2022

Development of plant-produced bispecific monoclonal antibody targeting PD-L1 and CTLA-4 for cancer immunotherapy

Christine Joy Isip Bulaon
Faculty of Pharmaceutical Sciences

DEVELOPMENT OF PLANT-PRODUCED BISPECIFIC MONOCLONAL ANTIBODY TARGETING PD-L1 AND CTLA-4 FOR CANCER IMMUNOTHERAPY

Miss Christine Joy Isip Bulaon

A Dissertation Submitted in Partial Fulfillment of the Requirements
for the Degree of Doctor of Philosophy in Pharmaceutical Sciences and Technology
FACULTY OF PHARMACEUTICAL SCIENCES
Chulalongkorn University
Academic Year 2022

การพัฒนาโมโนโคลนอลแอนติบอดีคู่จำเพาะต่อ PD-L1 และ CTLA-4 ที่ผลิตจากพืชสำหรับการรักษามะเร็งด้วยภูมิคุ้มกันบำบัด

น.ส.คริสติน จอย อีซิพ บูลาโอน

วิทยานิพนธ์นี้เป็นส่วนหนึ่งของการศึกษาตามหลักสูตรปริญญาวิทยาศาสตรดุษฎีบัณฑิต
สาขาวิชาเภสัชศาสตร์และเทคโนโลยี ไม่สังกัดภาควิชา/เทียบเท่า
คณะเภสัชศาสตร์ จุฬาลงกรณ์มหาวิทยาลัย
ปีการศึกษา 2565

Thesis Title	DEVELOPMENT OF PLANT-PRODUCED BISPECIFIC MONOCLONAL ANTIBODY TARGETING PD-L1 AND CTLA-4 FOR CANCER IMMUNOTHERAPY
By	Miss Christine Joy Isip Bulaon
Field of Study	Pharmaceutical Sciences and Technology
Thesis Advisor	Associate Professor WARANYOO PHOOLCHAROEN, Ph.D.

Accepted by the FACULTY OF PHARMACEUTICAL SCIENCES, Chulalongkorn University in Partial Fulfillment of the Requirement for the Doctor of Philosophy

..... Dean of the FACULTY OF PHARMACEUTICAL SCIENCES

(Professor PORNANONG ARAMWIT, Ph.D.)

DISSERTATION COMMITTEE

..... Chairman

(Associate Professor Anchanee Kubera, Ph.D.)

..... Thesis Advisor

(Associate Professor WARANYOO PHOOLCHAROEN, Ph.D.)

..... Examiner

(Assistant Professor SUPANNIKAR TAWINWUNG, Ph.D.)

..... Examiner

(Assistant Professor WANATCHAPORN ARUNMANEE, Ph.D.)

..... Examiner

(Assistant Professor NATAPOL PORNPUTTAPONG, Ph.D.)

คริสติน จอย อีซิพ บูลาโอน : การพัฒนาโมโนโคลนอลแอนติบอดีคู่จำเพาะต่อ PD-L1 และ CTLA-4 ที่ผลิตจากพืชสำหรับการรักษามะเร็งด้วยภูมิคุ้มกันบำบัด. (DEVELOPMENT OF PLANT-PRODUCED BISPECIFIC MONOCLONAL ANTIBODY TARGETING PD-L1 AND CTLA-4 FOR CANCER IMMUNOTHERAPY) อ.ที่ปรึกษาหลัก : รศ. ดร.วรัญญู พูลเจริญ

การรักษาด้วยภูมิคุ้มกันบำบัดแบบยับยั้งการทำงานของอิมมูนเช็คพอยต์เป็นการปฏิวัติแนวทางการรักษามะเร็งอย่างหนึ่ง โดยผลการวิจัยทางคลินิคพบว่าการใช้โมโนโคลนอลแอนติบอดีที่มีความจำเพาะต่ออิมมูนเช็คพอยต์นั้นเป็นที่น่าพอใจในการรักษามะเร็งหลายชนิด อย่างไรก็ตาม การใช้แอนติบอดีที่จำเพาะเพียงเป้าหมายเดียวทำให้ประสิทธิภาพในการรักษาถูกจำกัด ในงานวิจัยนี้ ได้พัฒนาการผลิตโมโนโคลนอลแอนติบอดี DVD-AT2C ที่จำเพาะต่อ 2 เป้าหมาย (bsAb) ได้แก่ PD-1/PD-L1 และ CTLA-4 ในพืชซึ่งเป็นอีกทางเลือกหนึ่งสำหรับผลิตรีคอมบิแนนท์โปรตีน ระดับการแสดงออกของโมโนโคลนอลแอนติบอดี DVD-AT2C ที่จำเพาะต่อ PD-1/PD-L1 และ CTLA-4 แบบชั่วคราวในต้นใบยาสูบ (*Nicotiana benthamiana*) ที่สูงสุดถูกพบในระยะเวลา 4 วัน bsAb ดังกล่าวที่ทำการบริสุทธิ์แล้วถูกนำมาศึกษาขนาดโมเลกุล โครงสร้าง คุณสมบัติ และหน้าที่ทั้งในหลอดทดลอง (*in vitro*) และในสิ่งมีชีวิต (*in vitro*) โครงสร้างโมเลกุลของ DVD AT2C ที่ผลิตในพืชนั้นเป็นไปตามที่ได้คาดการณ์ไว้และพบว่าส่วนใหญ่มีโครงสร้างแบบโมเลกุลเดี่ยวและมีการผลิตน้ำตาลแมนโนสและ N-glycan เชิงซ้อนสูง แอนติบอดี DVD-AT2C ที่ผลิตในพืชนั้นมีประสิทธิภาพในการจับกับโปรตีน PD-L1 และ CTLA-4 ในหลอดทดลอง นอกจากนี้ การทดสอบประสิทธิภาพการต้านมะเร็งของ bsAb ที่ผลิตจากพืชในมะเร็งลำไส้ของสิ่งมีชีวิตซึ่งเปรียบเทียบกับ Atezolizumab และ 2C8 ที่ผลิตจากพืชพบว่า DVD-AT2C ที่ผลิตจากพืชสามารถยับยั้งการเจริญของเซลล์มะเร็งอย่างมีนัยสำคัญโดยสามารถลดขนาดและน้ำหนักของเนื้องอกได้ แต่ผลต่อการต้านมะเร็งนั้นไม่ได้เหนือกว่าแอนติบอดีต้นแบบอย่าง 2C8 เท่าไรนัก ผลการศึกษาการเปลี่ยนแปลงน้ำหนักตัวบ่งชี้ว่าแอนติบอดีที่ผลิตในพืชดังกล่าวมีความปลอดภัยและทนทาน โดยรวมแล้วการศึกษานี้สามารถพิสูจน์ให้เห็นถึงประสิทธิภาพและความเป็นไปได้ของการผลิต bsAb ในพืชสำหรับการใช้ในการรักษาโรคมะเร็งด้วยภูมิคุ้มกันบำบัด

สาขาวิชา เภสัชศาสตร์และเทคโนโลยี ลายมือชื่อนิสิต .....

ปีการศึกษา 2565 ลายมือชื่อ อ.ที่ปรึกษาหลัก .....

6371002633 : MAJOR PHARMACEUTICAL SCIENCES AND TECHNOLOGY
KEYWORD: immune checkpoint inhibitor, bispecific antibody, N. benthamiana, cancer immunotherapy

Christine Joy Isip Bulaon : DEVELOPMENT OF PLANT-PRODUCED BISPECIFIC MONOCLONAL ANTIBODY TARGETING PD-L1 AND CTLA-4 FOR CANCER IMMUNOTHERAPY. Advisor: Assoc. Prof. WARANYOO PHOOLCHAROEN, Ph.D.

Checkpoint blockade immunotherapy has transformed the course of cancer treatments. The use of monoclonal antibodies (mAbs) specific against immune checkpoints has displayed satisfactory clinical benefits. However,its effectiveness is limited to just a small percentage of cancer patients. In this work, a recombinant DVD-AT2C bispecific antibody (bsAb) was developed for dual inhibition of PD-1/PD-L1 and CTLA-4 axes and produced in plants. Plant system was utilized as an alternative protein production platform. Transient expression of DVD-AT2C targeting PD-L1 and CTLA-4 in *Nicotiana benthamiana* was determined highest after 4 days of infiltration. The size, assembly, and protein properties of the purified bsAb were determined, and its function was investigated *in vitro* and *in vivo*. The molecular structures of plant-produced DVD AT2C are as expected, and it was mostly present as monomer. Expression of bsAb in wildtype plants produced high mannose-type and some complex N-glycans. The plant-produced DVD-AT2C showed *in vitro* binding to PD-L1 and CTLA-4 proteins. The antitumor activity of plant-produced bsAb was tested *in vivo* colon tumor and compared to plant-produced Atezolizumab and 2C8. Plant-produced DVD-AT2C significantly inhibited tumor growth by reducing tumor volume and weight. The antitumor effects, however, were not superior to monospecific parent 2C8. Body weight changes indicated that plant-produced bsAb was safe and tolerable. Overall, this proof-of-concept study demonstrated the viability of plants to produce functional plant-produced bsAb for cancer immunotherapy.

Field of Study:	Pharmaceutical Sciences and Technology	Student's Signature .....
Academic Year:	2022	Advisor's Signature .....

ACKNOWLEDGEMENTS

First and foremost, I want to thank my advisor, Associate Prof. Waranyoo Phoolcharoen, Ph.D., for allowing me to work on this research and for guiding me throughout my Ph.D. studies. Her unwavering encouragement and advice had helped me stay motivated and finish this thesis. Apart from my advisor, I'd like to thank my senior, Dr. Kaewta Rattanapisit, and the entire team of Research Unit for Plant-Produced Pharmaceuticals (RU-PPP) from Chulalongkorn University for their insightful suggestions and support throughout my five-year post-graduate studies. I am truly grateful to my committee members for making my thesis defense a pleasant experience, as well as for their valuable knowledge and their precious time.

Following that, I'd like to extend my heartfelt appreciation to Chulalongkorn University for awarding me the ASEAN and NON-ASEAN Scholarship to pursue my Ph.D. degree as well as to Baiya Phytopharm Co., Ltd. for financial assistance. I'm also grateful to the Pharmaceutical Sciences and Technology (PST) program for providing me with quality education, research opportunities, and the opportunity to broaden my knowledge.

Finally, my sincere gratitude goes to my beloved parents, family and friends for their constant help and support. I'd like to dedicate this work to the Lord for giving me the strength, patience, and mental and emotional stability.

Christine Joy Isip Bulaon

TABLE OF CONTENTS

LIST OF TABLES

Page

LIST OF FIGURES

Page

CHAPTER I INTRODUCTION

1.1.Research Background and Significance

Checkpoint blockade immunotherapy has become a revolutionary cancer treatment approach, with unprecedented long-term responses and favorable toxicity in a wide range of patients. However, the staggering success of immune checkpoint blockade is short-lived, revealing that only a fraction of cancer patients benefited from this intervention. Immune checkpoint inhibitor (ICI) resistance is caused, if not entirely in part, by a lack of immune cell infiltration and the buildup of immunosuppressive cells in the tumor microenvironment (1, 2), critically undermines their clinical utility and ultimately impedes positive therapeutic outcomes. One way to circumvent tumor resistance and augment the clinical efficacy of ICIs is to exploit the potential of combination immunotherapy. Based on several preclinical and early-phase clinical studies, the combined use of ICIs (Opdivo® and Yervoy®) has demonstrated dramatic response rates against advance melanoma; although, significant treatment-associated toxicities appear to have been reported in the majority of patients (3, 4). Therefore, challenges remain in determining the overall survival benefit of such combinations. For this reason, growing research efforts to develop novel treatments have focused on maximizing their advantages over monotherapies and combination cancer therapies.

Bispecific monoclonal antibody (BsMab, BsAb) is an antibody that recognizes two distinct antigens in one antibody molecule. It has long been postulated as potentially effective cancer treatment, but only recently have they shown promising results. BsAbs are currently receiving a great amount of attention due to the heightened interest for antibodies in general. Over 180 bsAbs are currently in preclinical trials, and more than 50 bsAbs have entered various stages of clinical investigations as of this writing (5). A remarkable turnaround in 2022 occurred with the approval of five bsAbs for marketing by FDA. Alternatively, while exploring the optimal immunotherapy approaches, the therapeutic potentials of bsAbs were considered in this study. This is why this research was conducted in order to develop a bsAb-based tumor immunotherapy with dual immune checkpoint blockade.

A dual-variable domain immunoglobulin (DVD-Ig™) bsAb was synthesized containing the antigen-binding variable fragments of both PD-L1 and CTLA-4 inhibitors. The idea of onbstructing the CTLA-4 and PD-1/PD-L1 mechanisms appears to be associated with increased levels of inhibitory PD-1 and PD-L1 immune checkpoints within the tumor microenvironment after anti-CTLA-4 treatment, suggesting an adaptive resistance mechanism (6). Thereby, the need for this research is further emphasized in examining the potential combinatorial effect and acceptable tolerability of dual receptors blockade with DVD-Ig™ bsAb targeting PD-L1 and CTLA-4 when compared to monospecific monoclonal antibody (mAb) therapy. The bsAb as well as its parental anti-PD-L1 and anti-CTLA-4 mAbs were produced for this purpose and tested in parallel assays.

BsAbs are rarely found in nature, and the method by which they are generated is critical and remains a major concern. Their development was once hampered by a number of obstacles, particularly chain mispairing issues and assembly. However, thanks to rapidly emerging production modalities, these challenges that bsAbs confront have been gradually resolved. Thus far, recombinant technology has dominated the bsAb platform (7), transforming and largely simplifying their manufacturing. Similarly, in this study, genetic recombination was utilized to produce the dual-targeting bsAb and parental mAbs. Plants, among other expression systems, have been spotlighted for many notable benefits, for instance, speed, flexibility, safety, scalability, and post-translational modifications (8). More importantly, the potential of plants to alleviate production costs implies attractiveness for the commercialization of anticancer antibodies. Therefore, considering all of its advantages, a plant expression system was utilized as an alternative expression system for immune checkpoint blocking antibodies.

1.2.Research Objectives and Hypotheses

In the current study, the bsAb heavy chain and light chain genes were synthesized and transiently co-expressed in *N. benthamiana* plants using geminivirus-derived vector. The experimental parameter of day post-infiltration or dpi (harvest time after infiltration) was controlled to determine the best condition with the

highest antibody expression. The bsAb was further characterized for its molecular structures (size), quality (purity, assembly, isoelectric point, and post-translational modification), and binding activity using several protein assays to fully elucidate the properties and specificity of plant-derived protein. Furthermore, preclinical evaluation of functionality was devised in this study to test the anticancer effects of plant-produced bsAb in humanized mouse model.

It is hypothesized that the recombinant bsAb can be transiently produced in *N. benthamiana* and that the plant-produced bsAb has significant antitumor activity *in vivo*. Moreover, dual-targeted plant-produced bsAb is hypothesized to display synergistic effect over parental antibodies and is well tolerated in tumor-bearing mice.

1.3.Research Scope

The study aimed to construct and analyze the quality and efficacy of a recombinant bsAb produced in *Nicotiana benthamiana*. The expression parameter dpi, which affects protein yield, was optimized. In addition, the physicochemical properties, *N*-glycan structures, binding and antitumor efficacy were evaluated in order to fully characterize the plant-produced bsAb. Based on our prior works (8-10), we have confirmed the feasibility of tobacco plants in producing immunotherapeutic mAbs and antigen. The contribution of this research is to additionally establish the robustness of plant platform for producing effective immune-oncology mAbs, as well as to provide preliminary results and a proof-of-concept for plant-based bsAb technology.

There are totally four main sections in the research methodology. Gene synthesis depicts a prior literature search and the application of gene construction and cloning in it. Transformation in *N. benthamiana* presents the procedures for plant preparation and infiltration and also the protein extraction and purification methods. The detailed characterization of plant-produced antibodies was followed and concluded with data collection and analysis. The flow of experimental design for each method is shown in Figure 1.

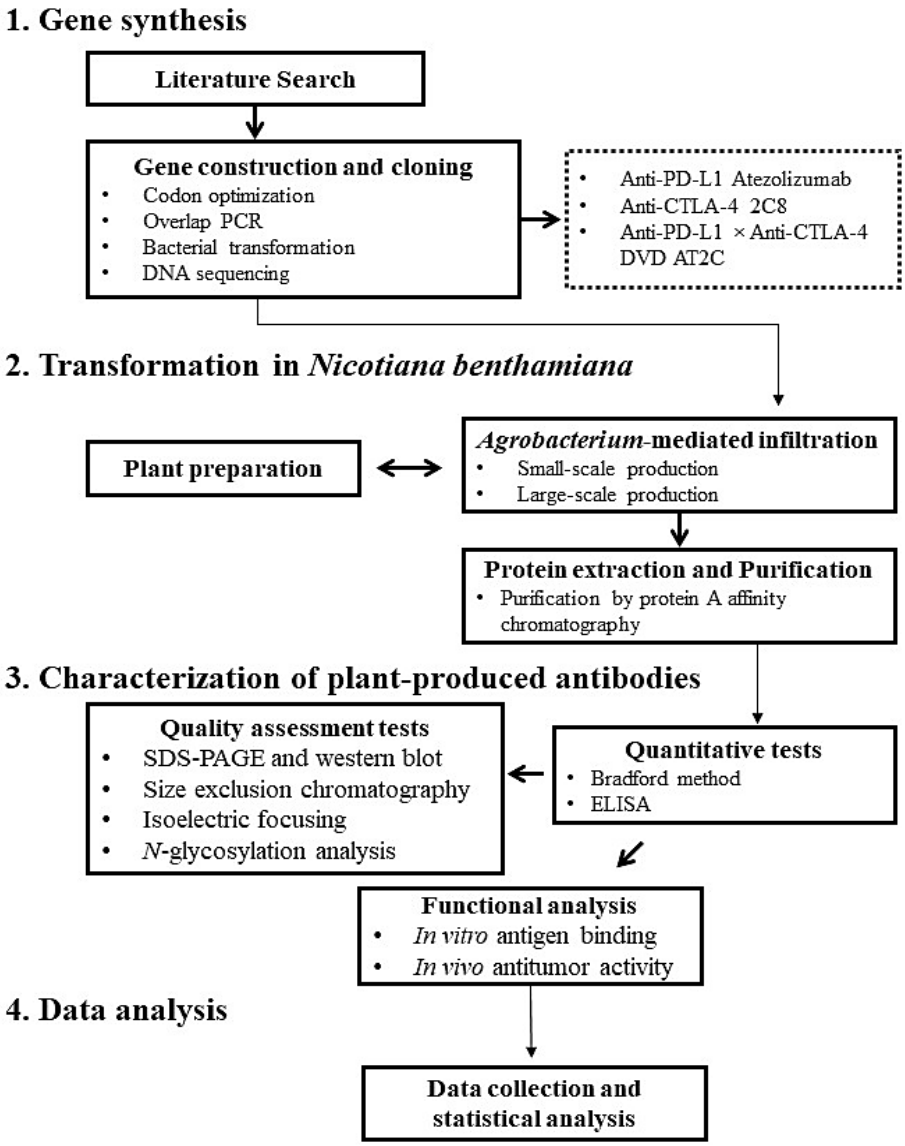

Figure 1. Flowchart of research study

1.4.Expected Benefits

This research establishes plants as an economically viable system for the production of anticancer bispecific antibodies and the plant-produced DVD AT2C can be regarded as an affordable, more effective, and safe bispecific antibody for cancer immunotherapy.

CHAPTER II LITERATURE REVIEW

2.1. Conventional cancer therapies

Cancer, one of the most prominent lethal diseases, is a public health dilemma responsible for nearly 10 million deaths worldwide. It is a multifactorial disorder characterized by abnormal cell growth, which causes tumor cells to grow haywire and spread throughout host's body, developing metastasis. Aside from that, cancer is incredibly complex because it continues to evolve and undergo mutations, making treatment extremely difficult.

Since then, three pillars of cancer therapies have been widely used: surgery, radiation, and chemotherapy. Of these medical interventions, surgical resection of tumors and radiotherapy with high-energy X-rays have primarily been considered in the early stages of cancer. Additionally, chemotherapy is another favored option which involves chemotherapeutic drugs to directly destroy cancer cells. Though, treatment with conventional treatments has proved to be satisfactory, a growing body of evidence shown that many patients suffer recurrence or fail to respond at all (11, 12), eventually limiting their clinical achievement. Besides, like any other treatment, these therapies also cause several harmful adverse events that can have a serious influence on one's quality of life (13, 14). Nonetheless, conventional cancer treatments remain mainstays up to date.

2.2. Immunotherapy

In attempt to develop more effective therapies after decades of disappointing results, immunotherapeutic strategies have emerged as the fourth pillar of cancer treatment. The immunological aspects of cancer therapy are gaining much attention, shifting the paradigm towards immune-based therapies. The groundbreaking advances in immunotherapy have expanded the treatment landscape for cancer. Immune checkpoint inhibitors (ICIs) and cellular immunotherapies, for example, has transformed the frontline standard of care for advanced malignancies. In this context, the role of immune system in cancer has come into limelight and is key determinant of its progression. As a matter of fact, tumors can develop when they outcompete

the immune system, thereby inducing suppression mechanism (15). Reactivating the immune system to effectively detect and eliminate cancer represents a promising treatment approach, which is realized in the concept of immunotherapy. Various types are currently used, with ICIs and adoptive T cell immunotherapy being the most common. Among these treatments, blocking of immune inhibitory pathways with ICIs will be covered briefly in the following section. However, as far as the treatment of cancer is concerned, there is no ideal treatment regimens presently known, although feats of immunotherapy unveil its promising future in the field of oncology.

2.3. Immune checkpoint blockade immunotherapy

Immunotherapy has taken the spotlight in recent years, with checkpoint blockade therapy gradually taking the forefront in medicine research. While endogenous immune responses are witnessed in preclinical and clinical trials, such responses are rendered ineffective as tumors stimulate tolerance amongst tumor-specific lymphocytes and exploit inhibitory checkpoint mechanisms (16). One method to positively regulate the T cell responses has been demonstrated via checkpoint blockade, which involves significant blocking of inhibitory checkpoint receptors hijacked by cancer. The advent of immune checkpoints has piloted enormous advancements in tumor therapy. Checkpoints that have received most interest include programmed cell death-1 protein (PD-1), programmed death-ligand 1 (PD-L1), and cytotoxic T-lymphocyte-associated protein 4 (CTLA-4) (Figure 2). Novel immune checkpoint molecules are also identified in recent studies (17) but exceed the scope of this research.

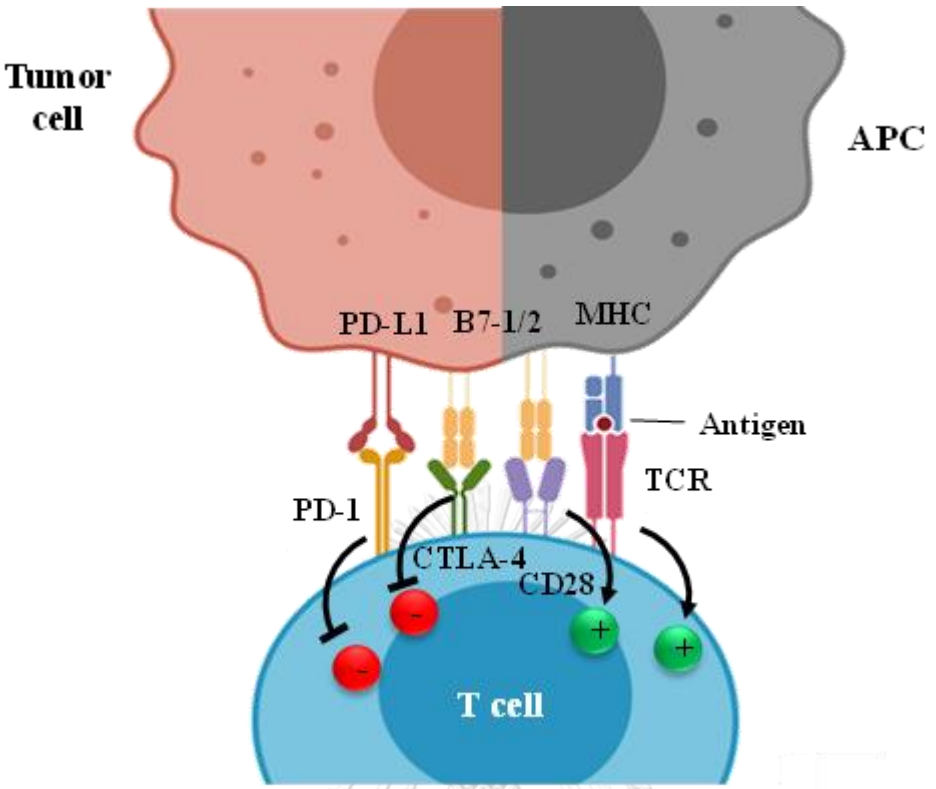

Figure 2. Interaction of immune checkpoints with immune cells or tumor cells. APC: Antigen presenting cell, MHC: Major histocompatibility complex, TCR: T cell receptor, B7-1: CD80, B7-2: CD86.

2.3.1. PD-1/PD-L1

The PD-1 is an immune checkpoint that has shown expression on a wide range of immune cells, predominantly T cells but also B cells, monocytes, dendritic cells (DCs) and natural killer (NK) cells (18, 19). It has essential roles in PD-1 signaling and is associated in the regulation of T cell responses during physiological conditions (19, 20). For instance, PD-1 expression reduces the risk of autoimmune reactions by inhibiting self-reactive lymphocytes. Conversely, the PD-1 inhibitory pathway can be co-opted in cancer to evade immune surveillance (19, 21), compromising antitumor immunity. PD-L1, one the contrary, a ligand of PD-1, was found to be expressed on both immune cells and tumor cells (22, 23). The engagement of PD-1 to PD-L1 within the tumor counteracts T cells and abrogates antitumor response, thereby limiting tumor cell destruction. These two immune checkpoints have gotten a lot of

attention as interesting targets for blocking monoclonal antibodies, which are already being developed and exploited in cancer immunotherapy.

2.3.2. CTLA-4

CTLA-4 is another immune checkpoint that is notably expressed by T cells. It controls the breadth of T cell activation throughout the initial stage. CTLA-4 binds with greater affinity to B7 ligand expressed by antigen presenting cells (APCs) than its homolog CD28 receptor. The competition for binding demonstrates that CTLA-4 thwarts CD28 function and, once bound, interferes with the CD28 costimulatory signaling. More so, the expression of CTLA-4 was found to be drastically different from that of CD28 (24), with increased levels of former on stimulated T cells and the latter on naïve T cells. This infers that CTLA-4 is necessary for T cell activation regulation because its absence brought about uncontrolled proliferation of T lymphocytes. In cancer, high expression of CTLA-4 is observed to downregulate T cell-mediated immune responses, potentially allowing tumor escape. Hence, blocking CTLA-4 engagement is being targeted and explored for anticancer therapies.

2.3.3. Mechanisms for CTLA-4 and PD-1/PD-L1 pathways

The CTLA-4 and PD-L1/PD-1 signaling is illustrated in Figure 3 and summarized in brief. T cell activation is multifaceted process that entails additional costimulatory signals. TCR recognition of peptide-MHC complexes initially provides specificity and stimulatory signal, however it is insufficient to mediate activation. The interplay of B7 ligand on APC and CD28 receptor on T cell provides positive costimulatory signal, leading to T cell signaling. The TCR signal in concert with CD28 costimulation are both needed for T cell activation. In early phases of activation, negative regulators, such as CTLA-4, are induced to counter overstimulation of the immune system (Figure 3A). CTLA-4 binds to B7, like CD28, but with much higher avidity (25). Nevertheless, the interaction between CTLA-4 and B7 produced an inhibitory signal unlike CD28. As such, competitive binding can prevent the positive signaling events initiated by CD28 costimulatory pathway (26). The relative levels of binding between CD28 and B7 vs. CTLA-4 and B7 decides if a T cell undergoes activation or becomes

anergic (27). In the context of cancer, CTLA-4 expression attenuates T cell responses, inducing tumor tolerance and T cell enervation. Monoclonal antibodies (mAbs) against CTLA-4 immune checkpoint can, though, block these inhibitory signals (Figure 3B). Anti-CTLA-4 mAbs can bind to this co-inhibitory receptor to dampen CTLA-4-mediated inhibition and reactivate effector functions, such as T cell killing of tumor cell (28).

PD-1 is another surface receptor that impedes activation of T cells by engagement to PD-L1 and PD-L2 ligands (Figure 3C, PD-L2 not shown). It is expressed by antigen-stimulated T lymphocytes that exerts negative signals once bound to its ligands on APCs or cancer cells. The T cell recognition of tumor antigens can activate T cell proliferation, cytokine secretion, and survival (29). However, following persistent antigen exposure, PD-1 expression can be upregulated and maintained, as seen during chronic viral infection and tumor progression (30, 31). Concurrent TCR and PD-1 binding ceases early TCR signaling and decreases T cell activation (32). Likewise, cancer cell can overexpress PD-1 ligands in consequence of inflammatory cytokines and other signaling networks (33). The interaction between PD-1 to PD-L1 triggers T cell dysfunction, resulting in poor control of infection and tumor. So, the PD-1 pathway has also been deemed to be a potential target for immune checkpoint blockade therapy. Blockade of PD-1-mediated inhibition with anti-PD-1 or anti-PD-L1 mAbs reverts T cell dysfunction and boosts T cells to combat cancer (Figure 3D).

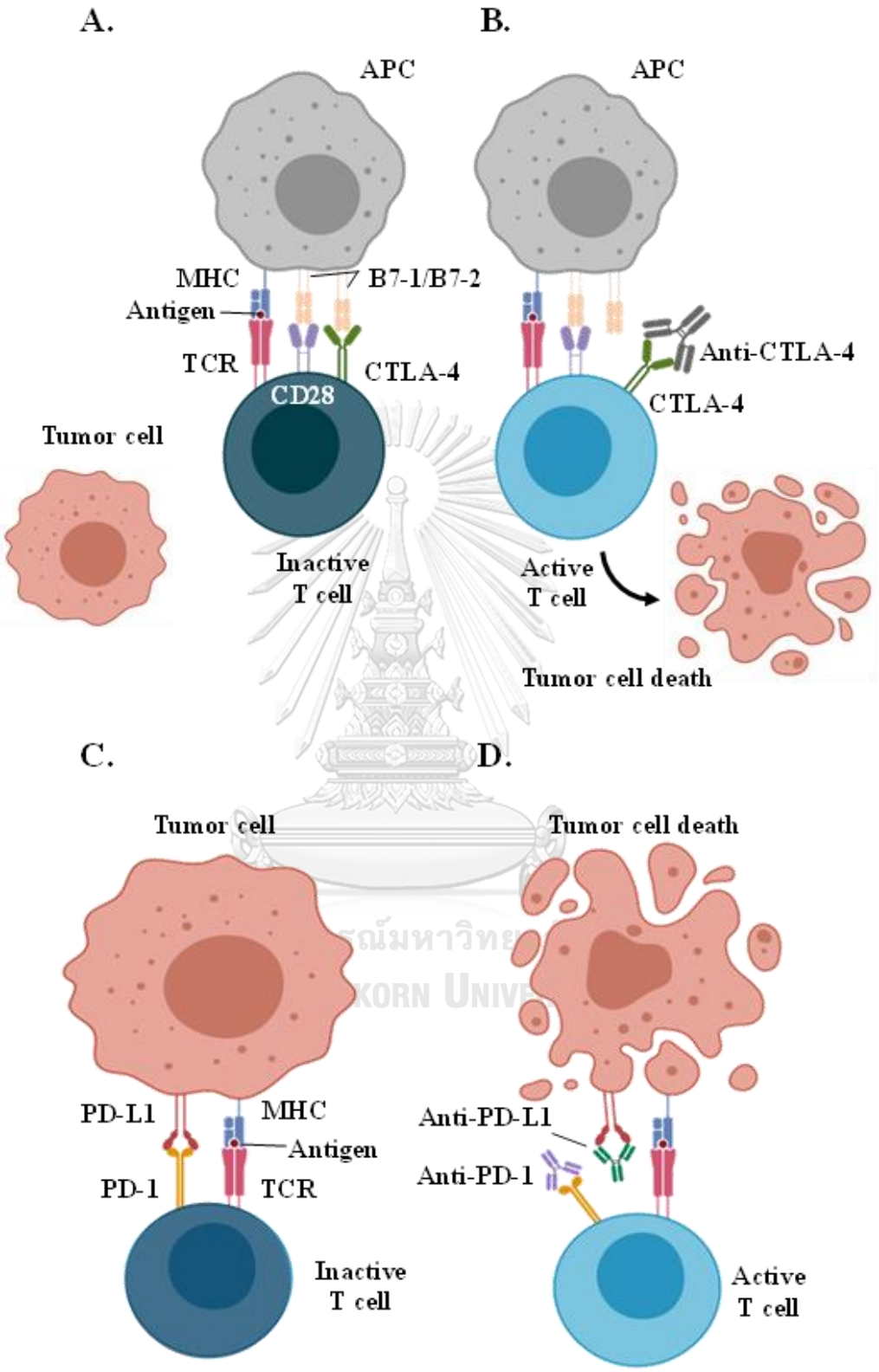

Figure 3. CTLA-4 and PD-L1/PD-1 pathways and modes of blockade. (A) TCR binding to antigen presented by MHC and CD28 binding to B7 drives T cell activation. The

binding of CTLA-4 to B7, same ligand for CD28, precludes full activation of T cells by inhibiting costimulatory signal. (B) mAbs specific for CTLA-4 reactivate CD28 costimulation and enable T cell effector function. (C) The engagement of PD-1 to PD-L1 in tumors negatively regulates T cell activation and hence occlude antitumor response. (D) PD-1 or PD-L1 specific mAbs occlude PD-1 signaling and permit activation of T cells. APC: Antigen presenting cell, MHC: Major histocompatibility complex, TCR: T cell receptor, B7-1: CD80, B7-2: CD86.

2.4. Success and challenges of ICI-based immunotherapy

ICIs are antibody-based immunotherapeutic agents that reinvigorate the host's immune response to cancer via blockade of inhibitory immune checkpoints. The US FDA has currently approved seven mAbs, which are listed in Table 1. Among the mAbs marked, data from Ipilimumab, Nivolumab and Atezolizumab will be concisely presented. This section reviews the benefits and drawbacks of these commercial antibodies against immunologic CTLA-4, PD-1, and PD-L1 receptors.

Ipilimumab, a CTLA-4 inhibitor, was the very first ICI authorized as first-line treatment for advanced and unresectable melanoma (34). According to a pooled meta-analysis of survival data, a 3-year survival rate of 22% in melanoma patients was projected from ipilimumab treatment (35). In line with this, ipilimumab therapy reported robust responses in a fraction of patients, with survival benefits in some lasting for over 3 years (35, 36). The importance of these findings is further underlined when compared to chemotherapy, where 3-year survival rates of melanoma patients treated with dacarbazine were just 12.2% (37). The applications of ipilimumab on several cancers i.e., non-small-cell lung carcinoma (NSCLC), renal cell carcinoma (RCC), prostatic adenocarcinoma and others are also being actively investigated. A review on recently completed clinical trials denotes that, although effectiveness against various malignancies is not as impressive as that shown in melanoma, a proportion of non-melanoma cancer patients have seen modest benefits in patient survival (38).

Nivolumab, a PD-1 inhibitor, was the first PD-1 specific ICI to be approved by the FDA as first-line treatment for melanoma without BRAF mutation. In a phase III

clinical trials, objective response rates (ORRs) with nivolumab therapy were greater than with dacarbazine following 40.0% vs. 13.9% of treated melanoma patients. This trial as well demonstrated improved progression-free survival and higher 1-year survival rates of anti-PD-1 mAb (5.1 months; 72.9%) against chemotherapy (2.2 months; 42.1%) (39). Furthermore, nivolumab has also been approved as either the first- or second-line therapy for a broad spectrum of malignancies, including squamous cell lung cancer, NSCLC, RCC, and head and neck squamous cell carcinoma. Following phase III trials from these cancer types, nivolumab had greater survival advantages than conventional treatments (40-43). Nivolumab achieved further licensed as the first ICI for hematological malignancy following two independent Phase I/II trials that reported combined ORR of 65% against classical Hodgkin lymphoma (44, 45).

Atezolizumab, a PD-L1 inhibitor, was the first ICI to be approved for PD-L1 blockade therapy. Since then, it has been utilized to treat multiple cancer indications, namely liver, skin and lung cancers, and approved as an adjuvant therapy for patients with stage II and IIIA PD-L1 positive (≥1%) NSCLC who had undergone surgery and chemotherapies (46). Additionally, the outcomes of phase III IMpassion130 trial demonstrating durable progression-free survival in atezolizumab-treated patients also led to FDA's accelerated approval for breast cancer in 2019 (47). A phase II study assessing the utility of atezolizumab in advanced bladder cancer shown better responses with increased PD-L1 expression (48), resulting to higher ORRs (26%) than those achieved without PD-L1 (8%). Moreover, in a phase II POPLAR trial, atezolizumab also had significant survival benefits over chemotherapy for the treatment of recurrent NSCLC tumors with moderate or high PD-L1 expression (49).

Despite these promising outcomes, there are also many challenges confronting immune checkpoint blockade immunotherapy. For instance, even though many of the patients receiving ICIs had complete and durable responses, some rather experienced disease recurrence or were completely unresponsive (28, 50). More so, response rates to these antibody therapies have barely surpassed 40% (51). Combination therapy with ICIs were exploited and have obtained meaningful

antitumor response, however adverse effects were exacerbated following combinatorial approach (3). In certain cases, poor response of some patients to ICIs may be caused by a compromised immune cell population as a result of prior rigorous treatments (50). The prerequisite for a pre-existing anti-tumor immunity may be another barrier to checkpoint blockade therapy (52, 53), as some patients who do not establish endogenous immune responses to cancer have perceived unfavorable therapeutic outcomes. Development of resistance could also render ICIs ineffective. For example, patients who are unresponsive to anti-PD-1 treatment may acquire tumor mutations, which could affect their sensitivity to PD-1 blockade (54). Alternatively, ICI therapies may also upregulate other inhibitory immune checkpoint proteins (6). More importantly, undesirable side effects and toxicities can also be associated with ICI treatment. Some examples of these aftereffects related to therapy are rash, dermatitis, diarrhea, colitis, hepatotoxicity and so on (50, 55). A review on these treatment-associated adverse events and their management is well-documented in other publications (56, 57).

Table 1. Immune checkpoint inhibitors approved by FDA.

Name	Target	Cancer indications
Ipilimumab (Yervoy®)	CTLA-4	Melanoma
Nivolumab (Opdivo®)	PD-1	Multiple solid tumors
Pembrolizumab (Keytruda®)	PD-1	Melanoma, NSCLC, HNSCC, classical Hodgkin lymphoma and UC
Cemiplimab (Libtayo®)	PD-1	Advanced cutaneous squamous cell carcinoma, basal cell carcinoma, and NSCLC
Atezolizumab (Tecentriq®)	PD-L1	NSCLC, liver cancer, advanced bladder cancer, SCLC, advanced melanoma
Avelumab (Bavencio®)	PD-L1	Advanced merkel cell carcinoma and advanced UC
Durvalumab (Imfinzi®)	PD-L1	Advanced UC, NSCLC, and SCLC

*Abbreviations: NSCLC - non-small cell lung cancer, HNSCC - head and neck squamous cell carcinoma, UC - urothelial carcinoma, SCLC - small cell lung cancer.

2.5. Overview of bispecific antibodies (bsAbs)

2.5.1. Formats of bsAbs

The conventional mAb is composed of two heavy chain and two light chain domains connected by four disulfide bridges (Figure 4). The heavy and light chain variable domains $(VH + VL)_2$ of mAb form the Fv region, which has single antigen specificity. Moreover, the Fab fragment is in charge of antigen binding, whereas the Fc region is a conserved sequence for crystallization with roles in binding to cellular receptors.

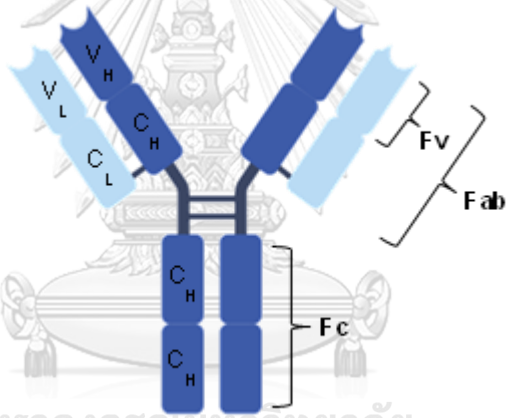

Figure 4. Classical IgG structure

BsAbs are antibodies that exhibit dual binding specificity and, in simple term, can target more than one antigen within the same agent. Compared with mAbs, bsAbs are advantageous in terms of higher binding avidity and specificity and slower rate of resistance development (58). Currently, there are more than 100 different bsAb types that have been engineered, and they are generally categorized as fragment-based molecules (Figure 5A) and immunoglobulin-like (IgG-like) molecules (Figure 5B).

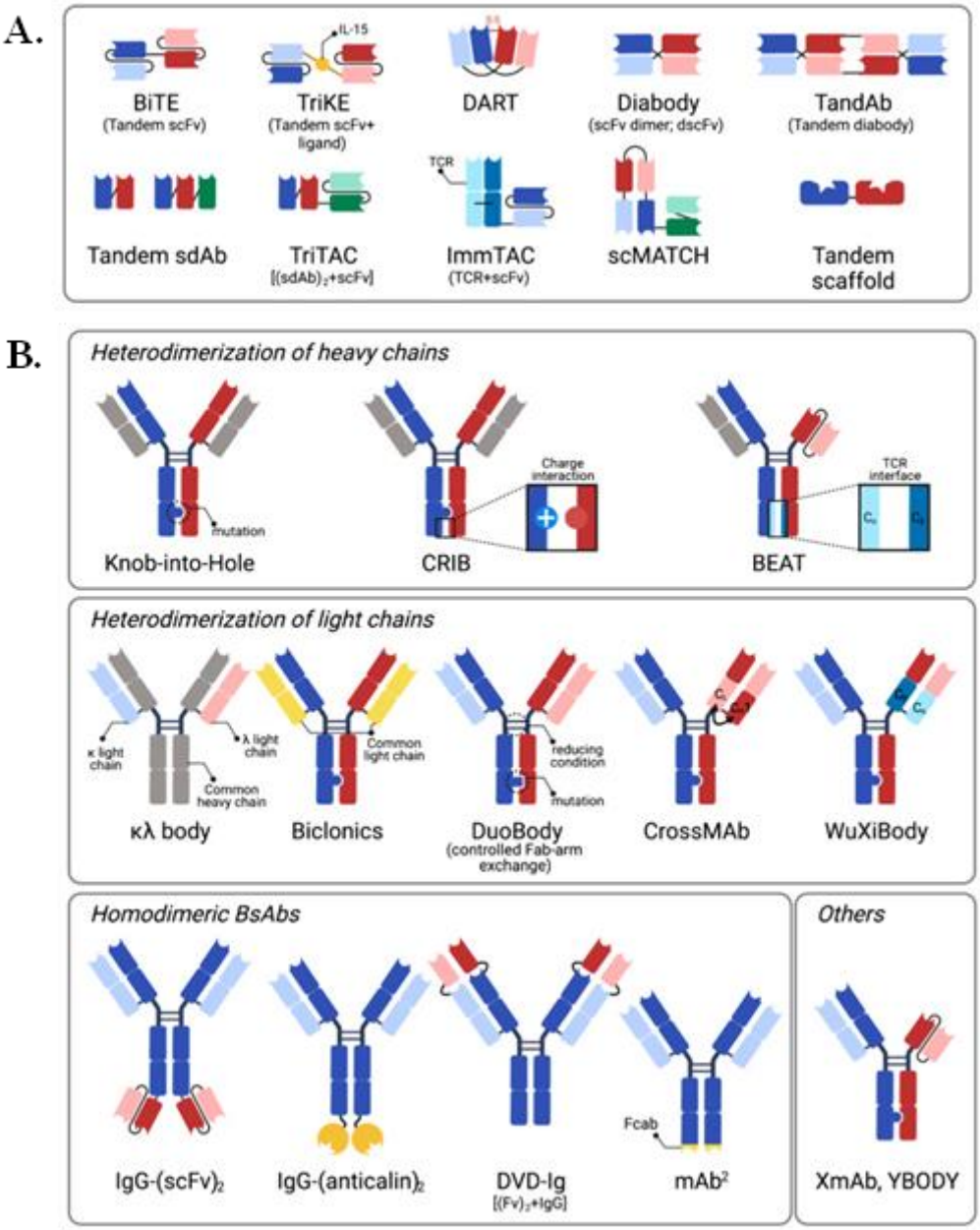

Figure 5. Illustration of bsAb representative structures. (A) Fragment-based bsAb formats (examples of bsAb lacking Fc). (B) IgG-like bsAb formats (examples of bsAb containing Fc region). Figure is modified and adapted from (59).

The fragment-based bsAbs lack the Fc region and thereby exert therapeutic effects via antigen binding. They offer benefits such as simplified production, low immunogenicity and improved tissue penetration. BiTE is a single-chain Fvs in tandem (scFv-based) bsAb that has been used to successfully treat leukemia. However, bsAbs in the BiTE format and other fragment-based forms generally have shorter serum

half-lives owing to their low molecular weight (60). The IgG-like bsAbs, in contrast, retain the Fc fragment of classical mAb, which enables purification and enhances stability and solubility. Moreover, these bsAbs commonly have extended half-lives because of their relatively large size and Fc-dependent effector function (60). Nonetheless, a significant bottleneck in IgG-like bsAb generation is the appropriate combination of distinct heavy and light chain chains. Several reports elsewhere (61, 62) have covered the development of various technologies to enhance the heterodimerization of both heavy chains and light chains. Another strategy is to develop homodimeric bsAbs, which are often employed in checkpoint blocking agents and other immunomodulating antibodies. So far, bsAbs have been postulated as the next-generation antibody therapy and their recent applications in therapy are introduced in the following section.

2.5.2. Applications of BsAbs

Therapeutic mAbs have become a hallmark in the treatment of several diseases and have so far proved to be overall beneficial. However, in some cases, these single targeting mAbs only achieve modest efficacy. Alternatively, bsAbs are engineered to cross-link two distinct epitopes and can thus target two disease mechanisms. They were discovered decades ago, but only become clinically relevant after the approval of blinatumomab by FDA. This bsAb is a dual-targeting CD19×CD3 antibody used to treat acute lymphoblastic leukemia (63). Since then, bsAbs have emerged as viable therapeutic strategy for difficult-to-treat illnesses, like cancer. The also hold great promise in variety of applications, including but not limited to immune effector cell redirection, distinctive receptor modulation, blocking two signaling pathways and disease mediators, and use as delivery vehicles (60).

This section focuses on the roles of bsAbs in restoring antitumor immunity through immune checkpoint blockade. Although ICI monotherapy has established significant impact in treating some cancer, its efficacy is limited in a subset of patients. BsAbs, with its aforementioned ability to target two immune checkpoints, may enhance immunomodulatory (immune blocking) functions. So far, checkpoint-targeted bsAbs are mostly used for treating solid tumors. Preclinical evaluation of

LY3434172, a PD-1×PD-L1 bsAb, revealed full blockade of inhibitory PD-1 pathway (64). This bsAb increased T cell response *in vitro* and stimulated strong antitumor response *in vivo* in comparison to single and combination ICIs treatment. Clinical evaluation of AK104, a PD-1×CTLA-4 bsAb, demonstrated favorable safety and encouraging antitumor response in patients with mesothelioma (65). Furthermore, phase I study of KN046, a bsAb targeting PD-L1 and CTLA-4, exhibited early evidence of efficacy in patients with metastatic thoracic tumors and acceptable safety, which is consistent with other ICIs (66). As listed in Table 2, several immune checkpoint bsAbs are currently undergoing clinical trials (59, 67, 68).

Table 2. BsAbs targeting PD-1/PD-L1 and CTLA-4 in clinical trials.

Candidate	Targets	Format	Clinical trials (highest phase)
LY3434172	PD-1 × PD-L1	KIH	NCT03936959 (Phase I)
AK104	PD-1 × CTLA-4	IgG-$(scFv)_2$	NCT04172454 (Phase II)
KN046	PD-L1 × CTLA-4	CRIB	NCT04040699 (Phase III)
MGD019	PD-1 × CTLA-4	DART	NCT03761017 (Phase I))
MEDI5752	PD-1 × CTLA-4	DuetMab/KIH	NCT04522323 (Phase I)
XmAb20717	PD-1 × CTLA-4	XmAb	NCT03517488 (Phase I)

*Abbreviations: KIH: Knob-into-hole, CRIB: Charge repulsion improved bispecific

2.6. Bispecific PD-L1×CTLA-4 checkpoint blockade

2.6.1. Dual-variable domain immunoglobulin structure

The selection of target antigen for possible combination is critical in the biosynthesis of bsAb. The rational design of our bsAb was inspired by (66), in which variable domains (VDs) of PD-L1 and CTLA-4 mAbs are fused together and linked with human IgG1 gamma and kappa chains. Likewise, this bsAb employs a proprietary dual-variable domain immunoglobulin (DVD-Ig™) format (Figure 6). A DVD-Ig™ is classified as an IgG-like bsAb that contains two variable heavy chain and light chain domains in tandem connected via peptide linker. Each binding arm of the resulting bsAb contains two antigen recognition sites. The outer VD of heavy chain and light chain are termed as VH1 and VL1, while the inner VD are termed as VH2 and VL2. In

concept, the DVD-Ig™ format could obstruct the complementarity-determining regions (CDRs) of VH2 and VL2, which are adjacent to the C-terminal constant domains, limiting structural and rotational flexibility. However, it has been discovered that affinity at the innermost domain may be affected in part by linkers (69). The choice of appropriate linkers between the variable domains are crucial for maintaining the desired properties of bsAb. Prior studies have presented that short-short peptide linkages of 5 to 6 amino acids assume a flexible and loop-like orientation that is suitable for connecting two variable domains (70, 71). This type of linkers provided dual targeting and binding of two antigens with full occupancy to both variable domains. The outermost domain is depicted as a swinging bucket that can capably move from one side to another with the help of linkers. In other cases, longer linkers of 12 to 13 amino acids tend to better conserve the parental domain actions, specifically the inner domain. Nevertheless, concerns are raised with long linkers as they may be prone for proteolytic degradation (71). DVD-Ig™ molecules offer advantages in terms of ease of purification, display pharmacological properties similar to that of classical mAbs, amenable for mass production and favorable efficacy in multiple preclinical models (70, 71).

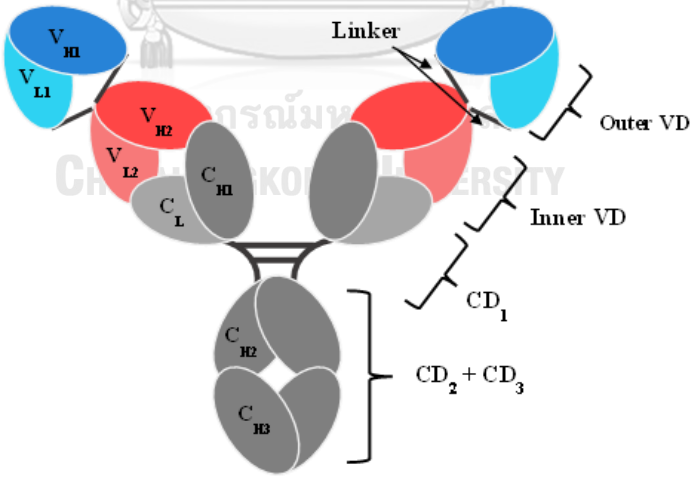

Figure 6. Structure of bispecific DVD-Ig™ protein. The figure shows a schematic representation of DVD-Ig™. VH: heavy chain, CH: constant heavy chain, VL: variable light chain, CL: constant light chain, VD: variable domain, CD: constant domain The outer VD and inner VD are coupled by linkers.

2.6.2. Proposed mechanism of action

In this study, our bsAb (DVD AT2C) aims to target the PD-L1/PD-1 and CTLA-4 inhibitory mechanisms for efficient dual receptors blockade (Figure 7) (28). During the priming phase, the anti-CTLA-variable domain of DVD AT2C engages to CTLA-4 receptor on the T cell and blocks receptor-ligand interaction. Inhibition of CTLA-4 binding to B7 will reestablish effector functions of T cells in the lymph nodes. Afterwards, stimulated T cells migrate to the tumor site in order to kill cancer cell. During effector phase, tumors and other immune cells may overexpress PD-L1 and consequently impede T cell function via engagement of PD-1 and PD-L1, inducing inhibitory signal. The anti-PD-L1 variable domain of DVD AT2C binds to the PD-L1 ligand on the tumor cell and blocks PD-L1 interaction with PD-1. PD-1 signaling obstruction will restore T cell effector function at the tumor site and enable tumor eradication. Additionally, since our DVD AT2C bsAb favors binding to PD-L1 more than CTLA-4, the bsAb can target tumor microenvironment with high PD-L1 expression. This idea also proposes that PD-L1 driven binding reduces treatment-associated toxicity, since low levels of CTLA-4 and PD-L1 proteins prevent bsAb from binding.

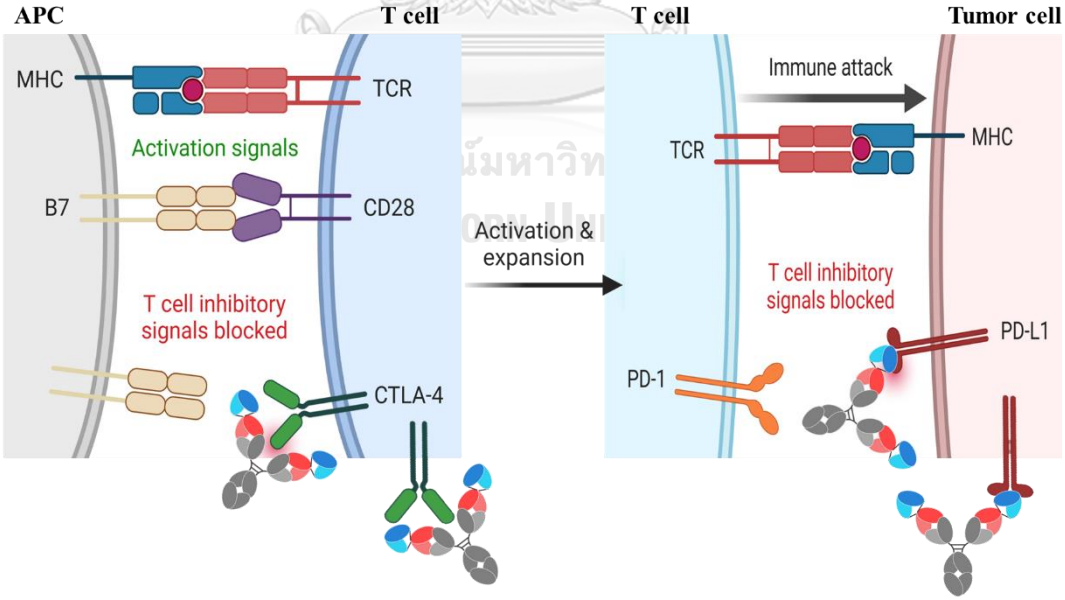

Figure 7. Modes of action of DVD AT2C bsAb. Created with BioRender.

CHAPTER III METHODOLOGY

This chapter explains the experimental procedures as well as the chemicals and equipment used in the study.

3.1. Materials

3.1.1. Gene sequences

2C8 (Patent No. US9758583B2)

Atezolizumab (Drugbank accession number: DB11595)

Human IgG1 gamma chain (Genbank accession number: AAA02914.1)

Human IgG1 kappa chain (Genbank accession number: AAA58989.1)

3.1.2. Enzymes

Q5 DNA polymerase (Promega, USA)

Restriction endonucleases *Afl*II (New England BioLabs, USA)

Restriction endonucleases *Bmt*I (New England BioLabs, USA)

Restriction endonucleases *Sac*I (New England BioLabs, USA)

Restriction endonucleases *Xba*I (New England BioLabs, USA)

T4 DNA ligase (Promega, USA)

Taq DNA polymerase (Promega, USA)

Trypsin (Promega, USA)

3.1.3. Vector

Plant expression vector (pBYR2eK2Md; pBY) (72, 73)

3.1.4. Commercial kits

DNA-spin™ plasmid DNA purification kit (iNtRON Biotechnology, Korea)

MEGAquick-spin™ plus fragment DNA purification kit (iNtRON Biotechnology, Korea)

3.1.5. Chemical reagents

2-N-morpholino-ethanesulfonic acid (MES), (ITW Reagents, Darmstadt, Germany)

2X sample buffer (LC5311, Bio-Rad, USA)

50x Tris-Acetate-EDTA (TAE) buffer (Vivantis, Malaysia)

Acrylamide (Himedia, India)

Agar powder (Titan Biotech Ltd., India)

Agarose powder (Vivantis, Malaysia)

Ammonium persulfate (AppliChem GmbH, Germany)

Bovine Serum Albumin (BSA) (HiMedia Laboratories, India)

Bromophenol blue (Labochem® International)

Citric acid monohydrate (VWR International, Beligum)

Coomassie Blue blue R-250 (AppliChem®, USA)

Enhanced chemiluminescence detection reagent (Abcam, UK)

Gentamicin (ITW Reagents, Germany)

Glacial acetic acid (Qrec, New Zealand)

Glycerol (Himedia, India)

Glycine (Vivantis, Malaysia)

Hydrochloric acid (HCl) (Merck, USA)

InstantBlue® Coomassie protein stain (Abcam, UK)

Kanamycin sulfate (ITW Reagents, Germany)

Magnesium Sulphate ($MgSO_4$) (Merck, USA)

Methanol (Honeywell, USA)

Peptone (Himedia, India)

Potassium chloride (KCl) (Merck, USA)

Potassium dihydrogen phosphate (KH_2PO_4) (Merck, USA)

Precision plus protein™ standards all blue (Bio-rad, USA)

Rifampicin (Thermo Fischer Scientific, USA)

SafeGreen (Vivantis, Malaysia)

Sodium chloride (NaCl) (VWR International, Beligum)

Sodium dodecyl sulphate (SDS) (Kemaus, Australia)

Sodium hydrogen phosphate (Na_2HPO_4) (Himedia, India)

Sulfuric acid (H_2SO_4) (Merck, USA)

TEMED (AppliChem GmbH, Germany)

TMB one solution substrate (Promega, USA)

Tris-base (Vivantis, Malaysia)

Tween 20 (Vivantis, Malaysia)

VC 1kb DNA ladder (Vivantis, Malaysia)

Yeast extract (Titan Biotech Ltd., India)

3.1.6. Laboratory materials

0.22 μm S-Pak membrane filter (Merck Millipore, USA)

0.45 μm Nitrocellulose membrane (Bio-Rad, USA)

96-well microtiter plate (269620, Thermo Scientific, USA)

Amicon® Ultra (50K) centrifugal filter (Merck, Germany)

Centrifuge tube 0.2-50 mL (Axygen®, USA)

Costar® 96-well ELISA plate (3690, Corning, USA)

Cuvette

MabSelect SuRe™ LX protein A resin (Cytiva, Sweden)

Medical X-ray green film (Carestream, USA)

NanoEase C18 column (Waters, USA)

NIPRO™ Disposable Syringe 1, 10, 20, and 50 mL and needle (Nipro, Thailand)

PCR tubes/strips (Axygen®, USA)

Petri dish Hycon plates (S.P.S. Lab Company, Thailand)

Pipet Tip sizes: 10, 200, 1000 μL and 5 mL (Axygen®, USA)

Polypropylene column (Qiagen, Germany)

SEC BEH 200 column (Waters, USA)

Snakeskin™ dialysis tubing (Thermo Scientific, USA)

3.1.7. Biological materials

Agrobacterium tumefaciens (GV3101 strain)

Escherichia coli (DH10B strain)

Mice (*Mus Musculus*) from Gempharmatech, China

Murine colon cancer (CT26) cell line

Tobacco (*Nicotiana benthamiana*)

3.1.8. Recombinant proteins and antibodies

Goat anti-human IgG-Fc specific antibody (ab97221, Abcam, United Kingdom)

HRP-conjugated anti-human gamma antibody (2040-05, SouthernBiotech, USA)

HRP-conugated goat anti-human kappa antibody (2060-05, SouthernBiotech, USA)

Human CTLA-4/His (11159-H08H, SinoBiological, China)

Human IgG1 (ab206198, Abcam, United Kingdom)

Human PD-L1/His (10084-H08H, SinoBiological, China)

Mouse CTLA-4/His (50503-M08H, SinoBiological, China)

Mouse PD-L1/His (50010-M08H, SinoBiological, China)

Plant-produced anti-PD-1 Nivolumab (8, 74)

Tecentriq® (Lot no. H0217B01, Roche)

Yervoy® (Lot no. ABQ8027, Bristol-myers Squibb)

3.2. Buffers

3.2.1. DNA loading 6x dye

38% (w/v) Glycerol, 0.08% (w/v) Bromophenol blue, 0.08% (w/v) Xylencyanol

3.2.2. 10X Non-reducing loading dye

125 mM Tris-HCl, 12% SDS, 10% Glycerol, 0.001% Bromophenol blue at pH 6.8

3.2.3. 10X Reducing loading dye

125 mM Tris-HCl, 12% SDS, 10% Glycerol, 0.001% Bromophenol blue, 22% (v/v) β-Mercaptoethanol at pH 6.8

3.2.4. 1X Phosphate-buffered saline (PBS)

137 mM NaCl, 2.7 mM KCl, 4.3 mM Na_2HPO_4 and 1.47 mM KH_2PO_4 at pH 7.4

Hyclone™ PBS with 0.0067 M PO_4 at pH 7.0-7.2 (Cytiva, Sweden)

3.2.5. 1X Phosphate-buffered saline-Tween (PBST)

1X PBS and 0.05% (v/v) Tween 20

3.2.6. Coomassie® blue stain solution

Coomassie Brilliant Blue R-250, Methanol, Glacial acetic acid, H_2O

3.2.7. Destaining solution

Glacial acetic acid, Methanol, H_2O

3.2.8. 1X Running buffer

25 mM Tris, 192 mM Glycine, 1% SDS

3.2.9. 1X Transfer buffer

25 mM Tris, 192 mM Glycine, 15% Methanol

3.2.10. 1X Infiltration buffer

10 mM MES, 10mM MgSO4 pH 5.5

3.3. Media

3.3.1. Luria Bertani Broth

1% NaCl, 0.5% Yeast, 1% Peptone

3.3.2. Luria Bertani Agar

1% NaCl, 0.5% Yeast, 1% Peptone, 1.5% Agar

3.4. Equipment

3.4.1. Machine and accessories

Blue LED transilluminator (Clare Chemical Research)

Grinding balls (Retsch, Germany)

MJ Mini™ 48-well Personal Thermal Cycler (Bio-Rad, USA)

Micropipette 2-1000 μg (Pipetman, USA)

Microplate incubator (Hercuvan Lab systems, UK)

Microplate reader (Hercuvan Lab Systems, Malaysia)

MicroPulser Electroporator (Bio-Rad, USA)

Mini Centrifuge (Bio-Rad, USA)

Multichannel pipette (Cleaver scientific, UK)

OTTO® Blender (OTTO, Thailand)

Orbitrap Exploris 480 mass spectrometer (Thermo Fisher Scientific, USA)

Tissue lyser (Retsch, Model: MM 400)

TOMY Autoclave sx series (Amuza Inc., Japan)

UHPLC system (Waters, USA)

Vanquish™ Neo UHPLC (Thermo Fisher Scientific, USA)

WIS-20 Precise Shaking Incubator (WiseCube®, Korea)

3.5. Methods

3.5.1. Synthesis of recombinant monospecific mAbs

The gene encoding sequences for the heavy chain (HC) and light chain (LC) of Atezolizumab (anti-PD-L1) and 2C8 (anti-CTLA-4) (75) mAbs were optimized *in silico* by Invitrogen GeneArt Gene Synthesis (Thermo Scientific, USA) with *Nicotiana benthamiana* codons. To generate the complete HC and LC sequences, the variable domains of Atezolizumab and 2C8 HCs was fused separately to the constant domain of human IgG1 gamma chain, whereby point mutations at N297A, D356E, and L358M were introduced into the gamma chain of Atezolizumab by overlap PCR using primers shown in Table 3. Whereas the variable domains of LC were linked to human IgG1 kappa chain. Both mAbs harbor an N-terminal signal peptide (SP) and a C-terminal SEKDEL peptide (Ser-Glu-Lys-Asp-Glu-Leu) of HC.

Table 3. Primers used to generate mutated Atezolizumab HC

Primer name	Sequence
XbaI-SP Forward	5’-GCTCTAGAACAATGGGCTGG-3’
SacI-SEKDEL Reverse	5’-CGAGCTCTCAAAGCTCATCCTTCTCAGA-3’
N-A Forward	5’-GAGAGAGGAACAGTACGCCAGCACGTACAGGGTTG-3’
N-A Reverse	5’-CAACCCTGTACGTGCTGGCGTACTGTTCCTCTCTC-3’
DEL-EEM Forward	5’-CCTCCATCTCGCGAGGAAATGACCAAGAACCAGG-3’
DEL-EEM Reverse	5’-CCTGGTTCTTGGTCATTTCCTCGCGAGATGGAGG-3’

3.5.2. Cloning of recombinant monospecific mAbs

The HC and LC gene inserts of Atezolizumab and 2C8 were digested from the recombinant plasmids using *Xba*I and *Sac*I restriction enzymes (Table 4) and ligated into geminiviral expression vector pBY individually (Tables 5 and 6). Then, ligated plasmids were transformed into *Escherichia coli* strain DH10B by heat shock method and spread onto Luria Bertani (LB) agar plate containing 50 mg/L kanamycin overnight at 37 °C. Transformants were verified by colony PCR and positive clones were inoculated in kanamycin-selective media at 37 °C for overnight with shaking (250

rpm). Next, plasmid DNAs were extracted following the DNA-spin™ plasmid DNA purification kit protocol and subjected to sequence analysis by Sanger sequencing (U2Bio, Thailand).

Table 4. Components for restriction endonuclease digestion

Components	Final concentration
Plasmid DNA	To be determined
10xCutsmart buffer	1x
XbaI restriction enzyme	10 units /50 µl reaction
SacI restriction enzyme	10 units /50 µl reaction
Nuclease-free water	Adjust to 50 µl

Table 5. Components for HC ligation

Components	Final concentration
pBY vector (*XbaI*/*Sac*I)	To be determined
HC gene (*XbaI*/*Sac*I)	To be determined
10xT4 DNA ligase buffer	1x
T4 DNA ligase	1 µl/ 20 µl reaction
Nuclease-free water	Adjust to 50 µl

Table 6. Components for LC ligation

Components	Final concentration
pBY vector (*XbaI*/*Sac*I)	To be determined
LC gene (*XbaI*/*Sac*I)	To be determined
10xT4 DNA ligase buffer	1x
T4 DNA ligase	1 µl/ 20 µl reaction
Nuclease-free water	Adjust to 50 µl

3.5.3. Construction of recombinant bispecific DVD AT2C mAb

To generate the anti-PD-L1 Atezolizumab × anti-CTLA-4 2C8 DVD-Ig™ bsAb (DVD AT2C), an overlap PCR strategy was carried out using the primers listed on

Tables 7 and 8. The PCR master mix contained primers, dNTP, $MgCl_2$, Q5 reaction buffer and Q5 Taq polymerase (Table 9). PCR amplification was performed using a MJ Mini™ 48-well Personal Thermal Cycler with the following conditions: initial denaturation at 98 °C for 7 min, 30 cycles of denaturation at 98 °C for 30 sec, annealing at 52 °C for 30 sec, and elongation at 72 °C for 1 min, and final elongation at 72 °C for 10 min. During the final elongation step of 2nd PCR, Taq polymerase was added to insert poly-A overhang at the 3' ends. The resulting PCR products were electrophorized in agarose gel and examined under blue light illumination.

Table 7. Primers used to generate DVD AT2C HC

Primer name	Sequence
XbaI-SP Forward	5'-GCTCTAGAACAATGGGCTGG-3'
DVD AT2C-L-HC Reverse	5'-CTGAACCTGTGGACCTTTGGTGCTAGCG-3'
DVD AT2C-L-HC Forward	5'-CAAAGGTCCACAGGTTCAGCTTCAACAATC-3'
SacI-SEKDEL Reverse	5'-CGAGCTCTCAAAGCTCATCCTTCTCAGA-3'

Table 8. Primers used to generate DVD AT2C LC

Primer name	Sequence
*Xba*I-SP Forward	5'-GCTCTAGAACAATGGGCTGG-3'
DVD AT2C-L-LC Reverse	5'-CTGAATATCGGGGGCGGCGACGGTGCG-3'
DVD AT2C-L-LC Forward	5'-GCCGCCCCCGATATTCAGCTGACCCAG-3'
SacI-SEKDEL Reverse	5'-CGAGCTCTCAAAGCTCATCCTTCTCAGA-3'

Table 9. Components for PCR

Components	Final concentration
dNTP (dATP/dTTP/dCTP/dGTP)	0.2 mM
Forward primer	0.2 mM
Reverse primer	0.2 mM
DNA template	0.1-250 ng
Q5 reaction buffer	1X
$MgCl_2$	2.0 mM

Taq or Q5 DNA polymerase	2 units/ 50 µl PCR
Nuclease-free water	Adjust to 15-25 µl

3.5.4. Cloning of recombinant bispecific DVD AT2C mAb

The obtained DNA bands were cut out of the agarose gel, eluted by MEGAquick-spin™ plus fragment DNA purification kit and then digested with *Xba*I and *Sac*I restriction endonucleases for both DVD AT2C HC and LC following Table 4. DNA bands were purified and ligated into pBY expression vector individually for two-piece ligation, as shown in Tables 5 and 6. The ligated plasmids were transformed into *E. coli* strain DH10B by heat shock and transformed cells were inoculated onto agar plate with 50 mg/L kanamycin. Transformants were randomly picked and screened by PCR for positive clones, which were further cultivated in kanamycin-selective broth medium at 37 °C for overnight. Plasmid DNAs were collected by DNA-spin™ plasmid DNA purification kit and analyzed by DNA Sanger sequencing (U2Bio, Thailand) to confirm the nucleotide sequences of DVD AT2C HC and LC. The resulting constructs are fused with a SP at the N-terminus and a SEKDEL motif at HC C-terminus.

3.5.5. Transformation into electro-competent *Agrobacterium* cells

The purified plasmids harboring anti-PD-L1, anti-CTLA-4 and DVD AT2C HC and LC genes in pBY vector were mobilized into *Agrobacterium tumefaciens* strain GV3101 using MicroPulser by electroporation and then cells were spread onto LB agar supplemented with kanamycin, rifampicin, and gentamicin (50 mg/L for each antibiotic). Agar plates were incubated at 28 °C for 48 h and colonies were screened by PCR using vector specific primers: 2e-3R plus 80bp Forward (5'-GGAGAGGACCTCGAGAAAC-3') and 2e-29e plus 78 bp Reverse (5'-GCTTTGCATTCTTGACATC-3') to verify presence of gene inserts. Positive colonies were cultured in an antibiotic-selective LB broth at 28 °C overnight with shaking (250 rpm). Then, *Agrobacterium* cultures were used for glycerol stock preparation and subsequent infiltration experiments.

3.5.6. Agroinfiltration of *Nicotiana benthamiana*

For small-scale infiltration, *Agrobacterium* liquid cultures containing pBY-HC and pBY-LC plasmids of either Atezolizumab, 2C8, or DVD AT2C antibodies were mixed at 1:1 ratio, pelleted by centrifugation at low-speed (4, 000×g for 15 min) and then resuspended in 1X infiltration buffer. The *Agrobacterium* was gently injected into the underside of six to eight-week-old *N. benthamiana* leaves via a needleless plastic syringe (1 mL). The infiltrated tobacco plants were maintained in a plant room with controlled conditions (16 h light/8 h dark cycle at 28 °C). To evaluate the level of antibody expression, transfected leaves were collected within 2-, 4-, and 6-days post-infiltration (dpi).

For large-scale infiltration, recombinant *Agrobacteria* harboring plasmids of pBY-HC and pBY-LC for each antibody were mixed together to OD_{600} of 0.2 at ratio 1:1 using 1X infiltration buffer and co-delivered into *N. benthamiana* by vacuum infiltration (600 – 760 mmHg for 1-2 min). Infiltrated plants were incubated in an indoor plant room and harvested at optimal dpi.

3.5.7. Extraction and quantification of plant-produced monoclonal antibodies

Small-scale infiltrated leaf samples were collected every 2 days between 2 to 6 dpi and chopped into small leaf discs (~30-50 mg leaf weight). Total soluble proteins (TSP) were extracted using a tissue lyser with stainless steel grinding balls (diameter 3 mm) in 200 µl of 1X PBS. Crude plant extracts were centrifuged (20, 000×g for 5 min) at 4°C. TSP concentration and protein yield was calculated by Bradford assay and enzyme-linked immunosorbent assay (ELISA).

A microtiter ELISA plate was coated with goat anti-human IgG-Fc specific antibody in 1X PBS (dilution 1:1,000) at 4 °C overnight. Then, plate was washed three times with 1X PBST and incubated with blocking solution of 5% (w/v) skim milk in 1X PBS at 37 °C for 2 h. Serial dilutions of commercial human IgG1 isotype as standard and protein samples were loaded into the plate and the plate was placed at 37 °C incubator for 2 h. Next, for antibody detection, an HRP-conjugated goat anti-human kappa antibody (dilution 1:2,500) in 1X PBS was incubated into the plate at 37 °C for 1 h. After washing with 1X PBST, plate was developed using TMB one solution

substrate. Finally, the reaction was impeded with 1M H_2SO_4 and the absorbance at 450 nm was read using a microplate reader (Hercuvan, Model: NS-100).

3.5.8. Purification of plant-produced monoclonal antibodies

Large-scale leaf samples were grinded in two volumes (w/v) of 1X PBS by blender. The crude lysates were centrifuged (13,000 rpm for 30 min) at 4 ℃ and supernatants were clarified by a cheesecloth and a sterile 0.22-μm S-Pak filter. Affinity chromatography with Protein A ligand was carried out for purifying the plant-produced mAbs. Briefly, a polypropylene column (diameter 15 mm) was packed with MabSelect SuRe™ LX protein A resin and equilibrated with 3 column volumes of 1X PBS. The filtered supernatant was slowly added into the column at 0.5 mL/min flow rate. Then, the column was washed with 10 bed volumes of 1X PBS and the plant-produced antibody was eluted with 5 bed volumes of 0.15 M citrate buffer at pH 2.7, which was immediately neutralized with 1.5 M Tris-HCl pH 8.8 to approximately pH 7. The purified plant-expressed antibody was further subjected to buffer-exchange using Snakeskin™ dialysis tubing (3.5K MWCO) with 1X PBS and concentrated in Amicon® Ultra (50K) centrifugal filter. The purity of antibody was evaluated by sodium dodecyl sulfate polyacrylamide gel electrophoresis (SDS-PAGE) and concentration was calculated using ELISA.

3.5.9. SDS-PAGE and western blot

The expression of antibody in crude extracts and in purified samples were determined using SDS-PAGE and western blot. Here, antibody samples either in non-reducing loading buffer or reducing loading buffer were separated in 4-15% SDS-polyacrylamide gel with 1X running buffer for 90-120 min. Then, proteins from the gel were electro-transferred to nitrocellulose membrane with 1X transfer buffer. The membrane was washed with 1X PBS and incubated withthe blocking solution of 5% (w/v) skim milk for 30-45 min. After blocking, membrane was incubated either with HRP-conjugated anti-human gamma antibody (1:5,000) or HRP-conjugated anti-human kappa antibody (1:5,000) in 3% (w/v) skim milk in 1X PBS for 2 h and then washed with 1X PBST three times for 10 min with shaking (30 rpm). The ECL plus detection

reagent was incubated with the membrane for 1 min with gentle shaking and later sprinkled onto the nitrocellulose membrane. Luminescence was detected and exposed to a medical X-ray green film. The quality of the purified plant-produced antibodies was visually examined using InstantBlue® staining of SDS gels.

3.5.10. Size exclusion chromatography (SEC)

The purity and aggregation of plant-produced Atezolizumab, 2C8 and DVD AT2C antibodies were further evaluated by SEC. Accordingly, a SEC BEH 200 column (4.6 x 300 mm) with 2.5 μM particle size mounted on an UHPLC system was used for the experiment. The plant-antibody samples were injected into the system and eluted with 1X PBS at 0.3 mL/min flow rate. Then, the column was maintained at 25 °C for 20 min of each chromatographic run. The ultraviolet absorbance at 280 nm was observed and the peak was integrated using Empower 3 software (Waters, USA).

3.5.11. Isoelectric focusing

The isoelectric points (pI) of purified plant-derived Atezolizumab, 2C8 and DVD AT2C antibodies were determined by isoelectric focusing. Antibody protein samples were resuspended with 2X sample buffer and electrophoresed through Invitrogen™ Novex™ pH 3-10 IEF Protein Gels (1.0 mm × 10-well) (EC6655BOX, Thermo Fischer Scientific, USA) for a total run time of 2 h and 30 mon at constant voltage (100 V for 1 h, 200 V for 1 h and 500 V for 30 min). Then, gel was incubated with a fixing solution of 12% trichloroacetic acid containing 3.5% sulfosalicylic acid for 30 min, stained with Coomassie® blue stain solution and destained with destaining solution.

3.5.12. *N*-glycosylation analysis

The *N*-glycan patterns of plant-produced Atezolizumab, 2C8 and DVD AT2C antibodies were assessed by liquid chromatography-electrospray ionization-mass spectrometry (LC-ESI-MS). Briefly, plant-produced antibodies were run in reducing SDS-PAGE and subjected to InstantBlue® staining. Then, the protein bands, which correspond to the HCs of plant-produced antibodies, were cut into slices, destained with acetonitrile, S-alkylated with carbamidomethylation reaction and digested with

trypsin. The glycopeptides were analyzed by LC-ESI MS with a Vanquish™ Neo UHPLC system coupled to an Orbitrap Exploris 480 mass spectrometer. Peptides were separated using C18 column. A C18 trapping column was used in line with the LC before separation with the analytical column.

3.5.13. Antigen binding ELISA

Recombinant human PD-L1/His, human CTLA-4/His, mouse PD-L1/His, and mouse CTLA-4/His were used to confirm the binding specificity of purified plant-produced Atezolizumab, 2C8 and DVD AT2C bsAb. Plant-produced Nivolumab and standard human IgG1 were tested in parallel assays and used as negative controls. Purified recombinant proteins at a concentration of 2 µg/mL were coated on microtiter plates at 4 °C overnight. Plates were then washed thrice with 1X PBST and incubated with 5% (w/v) skim milk blocking solution at 37 °C for 1 h. After blocking, two-fold serial dilution of purified plant-antibodies and controls were added into the plate and incubated at 37 °C for 2 h. Plates were washed with 1X PBST and incubated with HRP-conjugated anti-human kappa antibody (1:5,000) in 1X PBS at 37 °C for 2 h. The plates were washed again three times and developed using TMB solution substrate for 15 min, before quenching with 1 M H_2SO_4. Lastly, the absorbance at 450 nm was determined in a microplate reader (Hercuvan, Model: NS-100).

3.5.14. *In vivo* analysis of antitumor activity

3.5.14.1. Ethics statement

The study protocol along with any adjustment(s) or methods concerning the care and use of animals were assessed and approved by the Institutional Animal Care and Use Committee (IACUC) of GemPharmatech Co. prior to execution. Throughout the investigation, the care and use of animals were performed in compliance with the laws and regulations stated in the Association for Assessment and Accreditation of Laboratory Animal Care (AAALAC).

3.5.14.2. Animals

Six to eight weeks old BALB/c-hPD-1/hPD-L1/hCTLA-4 female mice from GemPharmatech Co., Ltd., China was used and a total of 36 mice were enrolled. All mice were housed on Aikelin cages and maintained at animal housing with 21-25 °C room temperature, 40-70% humidity and 12 h light/dark cycle.

3.5.14.3. Cell culture and inoculation

CT26-hPDL-1 cell line was developed by knocking-out mouse *PD-L1* gene using CRISPR/Cas9 technology and inserting a constitutively expressed human *PD-L1* gene. Mycoplasma-free CT26-hPDL-1 murine colon cancer cells were thawed and cultured, and then collected and resuspended in Dulbecco's PBS at a cell density of 1×10^7 cell/mL. Cell viability was calculated before and after inoculation, and each mouse was inoculated with 1×10^6/100 µL cells subcutaneously into the right hind flank depicted in Figure 8.

Figure 8. Tumor inoculation site

3.5.14.4. Randomization and dosing

When the average tumor size reached roughly 100.07 mm^3, all mice (n = 36) were fairly allocated into 6 groups with 6 mice each. The experimental design is shown in Table 10. Test groups include plant-produced Atezolizumab, 2C8 and DVD AT2C antibodies along with commercially available Tecentriq® and Yervoy®. PBS will be used as the control group. The day of grouping was considered as day 0 and administration of antibodies and control started on day 0. The tumor bearing mice were administered with commercial and plant-produced anti-PD-L1 and anti-CTLA-4 mAbs at 3 mg/kg dose and plant-produced DVD AT2C bsAb at 5 mg/kg dose for treatment. Route of administration (ROA) was via., intraperitoneal injection (i.p.) on

days 0, 3, 6, 9, 12, 15 with the adjustment of dosing volume based on mouse body weight (10 µl/g).

Table 10. Experimental design

Group	No.	Treatment	Dosage (mg/kg)	ROA	Frequency
G1	6	Vehicle	-	*i.p.*	Q3D × 6 times
G2	6	Tecentriq	3	*i.p.*	Q3D × 6 times
G3	6	Plant-produced Atezolizumab	3	*i.p.*	Q3D × 6 times
G4	6	Ipilimumab	3	*i.p.*	Q3D × 6 times
G5	6	Plant-produced 2C8	3	*i.p.*	Q3D × 6 times
G6	6	Plant-produced DVD	5	*i.p.*	Q3D × 6 times

3.5.14.5. Data collection and study endpoint

Tumor volume and mouse body weight were measured twice per week for the first week of drug administration and then three times a week for the following weeks based on tumor growth. The tumor volume is expressed as mm^3 using the formula: TV = 0.5 a x b^2, where a and b are the long and short diameters of the tumors. The body weight changes, tumor growth inhibition based on tumor volume (TGI_{TV}) and tumor weight (TGI_{TW}) were analyzed at the endpoint. Body weight changes were measured with an electronic weighing scale, and tumor volume with vernier calipers.

The calculation of TGI_{TV} is as follows:

$$RTV_n = \frac{V_{nt}}{V_{n0}}$$

$$TGI = \left(1 - \frac{meanRTV_{treat}}{meanRTV_{vehicle}}\right) \times 100\%$$

V_{nt} : Tumor volume on day treated (t) of mouse n;

V_{n0} : Tumor volume on day 0 of mouse n;

RTVn : Relative tumor volume on day n of mouse n;

$meanRTV_{treat}$: Mean RTV of administration group;

$meanRTV_{vehicle}$: Mean RTV of vehicle group;

The calculation of TGI_{TW} is as follows:

$$TGI_{TW} = \left(1 - \frac{meanTW_{treat}}{meanTW_{vehicle}}\right) \times 100\%$$

$meanTW_{treat}$: average tumor weight on some day in treatment group.

$meanTW_{vehicle}$: average tumor weight on some day in vehicle group.

3.5.15. Data and statistical analyses

The data was expressed as mean ± standard deviation (Mean ± SD). For comparison among three or more groups, one way analysis of variance (ANOVA) followed by multiple comparison procedures were performed. Data were analyzed with SPSS and statistical significance will be established as *** $p \leq 0.001$; ** $p < 0.01$; * $p < 0.05$. GraphPad Prism was used for data visualization.

CHAPTER IV RESULTS AND DISCUSSION

This chapter presents the data collection and the findings obtained in this study. The results were analyzed and discussed in the context of prior reports and relevant literature, as appropriate, to highlight similarities and differences between this study and earlier studies.

4.1. Construction and cloning of recombinant monospecific mAbs

The heavy chain (HC) and light chain (LC) gene sequences of Atezolizumab and 2C8 were synthesized to contain a 19 amino acid leader sequence peptide, MGWSCIILFLVATATGVHS (Accession No. P01750), at the N-terminus. This study used a leader sequence peptide, also referred as signal peptide (SP), which was derived from the murine immunoglobulin heavy chain to effectively secrete recombinant mAbs expressed in *N. benthamiana* (76). Moreover, a 6-residue retention sequence peptide, SEKDEL, was incorporated at the C-terminus of the HC to induce specific localization of mAbs in the endoplasmic reticulum (ER). In principle, nascent recombinant protein first folds and assembles to form the mature protein in the ER before completing polypeptide translation and being transported to its final destination (77, 78). Accordingly, our idea was that the HC with SEKDEL could initially form dimers that are stabilized by disulfide bonds, and that LC could be joined by disulfide bridges between the HC and LC constant domains (C_L and C_H1), in accordance with relevant references (79, 80). When SEKDEL is attached, the recombinant proteins could be retained in, or retrieved to, the ER by retrograde transport (78, 81). In addition, ER retention was associated with higher protein production levels in seeds and plants (82, 83). The nucleotide and amino acid sequences of both antibodies were provided in Appendices A to D.

With the commercial Atezolizumab drug sequence as a guide, overlap PCR was carried out using the primers in Table 3 and plant-produced glycosylated anti-PD-L1 as the matrix (84) in order to introduce amino acid substitutions on the Fc portion of Atezolizumab. The process of overlap PCR and the predicted mutations on the IgG1 HC are depicted in Figure 9.

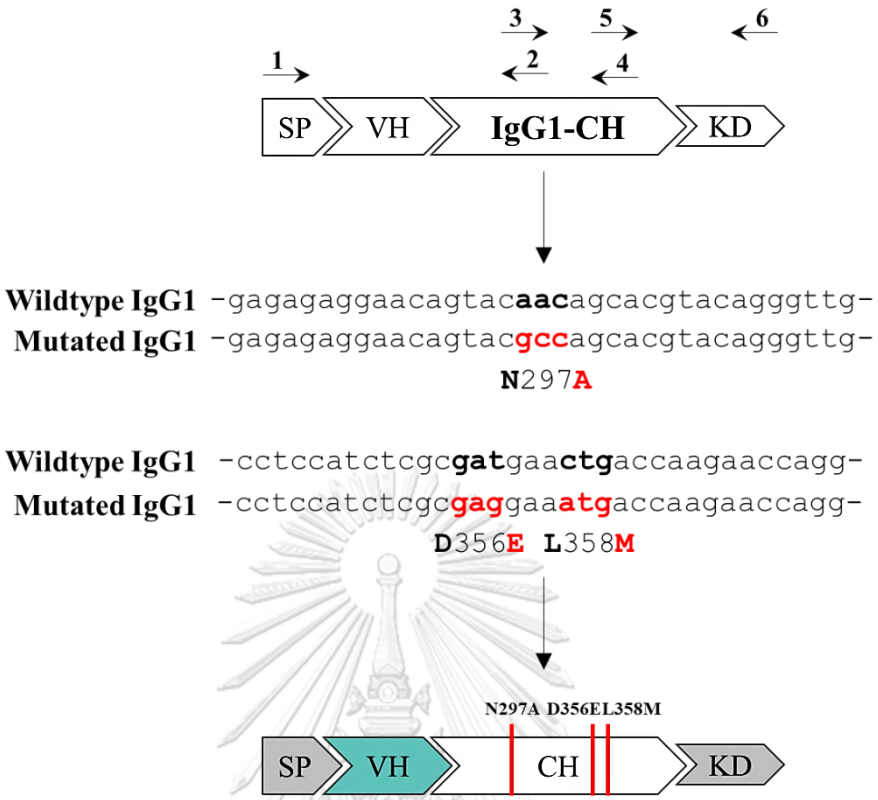

Figure 9. The overall scheme for the construction of mutant Atezolizumab IgG1.

The amplified PCR product for the mutated version of Atezolizumab was purified and digested with restriction enzymes *Xba*I and *Sac*I (Appendix E) for *in vitro* ligation. Meanwhile, the variable HC domain of 2C8 and variable LC domains of both Atezolizumab and 2C8 were commercially synthesized into the pUC57 vector and cut with restriction enzymes using *Xba*I and *Bmt*I (Appendix E) for HC and *Xba*I and *Afl*II (Appendix E) for LC. All digested products were individually ligated with the appropriate constant IgG1 gene fragments (C_H or C_L) bearing respective restriction enzymes into the pBY vector (Figure 10A). The pBY geminiviral expression vector (Appendix F) was generously provided by Professor Hugh Mason (Arizona State University, USA). The ligated plasmids were artificially transformed into *E. coli* DH10B strain competent cells by using heat shock technique. Clones for each antibody construct was screened by colony PCR using specific primer pairs and loaded on a 1% agarose gel to visualize the positive DNA bands. Here, findings revealed the

presence of gene inserts at approximately >1,450 bp for HCs and >730 bp for LCs as expected (Figure 10B,C).

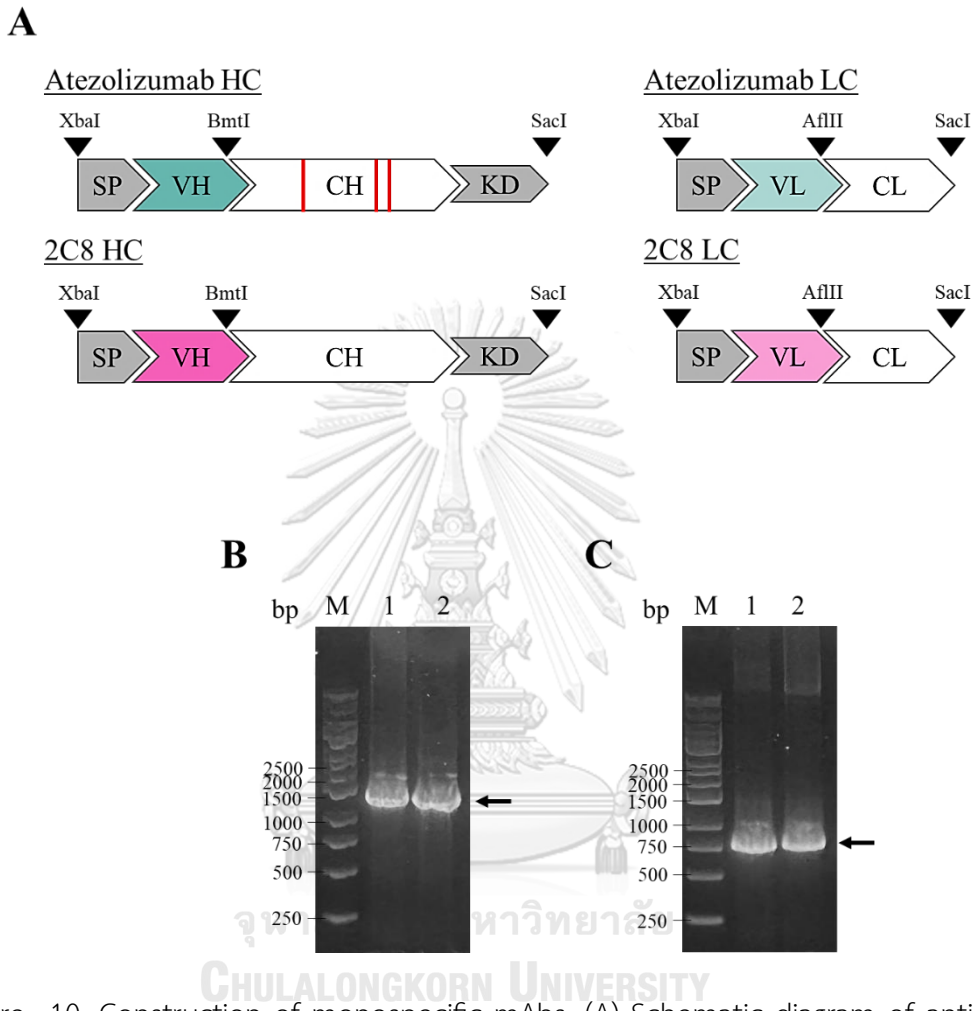

Figure 10. Construction of monospecific mAbs. (A) Schematic diagram of anti-PD-L1 Atezolizumab and anti-CTLA-4 2C8 HCs and LCs with corresponding domains and restriction enzymes. PCR analysis of E. coli transformants for the presence of HCs (B) and LCs (C) in the pBY plasmid. M: DNA ladder, 1: Atezolizumab HC/LC, 2: 2C8 HC/LC. The arrow indicates the genes of interest.

4.2. Construction and cloning of recombinant bsAb

The generation of recombinant bsAb with a DVD-Ig™ format initially started with the molecular cloning of parental Atezolizumab and 2C8 mAbs. To create the dual-specific DVD AT2C bsAb, their corresponding HC and LC gene fragments served as matrices for overlapping PCR using specific primers in Tables 7 and 8. An overview of DVD-Ig™ construction is depicted in Figure 11.

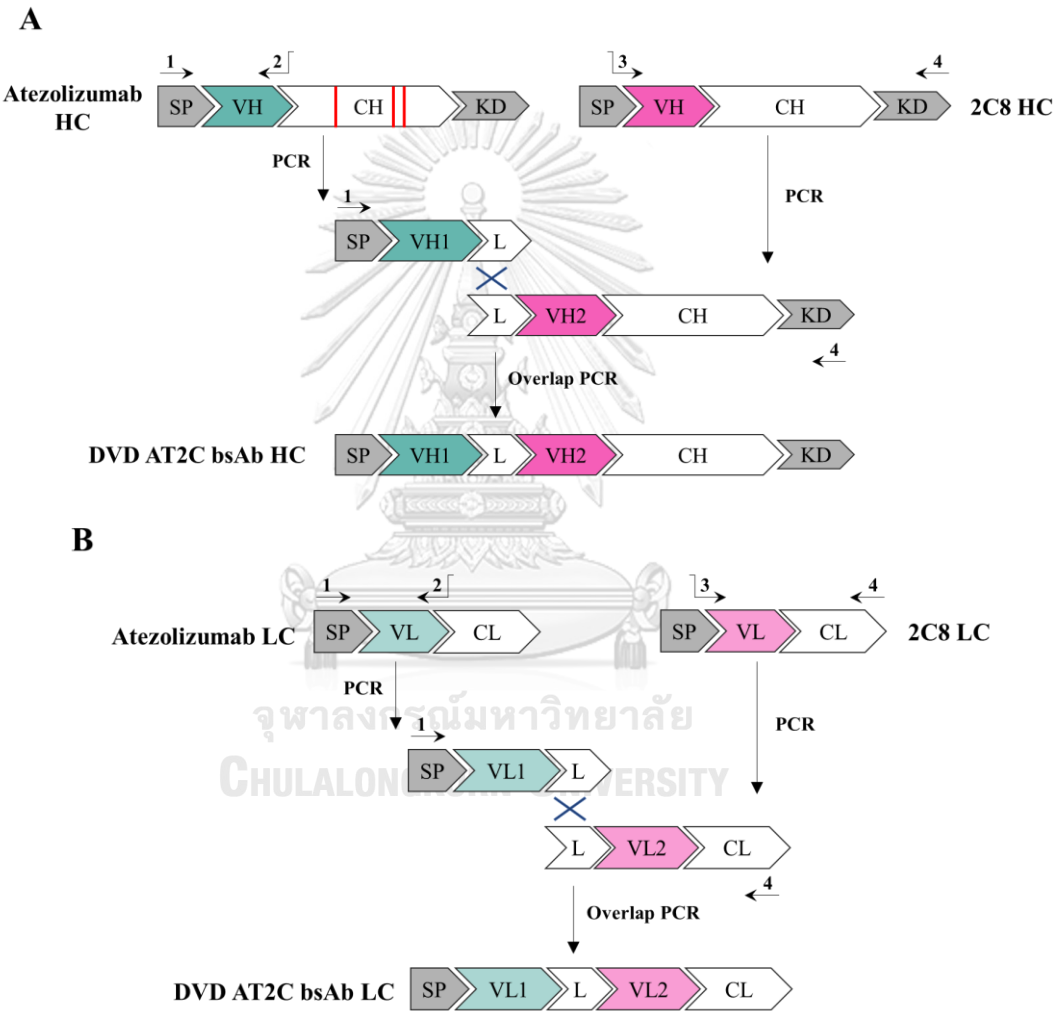

Figure 11. Summary of DVD AT2C HC (A) and LC (B) construction.

Herein, overlapping PCR strategy involves two PCR cycles. In the first cycle, two independent rounds of PCR amplification were carried out. The 1st round of PCR used primers 1 and 2 to amplify the SP, N-terminal outer variable domains and linker peptide, while the 2nd round of PCR used primers 3 and 4 to amplify the linker

peptide, C-terminal inner variable domain and constant domain sequences. Since the amplified products from PCR both contain the linker sequence, they can be linked together by a second cycle of PCR (overlap PCR) to obtain the full-length DVD AT2C HC and LC. Based on the results, every amplified product in every round of PCR was visualized on 1% agarose gel at the predicted size. In the first cycle, the amplified products for DVD AT2C HC contained DNA bands of approximately 465 bp (1st PCR) and 1399 bp (2nd PCR) (Figure 12, lanes 1 and 2), whereas the amplified products for DVD AT2C LC contained DNA bands of approximately 432 bp (1st PCR) and 663 bp (2nd PCR) (Figure 13, lanes 1 and 2). In the second cycle, the overlap of two PCR products for DVD AT2C HC and LC yielded in the complete amplification of bsAb at sizes of roughly 1,845 bp for HC (Figure 12, lane 3) and 1,077 bp for LC (Figure 13, lane 3).

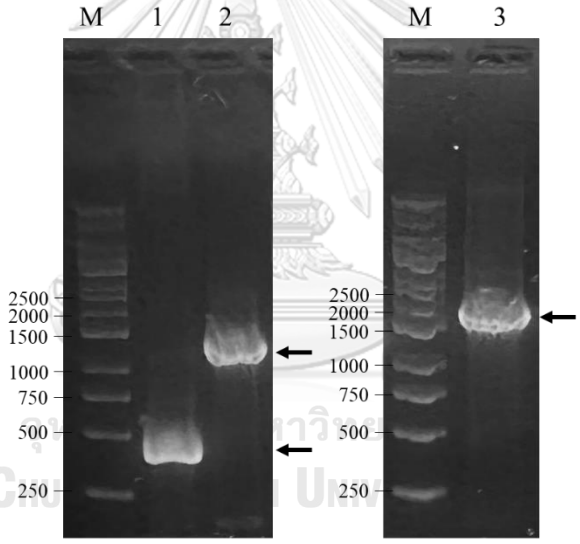

Figure 12. Amplification of DVD AT2C HC construct. (A) M: DNA ladder, 1: SP-VH1-Linker, 2: Linker-VH2-CH-KD, 3: SP-VH1-Linker-VH2-CH-KD. The arrow indicates the genes of interest.

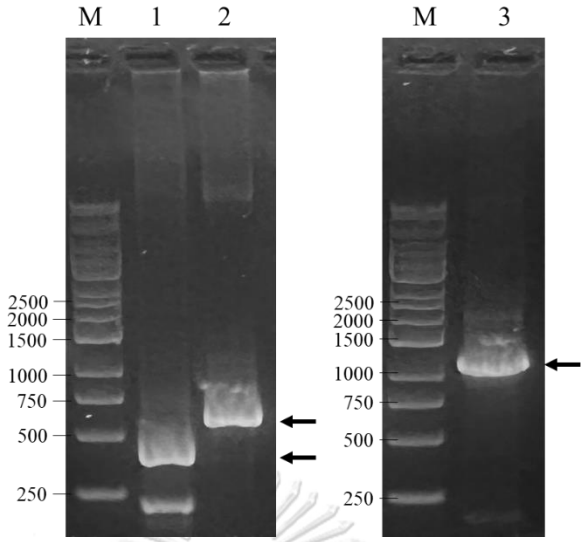

Figure 13. Amplification of DVD AT2C LC constructs. M: DNA ladder, 1: SP-VL1-Linker, 2: Linker-VL2-CL, 3: SP-VL1-Linker-VL2-CL. The arrow indicates the genes of interest.

The developed DVD AT2C HC and LC genes were confirmed by DNA sequencing and showed sequence similarity with the expected nucleotide sequences (Appendix G and H). The HC and LC fragments of bsAb were then cloned into pBY expression vector and transformed into *E. coli* cells strain DH10B. All obtained pBY plasmids that harbor the HC and LC genes of anti-PD-L1 Atezolizumab, anti-CTLA-4 2C8 and DVD AT2C bsAb were ultimately mobilized into *Agrobacterium tumefaciens* (GV3101) by electroporation. The plasmids were digested with *Xba*I and *Sac*I restriction enzymes for verification. As expected, results confirmed the presence of the pBY vector at roughly >13,000 bp and the HC and LC gene inserts (Figure 14A and B). Prior to agroinfiltration in plants, the Agrobacterium clones containing pBY-HC and pBY-LC were additionally screened by PCR, as shown in Figures 14C and D.

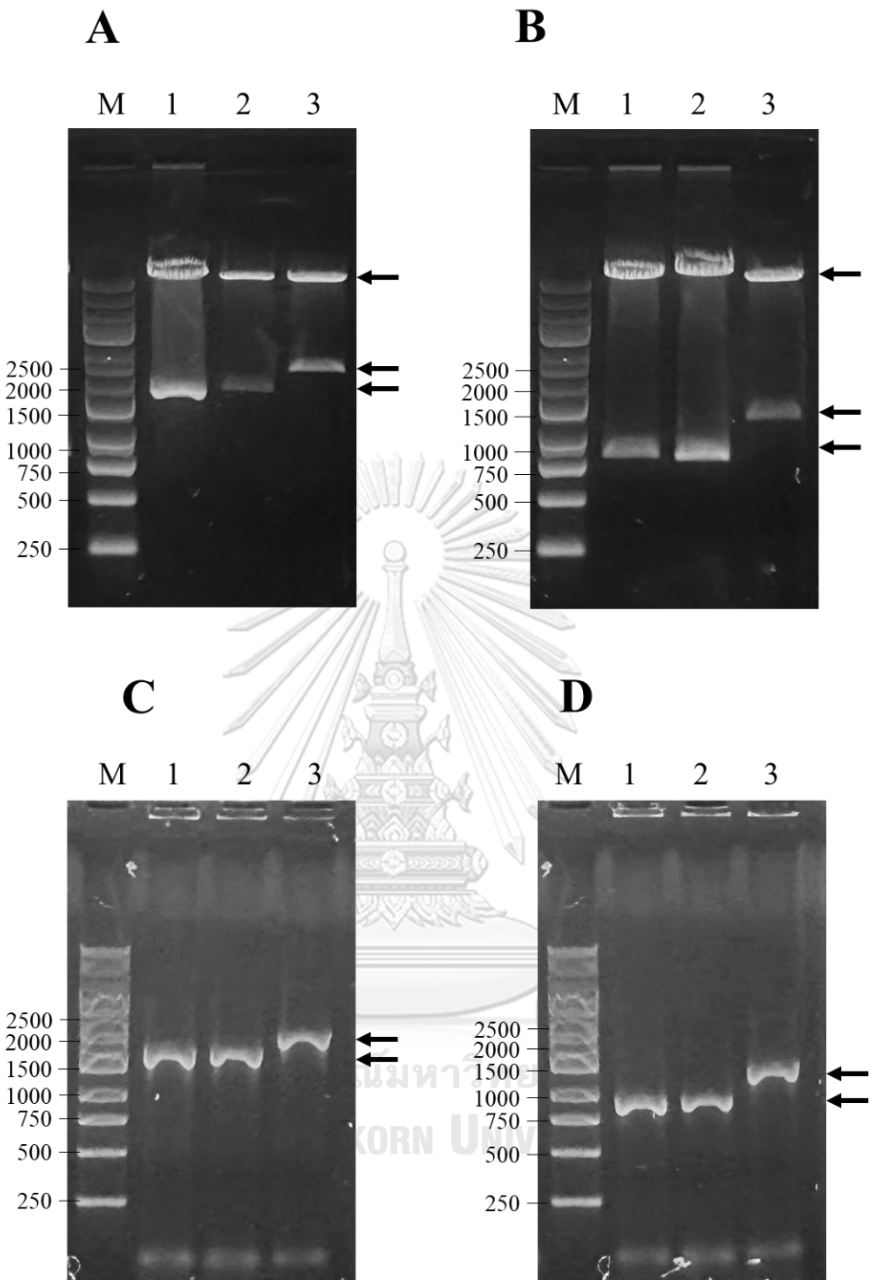

Figure 14. Enzyme cut and PCR analyses of pBY-HC and pBY-LC plasmids used in the study. Restriction enzyme digestion of pBY-HC vectors (A) and pBY-LC vectors (B). PCR amplification of A. tumefaciens clones containing pBY-HC constructs (C) and pBY-LC constructs (D). M: DNA ladder, 1: Atezolizumab HC/LC, 2: 2C8 HC/LC, 3: DVD AT2C HC/LC. The arrow indicates the vector and genes of interest.

4.3. Expression of recombinant monospecific and bispecific mAbs in *Nicotiana benthamiana*

The production of parent and dual-specific mAbs was carried out by the co-expression of HC with LC in *N. benthamiana* via agrobacterium-mediated infiltration. The geminiviral replicon system (pBY) was employed to express recombinant mAbs. The pBY-HC and pBY-LC expression cassettes were both controlled by the dual-enhancer CaMV 35S promoter, which is a a strong constitutive plant promoter intended for maximum transcription. The vector also contained the silencing suppressor p19 gene from tomato bushy stunt virus for improved protein expression (73). Furthermore, the genes of interest were placed between the long intergenic region and short intergenic region (LIR and SIR), respectively, in the vector to replace the genes for viral movement and coat proteins. The expression of the viral Rep protein (C1/C2 gene), which is connected to the expression cassette, is required for the amplification of geminiviral replicons (85). In this case, geminiviruses utilize a rolling-circle replication mechanism for DNA synthesis in which Rep protein facilitates the nicking and ligating processes (72). Figure 15 shows a schematic illustration of the T-DNA construct for the geminiviral expression vector used in the study. This T-DNA region represents the DNA that *Agrobacterium* will transfer to plant tissue.

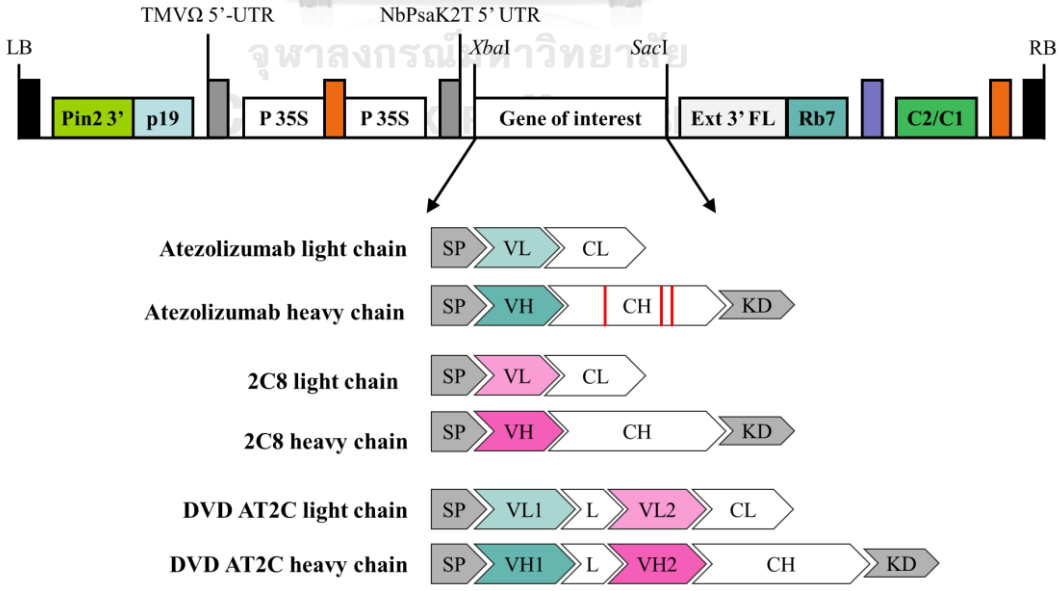

Figure 15. Schematic representation of pBY expression vector map of the antibodies used in this study. PinII 3′: terminator from potato proteinase inhibitor II gene, P19: P19 gene from TBSV, TMVΩ 5′-UTR: 5′ untranslated region of tobacco mosaic virus Ω, P35S: CaMV 35S promoter, long intergenic region of BeYDV genome (orange box), NbPsaK2T 5′UTR: 5′ UTR of Nicotiana photosystem I reaction center subunit psaK, Ext3′FL: 3′ full length of the tobacco extension gene, Rb7: tobacco RB7 promoter, short intergenic region of BeYDV genome (purple box), C2/C1: BeYDV ORFs C1 and C2 encoding for replication initiation protein (Rep) and RepA, LB and RBL left and right borders of the T-DNA region. The HC and LC of each antibody is individually inserted into the gene of interest site (white box with restriction enzymes).

The expression of mAbs was accomplished through syringe co-infiltration of *Agrobacterium* cultures containing pBY-HC and pBY-LC into *N. benthamiana* plants.

Expressed Atezolizumab, 2C8 and DVD AT2C bsAb caused necrosis in infiltrated leaves, as shown in Figure 16 and Appendix I.

Figure 16. Phenotype of infiltrated N. benthamiana leaves on day 4. Tobacco leaves were co-infiltrated with Agrobacterium containing pBY-HC and pBY-LC for Atezolizumab (1), 2C8 (2), and DVD AT2C (3) expression. Black circle indicates infection site. The leaves were photographed on 4 dpi.

To measure the antibody expression levels, transfected leaves were harvested and extracted on different days post-infiltration (2, 4, and 6 dpi). The yield of IgG in relation to the protein standard used was assessed using the crude extracts by ELISA. Based on the results, the highest antibody expression was observed within

4-6 days after agroinfiltration (Figure 17). Briefly, the Atezolizumab mAb was highly expressed on 6 dpi, with yields of up to 148.09 ± 43.9 µg/g fresh weight, whereas the 2C8 mAb was expressed on 4 dpi, with maximum yields estimated to be 39.65 ± 8.42 µg/g fresh weight. In addition, the expression level of DVD AT2C bsAb peaked at 4 dpi, reaching up to 81.63 ± 17.56 µg/g fresh weight. Our findings demonstrated the rapid transient production of antibodies in plants in less than a week when compared with other expression platforms (86, 87) and transgenic plants (88). The

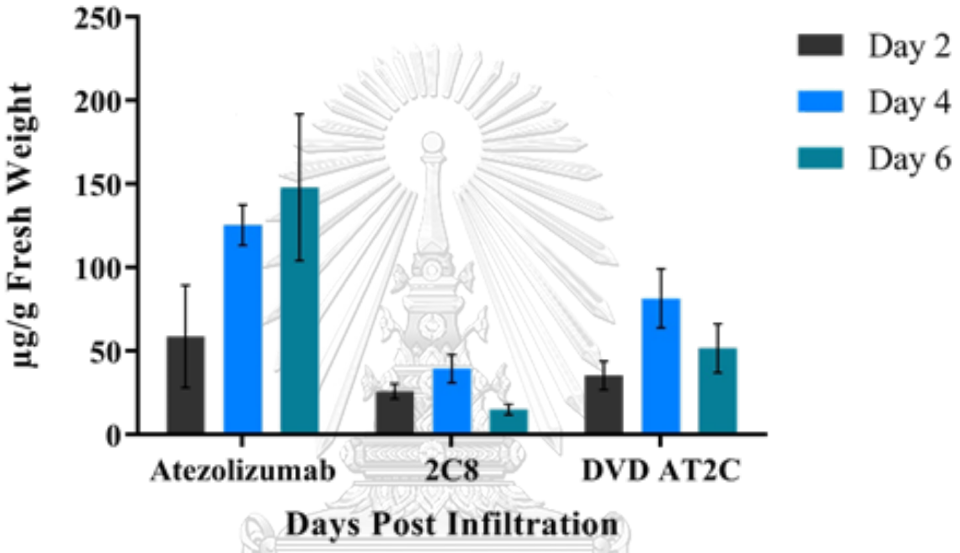

time course of expression on different dpi revealed the optimal harvest time for each antibody, which was later on considered in further experiments.

Figure 17. Transient expression of mAbs and bsAb in N. benthamiana plants. Expression levels of plant-produced antibodies at different days after agroinfiltration. The leaves were collected within 2, 4 and 6 dpi. Data are presented as mean ± SD from three replicates.

The presence of plant-produced mAbs in crude samples was also verified by immunoblotting technique with anti-human IgG gamma antibody. Infiltrated crude extracts of Atezolizumab, 2C8 and DVD AT2C showed protein bands at 150 kDa for mAbs and 250 kDa for bsAb under a non-reduced condition, while wildtype crude extract did not show any detectable band (Figure 18). Therefore, our results indicated that recombinant mAbs and bsAbs were produced rapidly and transiently in plants.

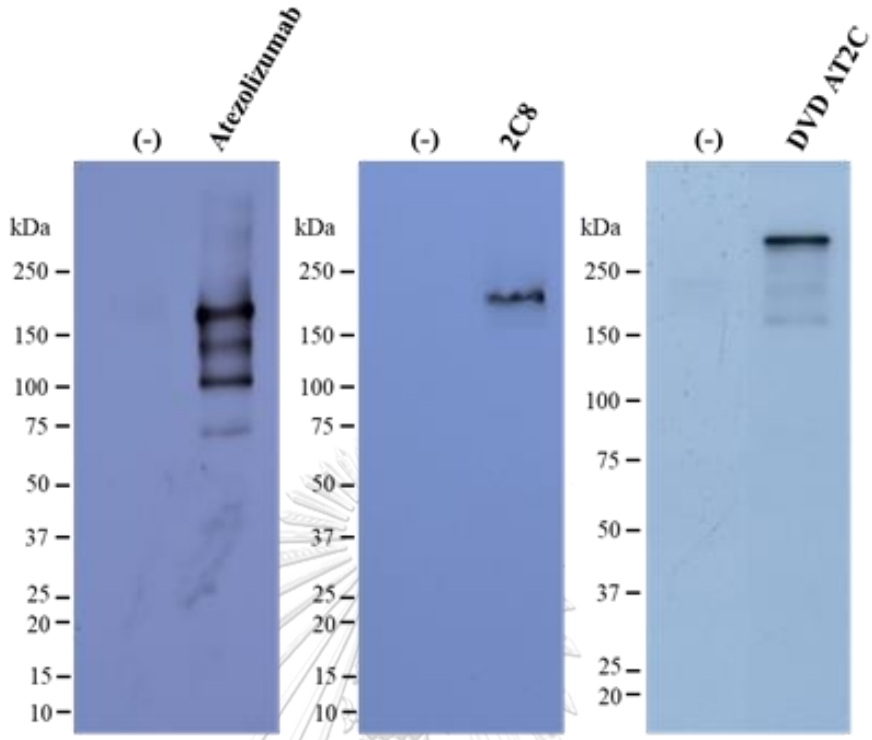

Figure 18. Expression of plant-produced antibodies from crude extracts. The samples were assayed by western blot and detected by anti-human IgG gamma chain antibody. (-) non-infiltrated wildtype extract.

4.4. Purification of plant-produced antibodies from *N. benthamiana*

The production of plant-made mAbs and bsAb was scaled up by *Agrobacterium*-mediated vacuum infiltration method. As evidenced by our previous studies (8, 9, 76, 89-91), this mode of transfection *in planta* has been used to generate several vaccine candidates and mAbs against viral infections and cancer, as well as for other biopharmaceutical applications. To this work, the plant-produced Atezolizumab, 2C8 and DVD AT2C were isolated and purified from plant crude supernatants by one-step protein A affinity chromatography. Protein A is a useful and economic chromatographic technique for purifying mAbs. It specifically binds to the Fc region of IgG with high affinity, allowing the separation of mAbs from crude proteins (92, 93). Protein A chromatography has since been widely used for the purification of various mAbs (94-96), though additional purification steps may be necessary to meet commercial quality standards.

The purity of plant-produced antibodies was evaluated by staining SDS-PAGE gel with InstantBlue® dye under reduced and non-reduced conditions. The preparation of mAbs and bsAB were estimated to be approximately >80% pure according to visual assessment of the SDS-stained gels (Figure 19). Purified antibody and antibody fragments of varying apparent molecular weights were observed in gels. Under non-reducing condition, both the plant-produced Atezolizumab and 2C8 mAbs were observed at roughly 150 kDa, as expected, whereas purified plant-produced DVD AT2C bsAb showed a major protein band at approximately 250 kDa, with trace levels of antibody fragments also observed (Figure 19A). Under reducing condition, protein bands of about 50 kDa and 25 kDa were identified, corresponding to the predicted heavy chain and light chain of plant-produced Atezolizumab and 2C8. Meanwhile, protein bands with molecular weights of 65 kDa and 37 kDa were found for heavy chain and light chain of purified plant-produced bsAb (Figure 19B).

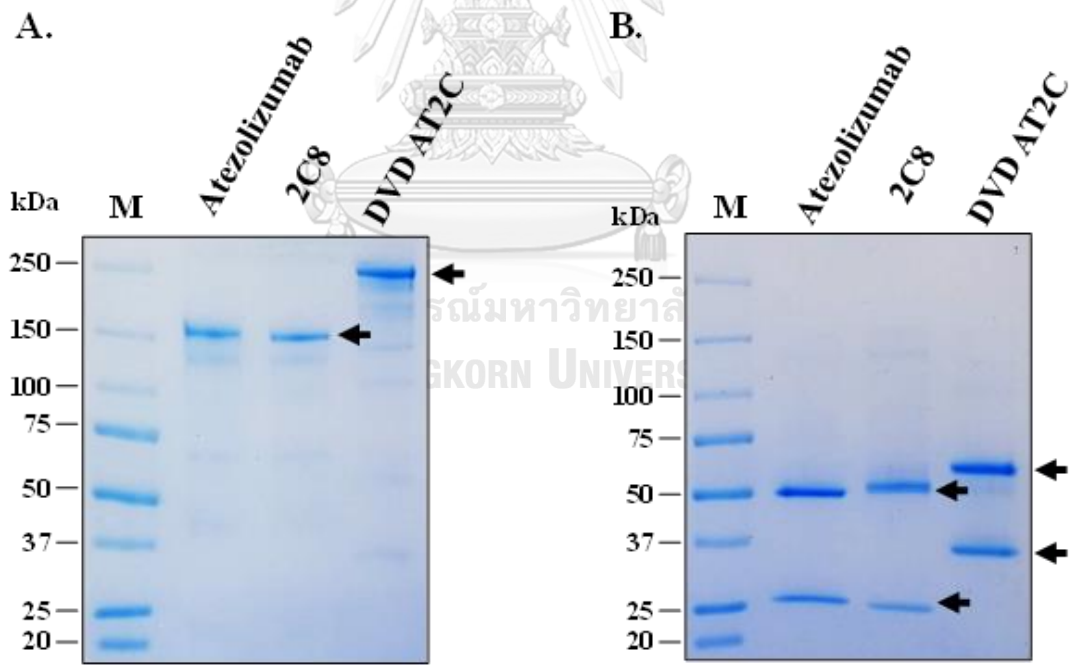

Figure 19. InstantBlue® staining of purified plant-produced antibodies. (A) Non-reducing condition and (B) reducing condition. M: Protein ladder. Arrow indicates major bands for full-antibody, heavy chain and light chain.

The assembly and folding of purified plant-produced antibodies were further confirmed by immunoblotting with specific anti-human gamma and anti-human kappa antibodies. A schematic representation of plant-derived mAbs and bsAb for production in tobacco plants is illustrated in Figure 20A. Western blot analyses under non-reduced conditions displayed distinct bands at 150 kDa and 250 kDa when probed with anti-heavy chain (Figure 20B) or anti-kappa chain (Figure 20C), respectively. These bands correspond to the expected sizes of plant-produced Atezolizumab, 2C8, and DVD AT2C bsAb. Additionally, under reduced conditions, anti-human gamma antibody bound to 50 kDa and 65 kDa heavy chain proteins (Figure 20C), while anti-human kappa antibody bound to 25 kDa and 37 kDa LC proteins (Figure 20D). Membranes probed with specific antibodies detected bands with higher molecular weights, which is consistent with plant-based bsAb under non-reduced or reduced conditions. The obtained protein bands also matched the band profile on previously stained gels. Thus, our results confirmed the proper folding and assembly of a full-length IgGs expressed in *N. benthamiana*.

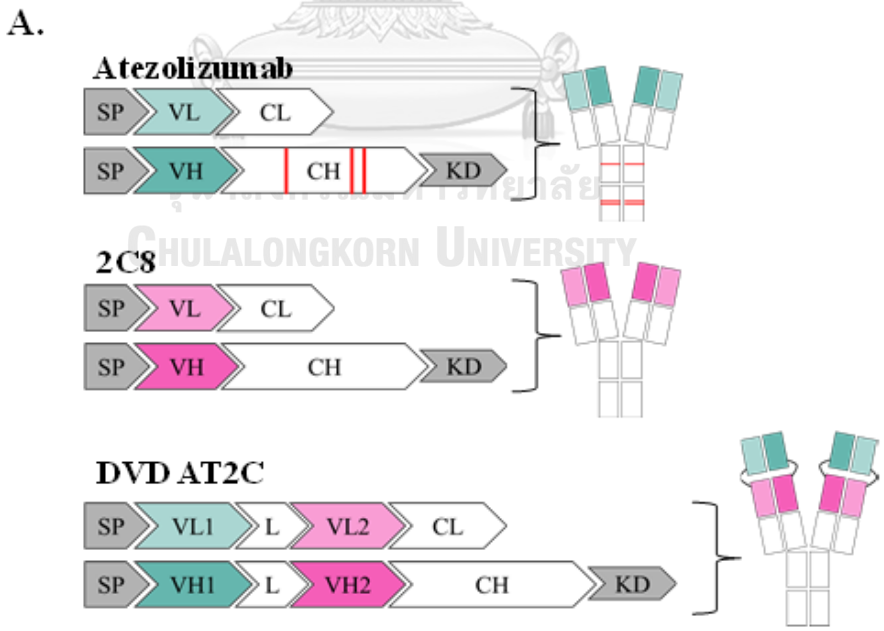

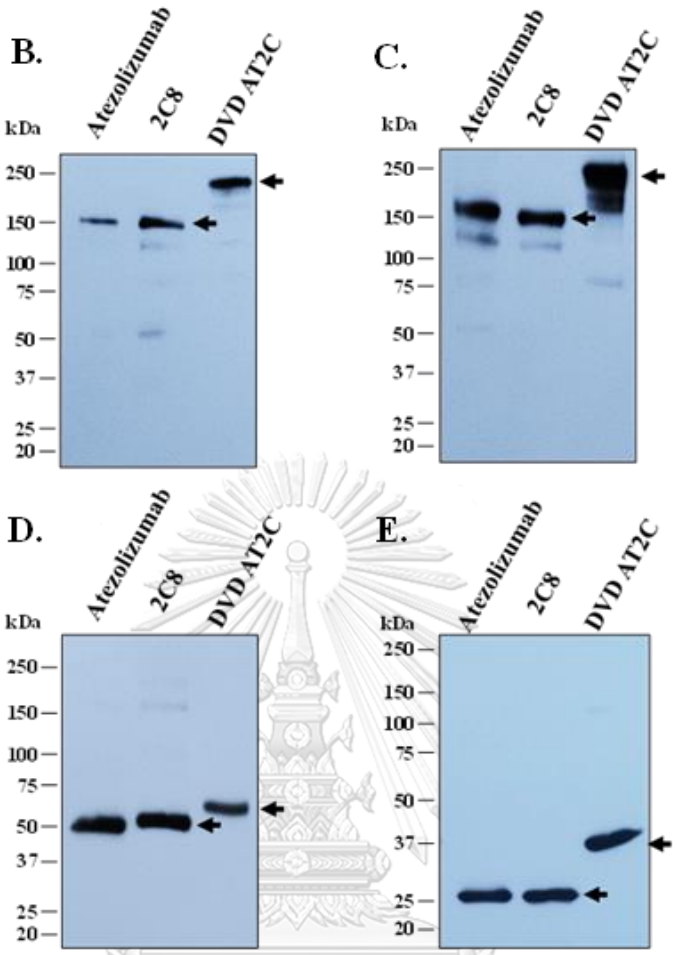

Figure 20. Western blotting of purified plant-produced antibodies. (A) Diagrammatic representation of Atezolizumab, 2C8, and DVD AT2C assembly (B and D) Anti-human gamma chain conjugated HRP detection and (C and E) anti-human kappa chain conjugated HRP detection in non-reducing (top) and reducing (bottom) conditions. M: protein ladder. Arrow indicates major bands for full-antibody, heavy chain and light chain.

4.5. Characterization of purified plant-produced antibodies

To analyze intact antibodies and their aggregates, size exclusion chromatograpy (SEC) was performed. SEC is a useful and validated tool for monitoring antibody aggregation, and it is widely used due to its speed and reproducibility (97, 98). Additionally, it has been used to separate biologics such bispecific and monospecific antibodies, antibody drug conjugates, and others. As

protein-based therapeutics have increasingly and recently gained attention, quality attributes are critically assessed, including quantitation of aggregates, such as multimers and dimers, of biologically active protein. Protein aggregates are thought to compromise safety and efficacy (99), so their presence warrants special concern.

In the present study, plant-produced Atezolizumab, 2C8 and DVD AT2C were examined by SEC separation. Figure 21 shows the chromatograms of SEC fractions containing the plant-produced mAbs and bsAb. Based on the results, the apparent elution positions of all antibodies indicate that they exist in their native states as monomers (major peak). Relatively small amounts of dimers and multimers were also eluted from the SEC column (minor peaks), suggesting that higher molecular weight species/aggregates were formed. There were no antibody fragments seen in any of the chromatograms. The peaks integrated using Empower 3 software are summarized in Table 11 and appendix J and K. From Table 11, the plant-produced Atezolizumab occurs as a monomer in about 90.01%, and as larger aggregates in 9.99%. Likewise, the plant-derived 2C8 assembled into a complete IgG, showing a monomeric peak of 94.13%, and with some aggregate forms of 5.87%. In the case of plant-produced bsAb, only a small amount of dimer (12.08%) was seen to elute before the monomer, and the major peak corresponding to DVD AT2C monomer was estimated to be of 87.92%. Aggregation of mAbs may have occurred during extraction and purification and caused by a number of variables, including pH, agitation, temperature etc. (100, 101). Since even a minute quantity of antibody aggregates can induce an immunogenic response, it is crucial to remove them for medicinal applications (102). Nonetheless, according to the results, it can be concluded that each individual plant-derived antibodies largely assembled and remained intact as monomeric species.

Table 11. Percentage (%) peak area

Antibody	% Area	
	Aggregate	Monomer
Plant-produced Atezolizumab	9.99	90.01
Plant-produced 2C8	5.87	94.13

Plant-produced DVD AT2C	12.08	87.92

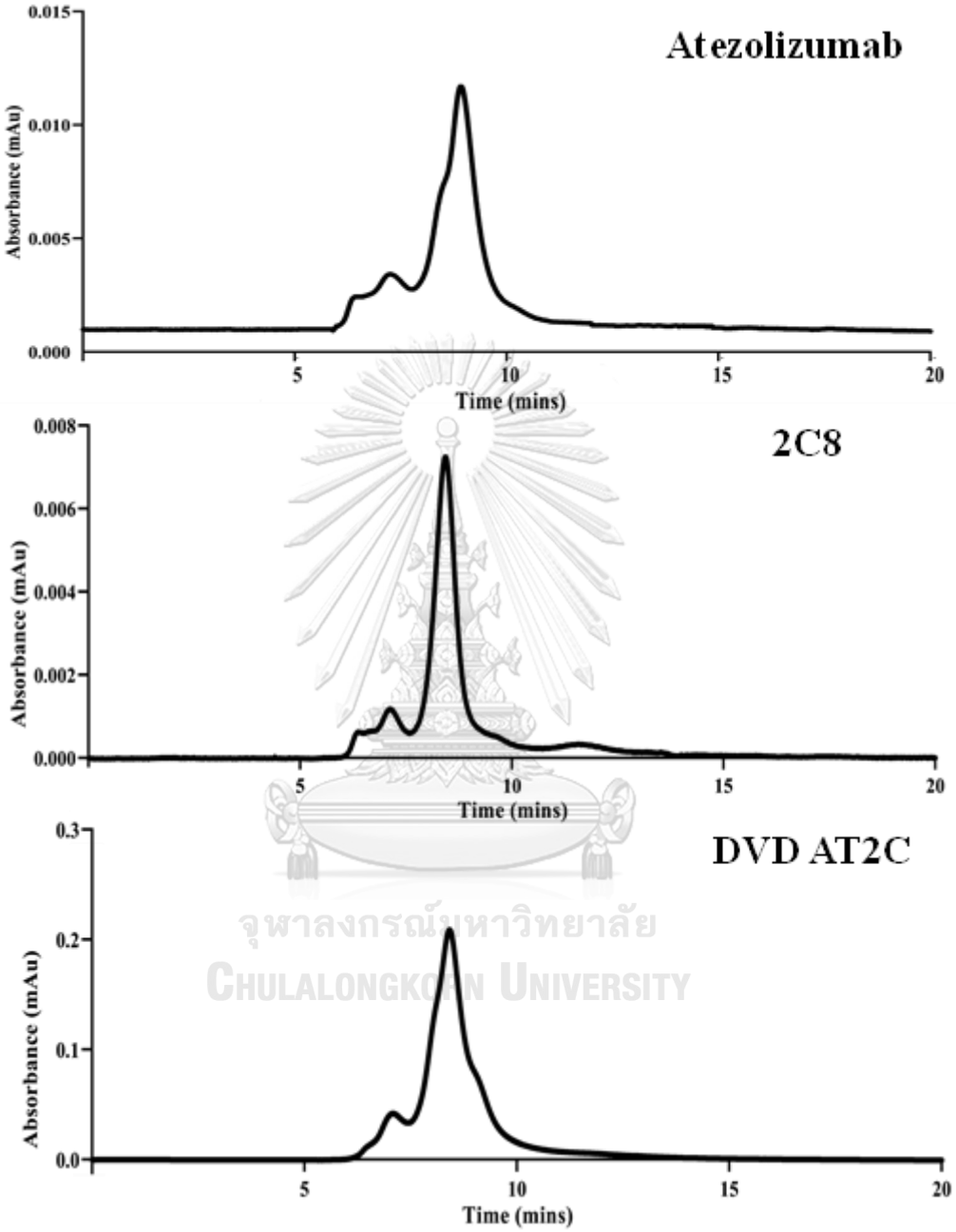

Figure 21. Size exclusion chromatography of plant-produced antibodies.

Isoelectric focusing (IEF) was used to further analyze the quality attributes of plant-produced antibodies based on their isoelectric point (p*I*). It is an electrophoretic method used for determining the p*I* of a protein, which is the pH value that indicates when the protein becomes neutral, or for separating protein

mixtures and other charged variants according to their p*I* (103). In the current study, the identity and charge distribution of mAbs were assessed using IEF on plant-produced Atezolizumab, 2C8, and DVD AT2C. The antibodies were electrophorized through a gel with an immobilized pH gradient and then migrated to the pH range that corresponded to their p*I* (104). The use of Coomassie Brilliant Blue R-250 staining on IEF is a qualitative strategy for monitoring charged isoforms (105).

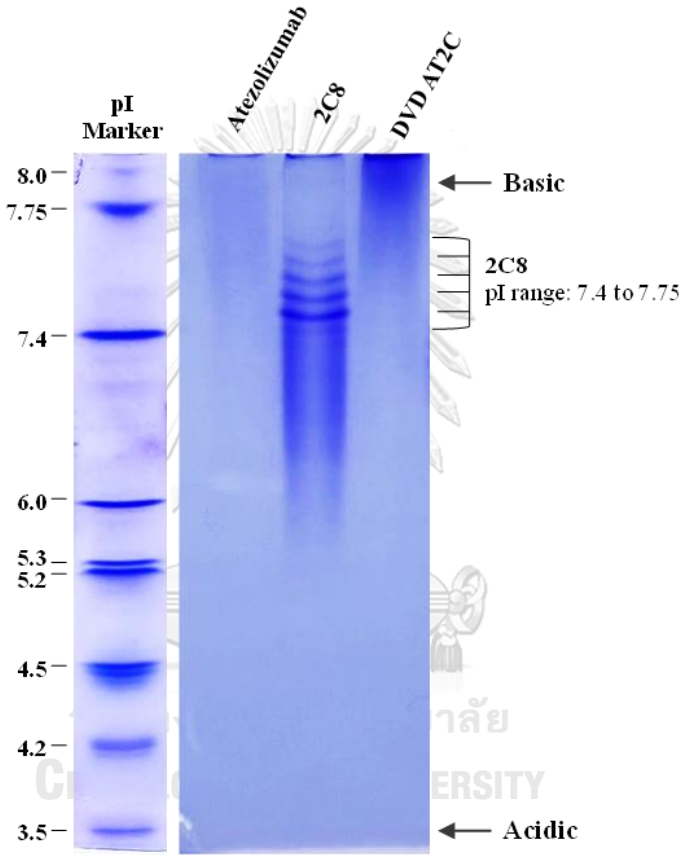

Figure 22. Isoelectric focusing of purified plant-produced antibodies.

Figure 22. depicts a Coomassie blue-stained IEF gel of plant-produced antibodies. Isoelectric positions of each antibody were compared to the positions of a p*I* marker, and their p*I*s were estimated. Multiple bands were visible in the gel for plant-produced 2C8, indicating a p*I* range of 7.4 to 7.75. The results are consistent with previous observations that affinity-purified mAbs typically exhibit a complex multiband pattern (106). Herein, the focusing of plant-produced IgGs revealed variable microheterogeneity as evidenced by different *pI* values from the mAb. This

microheterogeneity is often caused by differences in post-translational modifications (PTMs) such as protein S-thiolation, glycosylation and others (106, 107). On the contrary, smear bands were observed for both plant-produced 2C8 and DVD AT2C, implying a range of p*I* to be 7.75 to >8.0. These findings support prior reports indicating that mAbs have a fairly broad theoretical p*I* range, with some falling in the range of 8 to 9 (108, 109). In addition, the observed p*I* value for the plant-produced bsAb compares well with the range of theoretical p*I* values calculated using its HC, LC, and bsAb amino acid sequences (Table 12). Thus, the results presented here show that the plant-produced Atezolizumab, 2C8 and DVD AT2C have p*I* values ranging from 7.4 to >8.0, respectively.

Table 12. Predicted pI values for DVD AT2C proteins.

Protein	**Predicted pI (EMBOSS)**	**Predicted pI (ExPASy)**
DVD AT2C heavy chain	8.00	8.24
DVD AT2C light chain	7.53	7.52
DVD AT2C full	7.92	8.16

Differences in PTMs, such as glycosylation, was also investigated in the study. *N*-linked glycosylation differs in different cell compartments *in planta*. Among most organisms, the *N*-glycan processes in the ER appears conserved and limited to high-mannose type glycans, while the glycosylation in the Golgi is extremely diverse and produces hybrid and complex glycan structures (110, 111). Consequently, plant glycans typically carry complex glycan residues (β-1,2-xylose and α-1,3-fucose) that are not present from mammalian glycans (112-114), as a result, plant-based proteins differ from that of mammalian glycoproteins. This reserach aimed to analyze the *N*-glycan patterns of different mAbs and bsAb produced in plants.

In a more detail, purified plant-derived Atezolizumab, 2C8 and DVD AT2C were initially subjected to proteolytic digestion and the resulting glycopeptide EEQYNSTYR was examined by LC-ESI-MS. Findings revealed that the plant-produced Atezolizumab did not contain any *N*-linked glycans (Figure 23 and Appendix L). This is anticipated since the *N*-glycosylation site (N297) on the Fc region of the plant-

produced mAb was mutated, which inhibited the *N*-glycosylation processing (115, 116). The results confirm the successful removal of *N*-glycan structures and are consistent with the aglycosylated Tecentriq® data, as shown in Appendix L. Meanwhile, in an attempt to modify glycan processing in plants, an ER retention motif (SEKDEL) was incorporated into the C-terminus of both plant-produced 2C8 and DVD AT2C. The plant-derived 2C8 carried mainly oligomannose type *N*-glycans (Man5-9GlcNAc2) (Figure 23 and Appendix M) as predicted for ER-retained proteins. The results agree with previous studies in which the use of SEKDEL could restrict glycosylation to oligomannosidic *N*-glycans (82, 117-119). However, complex *N*-glycans bearing β-1,2-xylose and α-1,3-fucose (e.g., GnGnXF) and a small number of oligosaccharides carrying xylose or fucose were identified alongside high-mannose-type *N*-glycans on plant-produced DVD AT2C (Figure 23 and Appendix M). This contradicts earlier findings that glycans of SEKDEL-tagged proteins were mostly of oligomannose type. Even so, as evidenced by previous research, targeted and strict retention in the ER via SEKDEL peptide may not be sufficient (120) or alternatively retrieval into the ER could occur from distal Golgi stacks (121, 122). In addition, the presence of plant glycans had no effect on the binding affinity of plant-produced antibodies to their targets (9, 84).

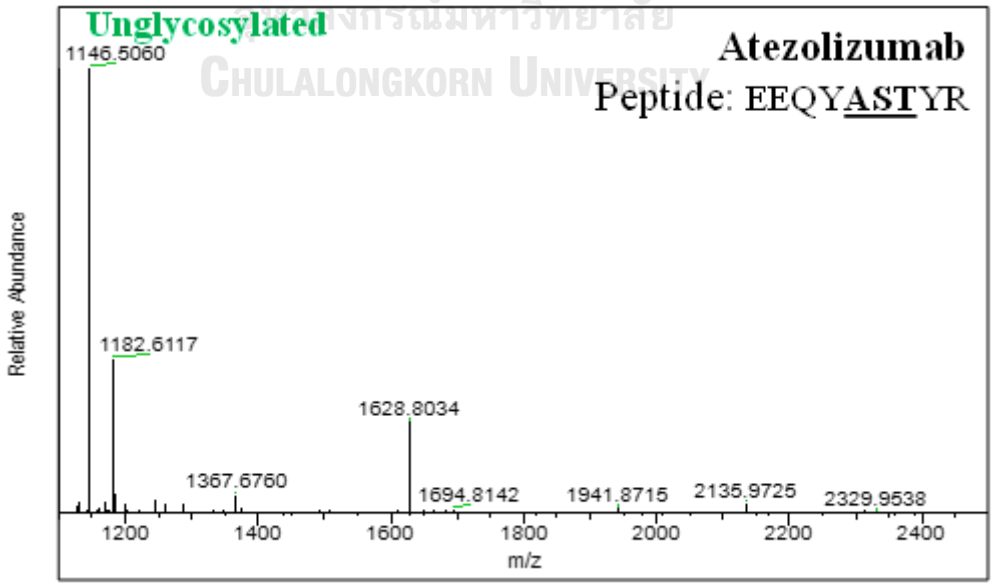

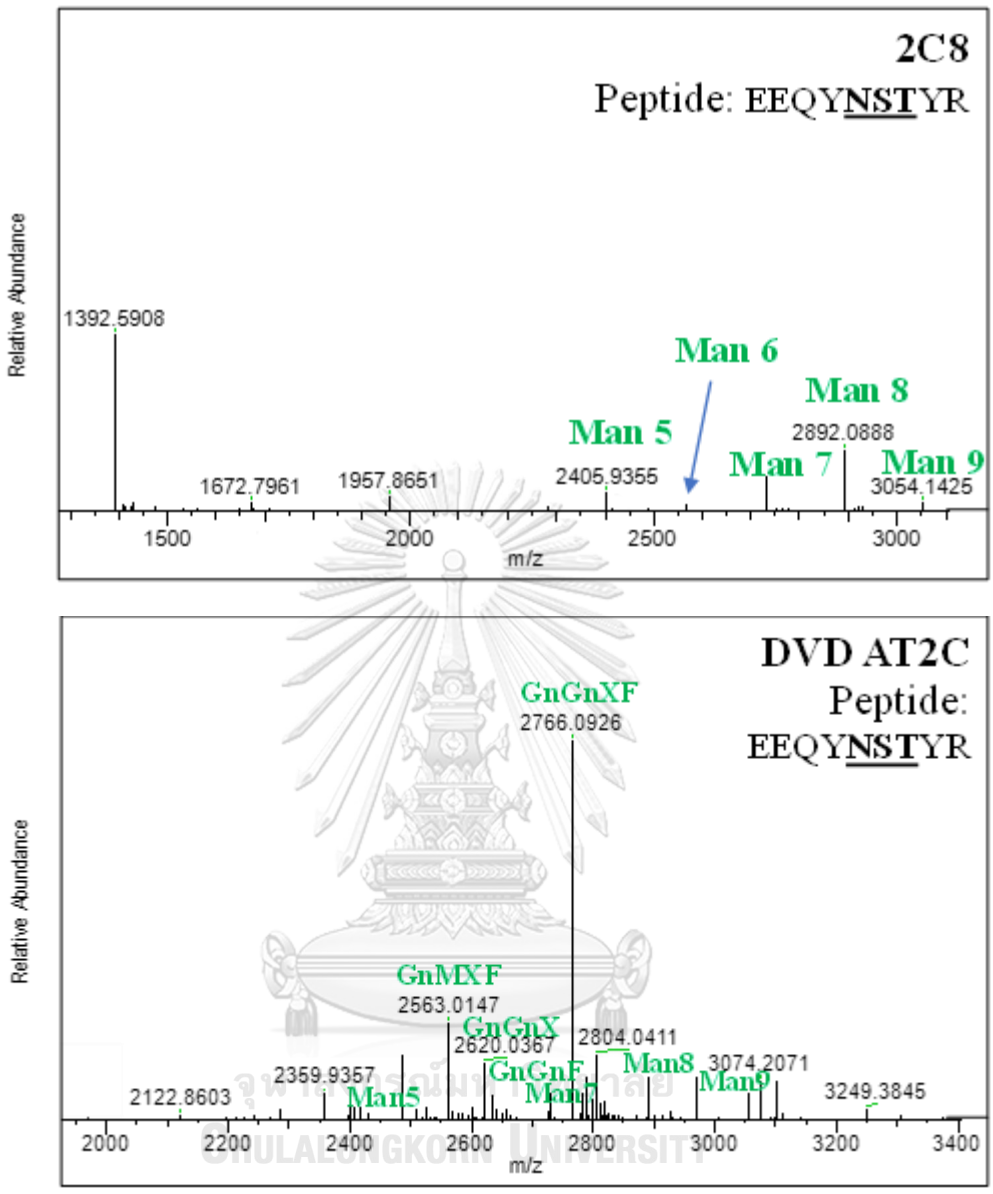

Figure 23. The N-glycosylation profile of plant-produced glycopeptide EEQYNSTYR (glycosylation site is underlined) from the Fc domain is shown, and the major glycosylated peaks are described.

It is important to note that the plant-produced bsAb has a functional Fc region and hence may exhibit binding for Fc gamma receptors (FγRs) typical of IgG1 (123). On the other hand, glycans attached to the Fc fragment are known to influence antibody binding to Fc receptors and Fc-dependent functions (124). Given the presence of plant mannosidic and complex *N*-glycans in the Fc region of plant-based DVD AT2C, the interaction of bsAb with human FcγRs may be affected. As

previously reported in the literature (125), plant glycan structures affect binding affinity by causing steric constraints in the FcγR binding site, thereby limiting or abrogating receptor engagement. This phenomenon opens up possibilities for modulating effector functions, which could be beneficial for bsAb-based immunotherapy.

4.6. *In vitro* binding activity of plant-produced antibodies

The plant-produced DVD AT2C was tested for its binding efficacy to its own specific targets using functional ELISA on recombinant purified PD-L1 and CTLA-4 proteins. Accordingly, serial dilutions of plant-produced DVD AT2C were added to the coated microtiter plates, and the captured bsAb was detected using anti-human kappa chain. Both the plant-produced Atezolizumab and 2C8 were used as experimental positive controls in parallel assays. By contrast, plant-produced Nivolumab, which confers binding specificity to PD-1 (8), was used as a possible negative control alongside the commercial human IgG1 isotype.

The results demonstrated that plant-derived DVD AT2C and plant-derived Atezolizumab could specifically bind to both human (Figure 24A) and mouse (Figure 24B) PD-L1 proteins. Plant-derived 2C8, on the other hand, did not exhibit any specific binding to both human and mouse PD-L1 targets, as expected. Further, plant-produced DVD AT2C and 2C8 bound with high specificity to both human (Figure 24C) and mouse (Figure 24D) CTLA-4 purified proteins, whereas only negligible binding was observed with plant-produced Atezolizumab. Neither plant-based Nivolumab nor human IgG1 isotype bound to any of the coated proteins, as predicted. Interestingly, the plant-produced bsAb had a higher affinity for the PD-L1 target than CTLA-4, which could be attributed to the imposition of certain binding constraints on the inner anti-CTLA-4 variable domain of the bsAb (70). Altogether, the DVD AT2C bsAb produced in *N. benthamiana* was confirmed to be functional as it can effectively bind to human PD-L1 and CTLA-4 proteins and cross-react with mouse recombinant proteins.

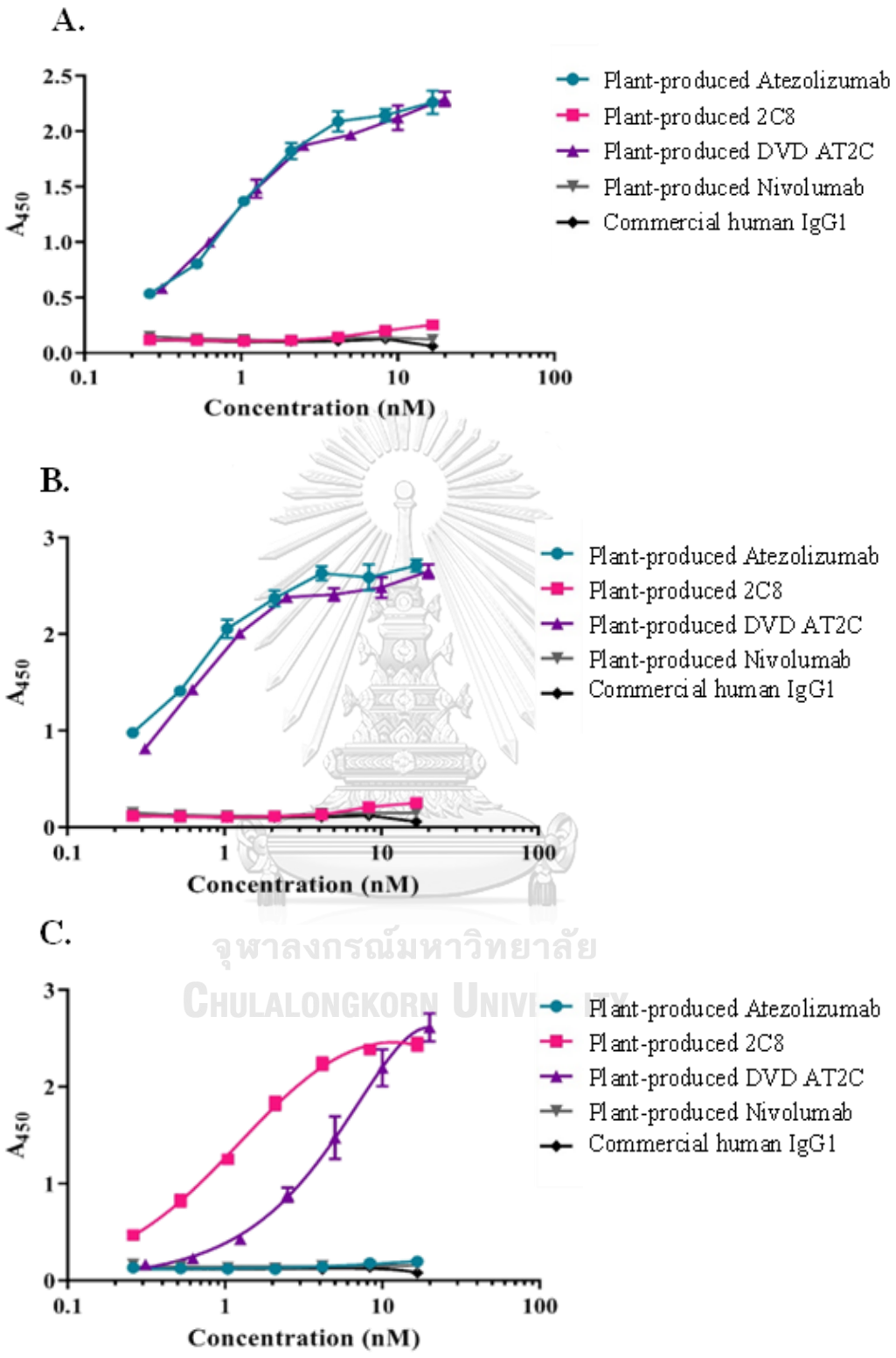

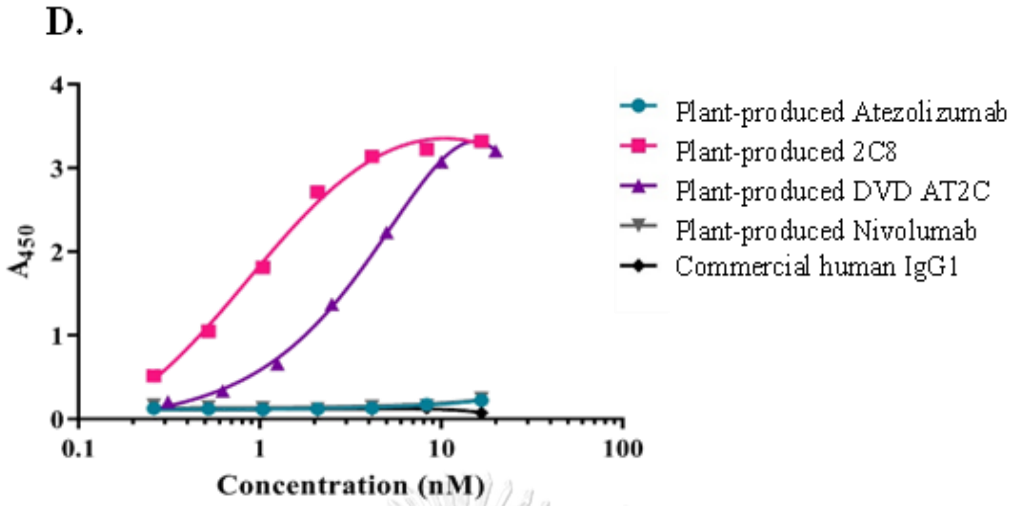

Figure 24. The binding activity of plant-produced antibodies. (A) Schematic diagram of antigen binding ELISA. Coated human PD-L1 (B) or mouse PD-L1 (C) or human CTLA-4 (D) or mouse CTLA-4 (E) were incubated with 0-20 nM of plant-Atezolizumab (blue), plant-2C8 (pink) and plant-DVD AT2C (purple), probed with anti-human kappa chain conjugated HRP and TMB substrate were used.

4.7. *In vivo* antitumor activity of plant-produced antibodies

The tumor growth inhibitory effects of plant-produced DVD AT2C on humanized mouse model were investigated to determine whether the plant-made bsAb elicits antitumor activity and whether these responses are superior to parent mAbs. To this aim, PD-L1 positive CT26 tumor cells were subcutaneously implanted in BALB/c-hPD-1/hPD-L1/hCTLA-4 mice, which were then treated with plant-produced DVD AT2C or plant-produced Atezolizumab and 2C8, used as experimental controls. For comparison with commercially available reference drugs, mammalian cell-produced Atezolizumab (Tecentriq®) and Ipilimumab (Yervoy®) were included as positive controls. Mice were given 5 mg/kg of plant-derived DVD AT2C (measured as conventional IgG equivalent) by intraperitoneal injection on days 0, 3, 6, 9, 12 and 15, while control groups received 3 mg/kg. On day 21, the plant-produced DVD AT2C (TGI_{TV}=36.22%) significantly regressed the tumor volume (TGI_{TV}) in mice relative to PBS, used as negative control (**p<0.01) (Figure 25 and Appendix N). Moreover, all of the control groups, including plant-produced Atezolizumab (TGI_{TV} = 41.90%,

p<0.001), Tecentriq® (TGI_{TV} = 24.59%, *p<0.05), plant-produced 2C8 (TGI_{TV} = 96.58%, ***p<0.001) and Yervoy® (TGI_{TV} = 98.83%, ***p<0.001) significantly reduced tumor growth when compared to the vehicle. Likewise, both the plant-produced Atezolizumab and 2C8 demonstrated comparable tumor volume reduction to that observed with Tecentriq® and Yervoy® drugs (p>0.05). Interestingly, tumor growth inhibition established by plant-produced DVD AT2C differs significantly from plant-produced 2C8 (p<0.001), but not from plant-produced Atezolizumab (p>0.05). Data of tumor volume changes of mice in different groups and tumor volume raw data are provided in Appendix O and P. Statistical analysis of tumor volume inhibitory rate and *P* value of mice in different groups are shown in Appendix Q, respectively.

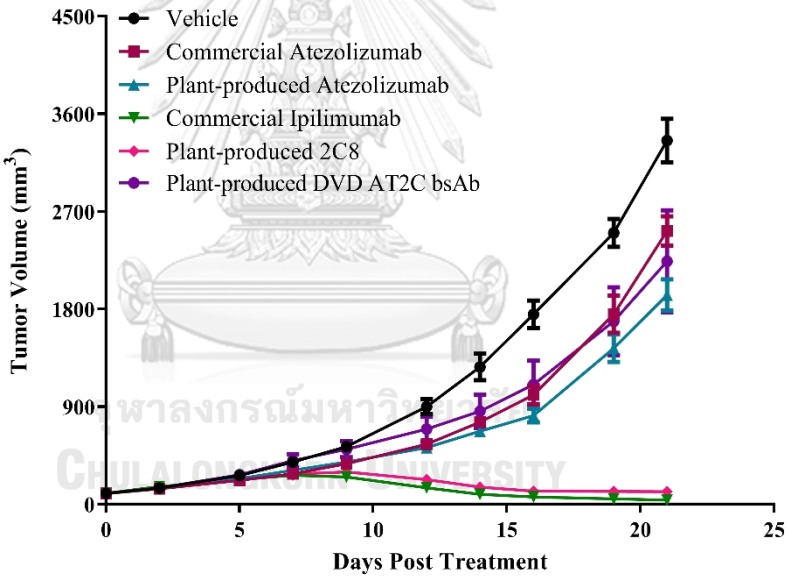

Figure 25. Tumor volume changes in different groups. Data are presented as mean ±SD.

At study endpoint, all mice were terminated, and tumors were collected and weighed (TW). Data was used as a reference for the evaluation of antitumor effect. As shown in Figure 26 and summarized in Table 13, tumor sizes in plant-produced DVD AT2C (TGI_{TW} = 34.62%) were significantly smaller than those in the PBS (*p<0.05). In addition, plant-produced Atezolizumab (TGI_{TW}= 12.29%, *p<0.05), plant-produced

2C8 (TGI_{TW} = 96.93%, ***p<0.001) and Yervoy® (TGI_{TW} = 99.20%, ***p<0.001) also significantly repressed tumor weights. Plant-produced monospecific mAbs and their mammalian cell-produced mAb counterparts both inhibited tumor growth to a similar extent based on tumor weight (p>0.05). In comparison with the plant-produced DVD AT2C, the tumor weight in Atezolizumab-treated group showed no significant difference (p>0.05), whereas the tumor weight in 2C8-treated group had significant difference (***p<0.001). The tumor weight raw data were shown in Appendix R. Photos of tumors and terminal mice are attached in Appendix S and T. Since no severe body weight loss (over 10%) was observed from continuous treatment administration during the study, it can be a parameter to show the good safety and tolerability of plant-produced antibodies (Figure 27 and Appendix U).

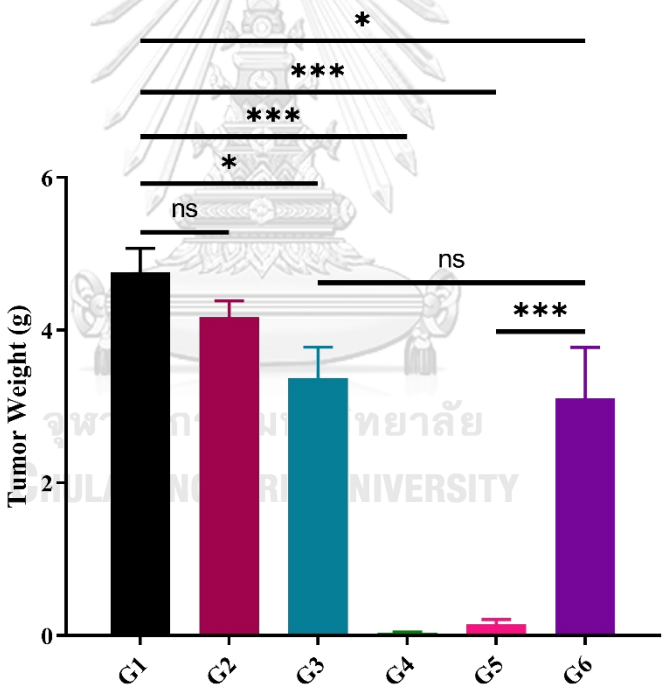

Figure 26. Tumor weight of mice in different groups. Data are presented as mean ±SD. Black box: PBS, Maroon box: Tecentriq®, Blue box: Plant-produced Atezolizuma, Green box: Yervoy®, Pink box: Plant-produced 2C8, Purple box: DVD AT2C

Table 13. Statistical analysis of tumor weight in different groups

Group	Tumor weight (g)	TGI_{TW}	*P* value (vs G1)	*P* value (vs G3)	*P* value (vs G4)	*P* value (vs G6)
G1	4.7548 ± 0.3183	-	-	-	-	-
G2	4.1704 ± 0.2159	12.29%	0.371	0.092	-	0.035*
G3	3.3746 ± 0.4031	29.03%	0.041*	-	-	0.581
G4	0.0380 ± 0.0096	99.20%	<0.001***	-	-	<0.001***
G5	0.1462 ± 0.0651	96.93%	<0.001***	-	0.814	<0.001***
G6	3.1087 ± 0.6653	34.62%	0.019*	-	-	-

Note: Data were shown as mean ± SD. Statistics performed using One-way ANOVA test, the post-hoc test was LSD, *: *P*<0.05, **: *P*<0.01, ***: *P*<0.001. G1: PBS, G2: Tecentriq®, G3: Plant-produced Atezolizumab, G4: Yervoy®, G5: Plant-produced 2C8, G6: Plant-produced DVD AT2C

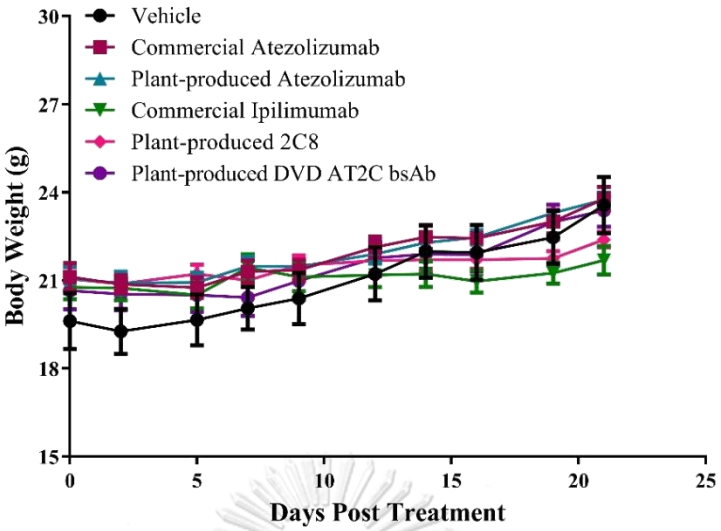

Figure 27. Body weight changes in different groups. Data were shown as mean ± SD.

Preclinical antitumor results present preliminary efficacy of the developed plant-produced bsAb. Here, plant-produced DVD AT2C was administered intraperitoneally to humanized BALB/c mice grafted with CT26-hPD-L1 tumors. The CT26 murine colon carcinoma has been classified as highly immunogenic (126) and has been used in a number of *in vivo* studies (127-129), including the current work. Since there is no immunomodulating (i.e., PD-L1/CTLA-4) bsAb drug available in the market and numerous reports in the literature (130, 131) indicate that commercial monospecific immune checkpoint inhibitors successfully induced tumor rejection *in vivo*, Tecentriq® and Yervoy®, were deemed useful for our research and were hence used as positive controls. Furthermore, plant-produced Atezolizumab and 2C8 were also analyzed concurrently as a basis for comparison with the bsAb. Tumor-bearing treated mice with plant-derived DVD AT2C showed significant regression of tumor volumes and weight. In contrast, vehicle treatment failed to control tumor growth. The antitumor effects of our plant-made bsAb were consistent with other mouse colon cancer models (CT26, Colon 26, and MC38) that demonstrated substantial sensitivity and durable responses to checkpoint blockades (127, 132). The ability of DVD AT2C bsAb to obstruct PD-L1 and/or CTLA-4 mechanisms marked the active immune response against cancer cells following T cell activation. Notably, plant-produced mAb treatments had similar effects on tumor size and weight reduction as

mammalian cell-produced mAbs, correlating with previous results reported in our study (74). As a result, plant-produced Atezolizumab and 2C8 can be used in place of their commercial counterparts for comparison purposes.

The anticancer responses from plant-produced DVD AT2C were comparable to those observed with plant-produced Atezolizumab, yet significantly lower than those observed with the plant-produced 2C8, which revealed more than 95% tumor reduction *in vivo*. This result is surprising since bsAb could not exert synergistic effects, contradicting our hypothesis and other efficacy data from dual immunomodulatory bispecifics (133, 134). Nonetheless, the antitumor effect of plant-produced DVD AT2C appears to be similar to that of plant-produced Atezolizumab, with no significant difference in tumor growth inhibition between the two groups. This is in line with the *in vitro* binding data, which showed that the plant-based bsAb had a higher affinity for PD-L1 than CTLA-4. It is important to note that the study lacks a dual-target bridging assay, which is necessary for determining the capability of bispecific molecules to bind to two targets simultaneously (135). This suggests that measuring the dual-target binding of DVD AT2C to both PD-L1 and CTLA-4 could help us better understand our findings and confirm the proposed mode of action. In addition, according to the data of this study, anti-CTLA-4 treatment is more sensitive in the established syngeneic CT26 tumor empirically, which agrees with clinical trials (34, 36, 136). Likewise, previous research has shown that higher doses of checkpoint inhibitor increased antitumor activity *in vivo* (130). Thus, future development of dose-escalation experiments for plant-produced DVD AT2C may be useful and will make a concerted effort to optimize tumor growth inhibitory response.

CHAPTER V CONCLUSION

The construction and development of dual-targeting bispecific antibody (bsAb) have been mainly explored in this study. Here, the variable domains of anti-PD-L1 Atezolizumab and anti-CTLA-4 2C8 were fused together to form a dual-variable domain immunoglobulin (DVD-Ig™) bsAb. The outcomes of the study confirmed that DVD Atezolizumab×2C8 (DVD AT2C) bsAb was successfully generated using overlap PCR approach, and co-expression of its heavy and light chain genes in *Nicotiana benthamiana* revealed rapid and high bsAb production on 4 days post-infiltration. To shed light on the authenticity of the plant-produced bsAb, protein properties and biological activity were compared to plant-produced parental monoclonal antibodies (mAbs), Atezolizumab and 2C8. Molecular weight determination by SDS-PAGE and western blotting indicated correct formation of bsAb with a protein band at higher molecular mass than the assembled plant-produced mAb. Size-exclusion chromatography was used to assess the presence of intact bsAb, which was found mostly as monomeric species. The isoelectric point of plant-produced DVD AT2C was determined to be greater than 8.0, and its expression in *N. benthamiana* wild type resulted in the generation of plant glycans. The plant-produced bsAb binds to both human and mouse PD-L1 and CTLA-4 proteins, but with a higher affinity for PD-L1. However, additional research is needed to confirm the simultaneous binding of bsAb to both antigens and support the envisioned mechanism of action. The plant-produced DVD AT2C also inhibited tumor growth in mice as a result of immune checkpoint inhibition, though the antitumor effects were less pronounced than the monospecific anti-CTLA-4 antibody. The preliminary safety of plant-produced bsAb showed no significant body weight loss throughout the study. This is the first report to our knowledge that shows the antitumor efficacy of plant-produced bsAb targeting immune checkpoints in an *in vivo* mouse colon carcinoma. This study provides evidence that complex antibody derivatives can be produced in plants. Future work will focus on improving next-generation multispecific antibody candidates for cancer immunotherapy.

REFERENCES

1. Jenkins RW, Barbie DA, Flaherty KT. Mechanisms of resistance to immune checkpoint inhibitors. British Journal of Cancer. 2018;118(1):9-16.
2. Schoenfeld AJ, Hellmann MD. Acquired Resistance to Immune Checkpoint Inhibitors. Cancer cell. 2020;37(4):443-55.
3. Larkin J, Hodi FS, Wolchok JD. Combined Nivolumab and Ipilimumab or Monotherapy in Untreated Melanoma. The New England journal of medicine. 2015;373(13):1270-1.
4. Postow MA, Chesney J, Pavlick AC, Robert C, Grossmann K, McDermott D, et al. Nivolumab and Ipilimumab versus Ipilimumab in Untreated Melanoma. 2015;372(21):2006-17.
5. Wu Y, Yi M, Zhu S, Wang H, Wu K. Recent advances and challenges of bispecific antibodies in solid tumors. Experimental Hematology & Oncology. 2021;10(1):56.
6. Gao J, Ward JF, Pettaway CA, Shi LZ, Subudhi SK, Vence LM, et al. VISTA is an inhibitory immune checkpoint that is increased after ipilimumab therapy in patients with prostate cancer. Nature Medicine. 2017;23(5):551-5.
7. Hosseini SS, Khalili S, Baradaran B, Bidar N, Shahbazi MA, Mosafer J, et al. Bispecific monoclonal antibodies for targeted immunotherapy of solid tumors: Recent advances and clinical trials. International journal of biological macromolecules. 2021;167:1030-47.
8. Rattanapisit K, Phakham T, Buranapraditkun S, Siriwattananon K, Boonkrai C, Pisitkun T, et al. Structural and In Vitro Functional Analyses of Novel Plant-Produced Anti-Human PD1 Antibody. Scientific Reports. 2019;9(1):15205.
9. Phakham T, Bulaon CJI, Khorattanakulchai N, Shanmugaraj B, Buranapraditkun S, Boonkrai C, et al. Functional Characterization of Pembrolizumab Produced in Nicotiana benthamiana Using a Rapid Transient Expression System. 2021;12.

10. Yiemchavee S, Wong-Arce A, Romero-Maldonado A, Shanmugaraj B, Monsivais-Urenda AE, Phoolcharoen W, et al. Expression and immunogenicity assessment of a plant-made immunogen targeting the cytotoxic T-lymphocyte associated antigen-4: a possible approach for cancer immunotherapy. Journal of biotechnology. 2021;329:29-37.

11. Tavare AN, Perry NJS, Benzonana LL, Takata M, Ma D. Cancer recurrence after surgery: Direct and indirect effects of anesthetic agents*. 2012;130(6):1237-50.

12. Alfarouk KO, Stock CM, Taylor S, Walsh M, Muddathir AK, Verduzco D, et al. Resistance to cancer chemotherapy: failure in drug response from ADME to P-gp. Cancer cell international. 2015;15:71.

13. Dilalla V, Chaput G, Williams T, Sultanem K. Radiotherapy side effects: integrating a survivorship clinical lens to better serve patients. Current oncology (Toronto, Ont). 2020;27(2):107-12.

14. Chan HK, Ismail S. Side effects of chemotherapy among cancer patients in a Malaysian General Hospital: experiences, perceptions and informational needs from clinical pharmacists. Asian Pacific journal of cancer prevention : APJCP. 2014;15(13):5305-9.

15. Farkona S, Diamandis EP, Blasutig IM. Cancer immunotherapy: the beginning of the end of cancer? BMC Medicine. 2016;14(1):73.

16. Drake CG, Jaffee E, Pardoll DM. Mechanisms of immune evasion by tumors. Advances in immunology. 2006;90:51-81.

17. Qin S, Xu L, Yi M, Yu S, Wu K, Luo SJMc. Novel immune checkpoint targets: moving beyond PD-1 and CTLA-4. 2019;18(1):1-14.

18. Agata Y, Kawasaki A, Nishimura H, Ishida Y, Tsubata T, Yagita H, et al. Expression of the PD-1 antigen on the surface of stimulated mouse T and B lymphocytes. International immunology. 1996;8(5):765-72.

19. Sharpe AH, Pauken KE. The diverse functions of the PD1 inhibitory pathway. Nature Reviews Immunology. 2018;18(3):153-67.

20. Francisco LM, Sage PT, Sharpe AH. The PD-1 pathway in tolerance and autoimmunity. Immunological reviews. 2010;236:219-42.

21. Pedoeem A, Azoulay-Alfaguter I, Strazza M, Silverman GJ, Mor A. Programmed death-1 pathway in cancer and autoimmunity. Clinical immunology (Orlando, Fla). 2014;153(1):145-52.

22. Zheng Y, Fang YC, Li J. PD-L1 expression levels on tumor cells affect their immunosuppressive activity. Oncology letters. 2019;18(5):5399-407.

23. Khan AR, Hams E, Floudas A, Sparwasser T, Weaver CT, Fallon PG. PD-L1hi B cells are critical regulators of humoral immunity. Nat Commun. 2015;6:5997.

24. Rudd CE, Taylor A, Schneider H. CD28 and CTLA-4 coreceptor expression and signal transduction. Immunological reviews. 2009;229(1):12-26.

25. Collins AV, Brodie DW, Gilbert RJ, Iaboni A, Manso-Sancho R, Walse B, et al. The interaction properties of costimulatory molecules revisited. Immunity. 2002;17(2):201-10.

26. Fallarino F, Fields PE, Gajewski TF. B7-1 engagement of cytotoxic T lymphocyte antigen 4 inhibits T cell activation in the absence of CD28. J Exp Med. 1998;188(1):205-10.

27. Krummel MF, Allison JP. CD28 and CTLA-4 have opposing effects on the response of T cells to stimulation. J Exp Med. 1995;182(2):459-65.

28. Seidel JA, Otsuka A, Kabashima K. Anti-PD-1 and Anti-CTLA-4 Therapies in Cancer: Mechanisms of Action, Efficacy, and Limitations. Frontiers in oncology. 2018;8:86.

29. Keir ME, Butte MJ, Freeman GJ, Sharpe AH. PD-1 and its ligands in tolerance and immunity. Annual review of immunology. 2008;26:677-704.

30. Barber DL, Wherry EJ, Masopust D, Zhu B, Allison JP, Sharpe AH, et al. Restoring function in exhausted CD8 T cells during chronic viral infection. Nature. 2006;439(7077):682-7.

31. Ahmadzadeh M, Johnson LA, Heemskerk B, Wunderlich JR, Dudley ME, White DE, et al. Tumor antigen–specific CD8 T cells infiltrating the tumor express high levels of PD-1 and are functionally impaired. Blood. 2009;114(8):1537-44.

32. Bennett F, Luxenberg D, Ling V, Wang IM, Marquette K, Lowe D, et al. Program death-1 engagement upon TCR activation has distinct effects on costimulation and cytokine-driven proliferation: attenuation of ICOS, IL-4, and IL-21, but not CD28, IL-7,

and IL-15 responses. Journal of immunology (Baltimore, Md : 1950). 2003;170(2):711-8.

33. Buchbinder EI, Desai A. CTLA-4 and PD-1 Pathways: Similarities, Differences, and Implications of Their Inhibition. American journal of clinical oncology. 2016;39(1):98-106.

34. Hodi FS, O'Day SJ, McDermott DF, Weber RW, Sosman JA, Haanen JB, et al. Improved survival with ipilimumab in patients with metastatic melanoma. The New England journal of medicine. 2010;363(8):711-23.

35. Schadendorf D, Hodi FS, Robert C, Weber JS, Margolin K, Hamid O, et al. Pooled Analysis of Long-Term Survival Data From Phase II and Phase III Trials of Ipilimumab in Unresectable or Metastatic Melanoma. Journal of clinical oncology : official journal of the American Society of Clinical Oncology. 2015;33(17):1889-94.

36. Farolfi A, Ridolfi L, Guidoboni M, Nicoletti SV, Piciucchi S, Valmorri L, et al. Ipilimumab in advanced melanoma: reports of long-lasting responses. Melanoma research. 2012;22(3):263-70.

37. Robert C, Thomas L, Bondarenko I, O'Day S, Weber J, Garbe C, et al. Ipilimumab plus dacarbazine for previously untreated metastatic melanoma. The New England journal of medicine. 2011;364(26):2517-26.

38. Topalian SL, Drake CG, Pardoll DM. Immune checkpoint blockade: a common denominator approach to cancer therapy. Cancer cell. 2015;27(4):450-61.

39. Robert C, Long GV, Brady B, Dutriaux C, Maio M, Mortier L, et al. Nivolumab in previously untreated melanoma without BRAF mutation. The New England journal of medicine. 2015;372(4):320-30.

40. Brahmer J, Reckamp KL, Baas P, Crinò L, Eberhardt WEE, Poddubskaya E, et al. Nivolumab versus Docetaxel in Advanced Squamous-Cell Non-Small-Cell Lung Cancer. The New England journal of medicine. 2015;373(2):123-35.

41. Borghaei H, Paz-Ares L, Horn L, Spigel DR, Steins M, Ready NE, et al. Nivolumab versus Docetaxel in Advanced Nonsquamous Non–Small-Cell Lung Cancer. 2015;373(17):1627-39.

42. Motzer RJ, Escudier B, McDermott DF, George S, Hammers HJ, Srinivas S, et al. Nivolumab versus Everolimus in Advanced Renal-Cell Carcinoma. 2015;373(19):1803-13.

43. Ferris RL, Blumenschein G, Fayette J, Guigay J, Colevas AD, Licitra L, et al. Nivolumab for Recurrent Squamous-Cell Carcinoma of the Head and Neck. 2016;375(19):1856-67.

44. Ansell SM, Lesokhin AM, Borrello I, Halwani A, Scott EC, Gutierrez M, et al. PD-1 Blockade with Nivolumab in Relapsed or Refractory Hodgkin's Lymphoma. 2014;372(4):311-9.

45. Younes A, Santoro A, Shipp M, Zinzani PL, Timmerman JM, Ansell S, et al. Nivolumab for classical Hodgkin's lymphoma after failure of both autologous stem-cell transplantation and brentuximab vedotin: a multicentre, multicohort, single-arm phase 2 trial. The Lancet Oncology. 2016;17(9):1283-94.

46. Herbst RS, Giaccone G, de Marinis F, Reinmuth N, Vergnenegre A, Barrios CH, et al. Atezolizumab for First-Line Treatment of PD-L1–Selected Patients with NSCLC. 2020;383(14):1328-39.

47. Kaplan A, Li MJ, Malani RJCOR. Treatments on the Horizon: Breast Cancer Patients with Central Nervous System Metastases. 2022:1-8.

48. Inman BA, Longo TA, Ramalingam S, Harrison MRJCCR. Atezolizumab: A PD-L1–Blocking Antibody for Bladder CancerAtezolizumab for Bladder Cancer. 2017;23(8):1886-90.

49. Mazières J, Park K, Lewanski C, Gadgeel S, Fehrenbacher L, Rittmeyer A, et al. 136PD_PR 3-year survival and duration of response in randomized phase II study of atezolizumab (atezo) vs docetaxel (doc) in 2L+ NSCLC (POPLAR). 2018;13(4):S79.

50. Hargadon KM, Johnson CE, Williams CJ. Immune checkpoint blockade therapy for cancer: An overview of FDA-approved immune checkpoint inhibitors. International immunopharmacology. 2018;62:29-39.

51. Pitt Jonathan M, Vétizou M, Daillère R, Roberti María P, Yamazaki T, Routy B, et al. Resistance Mechanisms to Immune-Checkpoint Blockade in Cancer: Tumor-Intrinsic and -Extrinsic Factors. Immunity. 2016;44(6):1255-69.

52. Ji R-R, Chasalow SD, Wang L, Hamid O, Schmidt H, Cogswell J, et al. An immune-active tumor microenvironment favors clinical response to ipilimumab. Cancer Immunology, Immunotherapy. 2012;61(7):1019-31.

53. Ayers M, Lunceford J, Nebozhyn M, Murphy E, Loboda A, Kaufman DR, et al. IFN-γ–related mRNA profile predicts clinical response to PD-1 blockade. The Journal of Clinical Investigation. 2017;127(8):2930-40.

54. Vinay DS, Ryan EP, Pawelec G, Talib WH, Stagg J, Elkord E, et al. Immune evasion in cancer: Mechanistic basis and therapeutic strategies. Seminars in cancer biology. 2015;35 Suppl:S185-s98.

55. Savoia P, Astrua C, Fava P. Ipilimumab (Anti-Ctla-4 Mab) in the treatment of metastatic melanoma: Effectiveness and toxicity management. Hum Vaccin Immunother. 2016;12(5):1092-101.

56. Kumar V, Chaudhary N, Garg M, Floudas CS, Soni P, Chandra ABJFip. Current diagnosis and management of immune related adverse events (irAEs) induced by immune checkpoint inhibitor therapy. 2017;8:49.

57. Puzanov I, Diab A, Abdallah K, Bingham CO, 3rd, Brogdon C, Dadu R, et al. Managing toxicities associated with immune checkpoint inhibitors: consensus recommendations from the Society for Immunotherapy of Cancer (SITC) Toxicity Management Working Group. J Immunother Cancer. 2017;5(1):95.

58. Schmid AS, Neri D. Advances in antibody engineering for rheumatic diseases. Nature reviews Rheumatology. 2019;15(4):197-207.

59. You G, Won J, Lee Y, Moon D, Park Y, Lee SH, et al. Bispecific Antibodies: A Smart Arsenal for Cancer Immunotherapies. Vaccines. 2021;9(7).

60. Fan G, Wang Z, Hao M, Li J. Bispecific antibodies and their applications. Journal of Hematology & Oncology. 2015;8(1):130.

61. Liu H, Saxena A, Sidhu SS, Wu D. Fc Engineering for Developing Therapeutic Bispecific Antibodies and Novel Scaffolds. Frontiers in immunology. 2017;8:38.

62. Zhang J, Yi J, Zhou P. Development of bispecific antibodies in China: overview and prospects. Antibody therapeutics. 2020;3(2):126-45.

63. Benjamin JE, Stein AS. The role of blinatumomab in patients with relapsed/refractory acute lymphoblastic leukemia. Therapeutic advances in hematology. 2016;7(3):142-56.

64. Kotanides H, Li Y, Malabunga M, Carpenito C, Eastman SW, Shen Y, et al. Bispecific Targeting of PD-1 and PD-L1 Enhances T-cell Activation and Antitumor Immunity. Cancer immunology research. 2020;8(10):1300-10.

65. Millward M, Frentzas S, Gan HK, Prawira A, Tran B, Coward J, et al. 1021O Safety and antitumor activity of AK104, a bispecific antibody targeting PD-1 and CTLA-4, in patients with mesothelioma which is relapsed or refractory to standard therapies. Annals of Oncology. 2020;31:S705-S6.

66. Richardson G, Kichenadasse G, Ganju V, Xu J, Van H, Kong P, et al. MA06.09 Preliminary Safety, Efficacy Results of KN046 (Bispecific Anti-PD-L1/CTLA4) in Subjects With Rare Thoracic Tumors. Journal of Thoracic Oncology. 2021;16(3):S154-S5.

67. Ma J, Mo Y, Tang M, Shen J, Qi Y, Zhao W, et al. Bispecific Antibodies: From Research to Clinical Application. Frontiers in immunology. 2021;12:626616.

68. Jin S, Sun Y, Liang X, Gu X, Ning J, Xu Y, et al. Emerging new therapeutic antibody derivatives for cancer treatment. Signal transduction and targeted therapy. 2022;7(1):39.

69. Digiammarino EL, Harlan JE, Walter KA, Ladror US, Edalji RP, Hutchins CW, et al. Ligand association rates to the inner-variable-domain of a dual-variable-domain immunoglobulin are significantly impacted by linker design. MAbs. 2011;3(5):487-94.

70. Jakob CG, Edalji R, Judge RA, DiGiammarino E, Li Y, Gu J, et al. Structure reveals function of the dual variable domain immunoglobulin (DVD-Ig™) molecule. MAbs. 2013;5(3):358-63.

71. Wu C, Ghayur T, Salfeld J. Generation and Characterization of a Dual Variable Domain Immunoglobulin (DVD-Ig™) Molecule. In: Kontermann R, Dübel S, editors. Antibody Engineering. Berlin, Heidelberg: Springer Berlin Heidelberg; 2010. p. 239-50.

72. Chen Q, He J, Phoolcharoen W, Mason HS. Geminiviral vectors based on bean yellow dwarf virus for production of vaccine antigens and monoclonal antibodies in plants. Human Vaccines. 2011;7(3):331-8.

73. Diamos AG, Mason HS. Modifying the Replication of Geminiviral Vectors Reduces Cell Death and Enhances Expression of Biopharmaceutical Proteins in Nicotiana benthamiana Leaves. Frontiers in plant science. 2019;9(1974).

74. Bulaon CJI, Sun H, Malla A, Phoolcharoen W. Therapeutic efficacy of plant-produced Nivolumab in transgenic C57BL/6-hPD-1 mouse implanted with MC38 colon cancer. Biotechnol Rep (Amst). 2023;38:e00794.

75. Wang C-I, Ngoh E, Yeo SP, inventors; Agency for Science, Technology and Research, assignee. Anti-CTLA-4 Antibodies. United States patent US9758583B2. 2017.

76. Shanmugaraj B, Rattanapisit K, Manopwisedjaroen S, Thitithanyanont A, Phoolcharoen W. Monoclonal Antibodies B38 and H4 Produced in Nicotiana benthamiana Neutralize SARS-CoV-2 in vitro. Front Plant Sci. 2020;11:589995.

77. Farràs M, Román R, Camps M, Miret J, Martínez Ó, Pujol X, et al. Heavy chain dimers stabilized by disulfide bonds are required to promote in vitro assembly of trastuzumab. BMC Molecular and Cell Biology. 2020;21(1):2.

78. Yamamoto K, Fujii R, Toyofuku Y, Saito T, Koseki H, Hsu VW, et al. The KDEL receptor mediates a retrieval mechanism that contributes to quality control at the endoplasmic reticulum. The EMBO journal. 2001;20(12):3082-91.

79. Feige MJ, Hendershot LM, Buchner J. How antibodies fold. Trends in Biochemical Sciences. 2010;35(4):189-98.

80. Weiner GJ. Building better monoclonal antibody-based therapeutics. Nature reviews Cancer. 2015;15(6):361-70.

81. Murshid A, Presley JF. ER-to-Golgi transport and cytoskeletal interactions in animal cells. Cellular and Molecular Life Sciences CMLS. 2004;61(2):133-45.

82. Petruccelli S, Otegui MS, Lareu F, Tran Dinh O, Fitchette AC, Circosta A, et al. A KDEL-tagged monoclonal antibody is efficiently retained in the endoplasmic reticulum in leaves, but is both partially secreted and sorted to protein storage vacuoles in seeds. Plant Biotechnol J. 2006;4(5):511-27.

83. Sharp JM, Doran PM. Characterization of monoclonal antibody fragments produced by plant cells. Biotechnol Bioeng. 2001;73(5):338-46.

84. Phetphoung T, Malla A, Rattanapisit K, Pisuttinusart N, Damrongyot N, Joyjamras K, et al. Expression of plant-produced anti-PD-L1 antibody with anoikis

sensitizing activity in human lung cancer cells via., suppression on epithelial-mesenchymal transition. PLoS One. 2022;17(11):e0274737.

85. Huang Z, Phoolcharoen W, Lai H, Piensook K, Cardineau G, Zeitlin L, et al. High-level rapid production of full-size monoclonal antibodies in plants by a single-vector DNA replicon system. Biotechnol Bioeng. 2010;106(1):9-17.

86. Akbarzadeh-Sharbaf S, Yakhchali B, Minuchehr Z, Shokrgozar MA, Zeinali S. Expression Enhancement in Trastuzumab Therapeutic Monoclonal Antibody Production using Genomic Amplification with Methotrexate. Avicenna J Med Biotechnol. 2013;5(2):87-95.

87. Dodev TS, Karagiannis P, Gilbert AE, Josephs DH, Bowen H, James LK, et al. A tool kit for rapid cloning and expression of recombinant antibodies. Sci Rep. 2014;4:5885.

88. Brodzik R, Glogowska M, Bandurska K, Okulicz M, Deka D, Ko K, et al. Plant-derived anti-Lewis Y mAb exhibits biological activities for efficient immunotherapy against human cancer cells. Proceedings of the National Academy of Sciences of the United States of America. 2006;103(23):8804-9.

89. Rattanapisit K, Shanmugaraj B, Manopwisedjaroen S, Purwono PB, Siriwattananon K, Khorattanakulchai N, et al. Rapid production of SARS-CoV-2 receptor binding domain (RBD) and spike specific monoclonal antibody CR3022 in Nicotiana benthamiana. Scientific Reports. 2020;10(1):17698.

90. Khorattanakulchai N, Manopwisedjaroen S, Rattanapisit K, Panapitakkul C, Kemthong T, Suttisan N, et al. Receptor binding domain proteins of SARS-CoV-2 variants produced in Nicotiana benthamiana elicit neutralizing antibodies against variants of concern. Journal of medical virology. 2022;n/a(n/a).

91. Bulaon CJI, Shanmugaraj B, Oo Y, Rattanapisit K, Chuanasa T, Chaotham C, et al. Rapid transient expression of functional human vascular endothelial growth factor in Nicotiana benthamiana and characterization of its biological activity. Biotechnology Reports. 2020;27:e00514.

92. Bauer K, Bayer PM, Deutsch E, Gabl F. Binding of enzyme--IgG complexes in human serum to Protein-A Sepharose CL-4B. Clinical chemistry. 1980;26(2):297-300.

93. Hober S, Nord K, Linhult M. Protein A chromatography for antibody purification. Journal of chromatography B, Analytical technologies in the biomedical and life sciences. 2007;848(1):40-7.

94. Rattanapisit K, Chao Z, Siriwattananon K, Huang Z, Phoolcharoen W. Plant-Produced Anti-Enterovirus 71 (EV71) Monoclonal Antibody Efficiently Protects Mice Against EV71 Infection. Plants (Basel). 2019;8(12):560.

95. Boonyayothin W, Kobtrakul K, Khositanon P, Vimolmangkang S, Phoolcharoen W. Development of a plant-produced recombinant monoclonal antibody against Δ-9-tetrahydrocannabinol (Δ9-THC) for immunoassay application. Biotechnology Reports. 2022;34:e00725.

96. Siegemund M, Richter F, Seifert O, Unverdorben F, Kontermann RE. Expression and purification of recombinant antibody formats and antibody fusion proteins. Methods in molecular biology (Clifton, NJ). 2014;1131:273-95.

97. Philo JS. Is any measurement method optimal for all aggregate sizes and types? The AAPS journal. 2006;8(3):E564-71.

98. Hong P, Koza S, Bouvier ES. Size-Exclusion Chromatography for the Analysis of Protein Biotherapeutics and their Aggregates. Journal of liquid chromatography & related technologies. 2012;35(20):2923-50.

99. Rosenberg AS. Effects of protein aggregates: an immunologic perspective. The AAPS journal. 2006;8(3):E501-7.

100. Fesinmeyer RM, Hogan S, Saluja A, Brych SR, Kras E, Narhi LO, et al. Effect of Ions on Agitation- and Temperature-Induced Aggregation Reactions of Antibodies. Pharmaceutical Research. 2009;26(4):903-13.

101. Amano M, Hasegawa J, Kobayashi N, Kishi N, Nakazawa T, Uchiyama S, et al. Specific racemization of heavy-chain cysteine-220 in the hinge region of immunoglobulin gamma 1 as a possible cause of degradation during storage. Analytical chemistry. 2011;83(10):3857-64.

102. Atis C. Separation of Monoclonal Antibodies by Analytical Size Exclusion Chromatography. In: Thomas B, editor. Antibody Engineering. Rijeka: IntechOpen; 2018. p. Ch. 7.

103. Kadakeri S, Arul MR, Bordett R, Duraisamy N, Naik H, Rudraiah S. 6 - Protein synthesis and characterization. In: Wei G, Kumbar SG, editors. Artificial Protein and Peptide Nanofibers: Woodhead Publishing; 2020. p. 121-61.

104. Friedman DB, Hoving S, Westermeier R. Chapter 30 Isoelectric Focusing and Two-Dimensional Gel Electrophoresis. In: Burgess RR, Deutscher MP, editors. Methods Enzymol. 463: Academic Press; 2009. p. 515-40.

105. Hunt G, Hotaling T, Chen AB. Validation of a capillary isoelectric focusing method for the recombinant monoclonal antibody C2B8. Journal of chromatography A. 1998;800(2):355-67.

106. Brasher MDR, Thorpe R. Isoelectric Focusing. In: Delves PJ, editor. Encyclopedia of Immunology (Second Edition). Oxford: Elsevier; 1998. p. 1510-4.

107. Bischoff R, Roecklin D, Roitsch C. Analysis of recombinant proteins by isoelectric focusing in immobilized pH gradients. Electrophoresis. 1992;13(4):214-9.

108. Boswell CA, Tesar DB, Mukhyala K, Theil FP, Fielder PJ, Khawli LA. Effects of charge on antibody tissue distribution and pharmacokinetics. Bioconjugate chemistry. 2010;21(12):2153-63.

109. Costello MA, Woititz C, Feo JD, Stremlo D, Wen L-FL, Palling DJ, et al. Characterization of Humanized Anti-Tac Monoclonal Antibody by Traditional Separation Techniques and Capillary Electrophoresis. Journal of Liquid Chromatography. 1992;15(6-7):1081-97.

110. Helenius A, Aebi M. Intracellular functions of N-linked glycans. Science. 2001;291(5512):2364-9.

111. Strasser R. Plant protein glycosylation. Glycobiology. 2016;26(9):926-39.

112. Strasser R, Stadlmann J, Schähs M, Stiegler G, Quendler H, Mach L, et al. Generation of glyco-engineered Nicotiana benthamiana for the production of monoclonal antibodies with a homogeneous human-like N-glycan structure. Plant Biotechnol J. 2008;6(4):392-402.

113. Fischer R, Emans N. Molecular farming of pharmaceutical proteins. Transgenic Res. 2000;9(4-5):279-99; discussion 7.

114. Gomord V, Chamberlain P, Jefferis R, Faye L. Biopharmaceutical production in plants: problems, solutions and opportunities. Trends in biotechnology. 2005;23(11):559-65.

115. Zhou Q, Jaworski J, Zhou Y, Valente D, Cotton J, Honey D, et al. Engineered Fc-glycosylation switch to eliminate antibody effector function. MAbs. 2020;12(1):1814583.

116. Borrok MJ, Jung ST, Kang TH, Monzingo AF, Georgiou G. Revisiting the role of glycosylation in the structure of human IgG Fc. ACS chemical biology. 2012;7(9):1596-602.

117. Conrad U, Fiedler U. Compartment-specific accumulation of recombinant immunoglobulins in plant cells: an essential tool for antibody production and immunomodulation of physiological functions and pathogen activity. Plant Mol Biol. 1998;38(1-2):101-9.

118. Ko K, Tekoah Y, Rudd PM, Harvey DJ, Dwek RA, Spitsin S, et al. Function and glycosylation of plant-derived antiviral monoclonal antibody. Proceedings of the National Academy of Sciences of the United States of America. 2003;100(13):8013-8.

119. Diego-Martin B, González B, Vazquez-Vilar M, Selma S, Mateos-Fernández R, Gianoglio S, et al. Pilot Production of SARS-CoV-2 Related Proteins in Plants: A Proof of Concept for Rapid Repurposing of Indoor Farms Into Biomanufacturing Facilities. 2020;11(2101).

120. Triguero A, Cabrera G, Cremata JA, Yuen CT, Wheeler J, Ramírez NI. Plant-derived mouse IgG monoclonal antibody fused to KDEL endoplasmic reticulum-retention signal is N-glycosylated homogeneously throughout the plant with mostly high-mannose-type N-glycans. Plant Biotechnol J. 2005;3(4):449-57.

121. Navazio L, Miuzzo M, Royle L, Baldan B, Varotto S, Merry AH, et al. Monitoring endoplasmic reticulum-to-Golgi traffic of a plant calreticulin by protein glycosylation analysis. Biochemistry. 2002;41(48):14141-9.

122. Pagny S, Cabanes-Macheteau M, Gillikin JW, Leborgne-Castel N, Lerouge P, Boston RS, et al. Protein recycling from the Golgi apparatus to the endoplasmic reticulum in plants and its minor contribution to calreticulin retention. The Plant cell. 2000;12(5):739-56.

123. Gombos RB, Gonzalez A, Manrique M, Chand D, Savitsky D, Morin B, et al. Toxicological and pharmacological assessment of AGEN1884, a novel human IgG1 anti-CTLA-4 antibody. PLOS ONE. 2018;13(4):e0191926.

124. Jefferis R. Recombinant antibody therapeutics: the impact of glycosylation on mechanisms of action. Trends in pharmacological sciences. 2009;30(7):356-62.

125. Stelter S, Paul MJ, Teh AY, Grandits M, Altmann F, Vanier J, et al. Engineering the interactions between a plant-produced HIV antibody and human Fc receptors. Plant Biotechnol J. 2020;18(2):402-14.

126. Lechner MG, Karimi SS, Barry-Holson K, Angell TE, Murphy KA, Church CH, et al. Immunogenicity of murine solid tumor models as a defining feature of in vivo behavior and response to immunotherapy. Journal of immunotherapy (Hagerstown, Md : 1997). 2013;36(9):477-89.

127. Sato Y, Fu Y, Liu H, Lee MY, Shaw MH. Tumor-immune profiling of CT-26 and Colon 26 syngeneic mouse models reveals mechanism of anti-PD-1 response. BMC Cancer. 2021;21(1):1222.

128. Jin Y, An X, Mao B, Sun R, Kumari R, Chen X, et al. Different syngeneic tumors show distinctive intrinsic tumor-immunity and mechanisms of actions (MOA) of anti-PD-1 treatment. Scientific Reports. 2022;12(1):3278.

129. Shi G, Yang Q, Zhang Y, Jiang Q, Lin Y, Yang S, et al. Modulating the Tumor Microenvironment via Oncolytic Viruses and CSF-1R Inhibition Synergistically Enhances Anti-PD-1 Immunotherapy. Molecular therapy : the journal of the American Society of Gene Therapy. 2019;27(1):244-60.

130. Li M, Zhao R, Chen J, Tian W, Xia C, Liu X, et al. Next generation of anti-PD-L1 Atezolizumab with enhanced anti-tumor efficacy in vivo. Scientific Reports. 2021;11(1):5774.

131. Graziani G, Lisi L, Tentori L, Navarra P. Monoclonal Antibodies to CTLA-4 with Focus on Ipilimumab. Experientia supplementum (2012). 2022;113:295-350.

132. Wei SC, Levine JH, Cogdill AP, Zhao Y, Anang NAS, Andrews MC, et al. Distinct Cellular Mechanisms Underlie Anti-CTLA-4 and Anti-PD-1 Checkpoint Blockade. Cell. 2017;170(6):1120-33.e17.

133. Selby M, Engelhardt J, Lu L-S, Quigley M, Wang C, Chen B, et al. Antitumor activity of concurrent blockade of immune checkpoint molecules CTLA-4 and PD-1 in preclinical models. Journal of Clinical Oncology. 2013;31(15_suppl):3061-.

134. Curran MA, Montalvo W, Yagita H, Allison JP. PD-1 and CTLA-4 combination blockade expands infiltrating T cells and reduces regulatory T and myeloid cells within B16 melanoma tumors. Proceedings of the National Academy of Sciences of the United States of America. 2010;107(9):4275-80.

135. Pei M, Wang Y, Tang L, Wu W, Wang C, Chen YL. Dual-target Bridging ELISA for Bispecific Antibodies. Bio-protocol. 2022;12(19).

136. Wolchok JD, Hoos A, O'Day S, Weber JS, Hamid O, Lebbé C, et al. Guidelines for the evaluation of immune therapy activity in solid tumors: immune-related response criteria. Clinical cancer research : an official journal of the American Association for Cancer Research. 2009;15(23):7412-20.

APPENDIX A

Sequence of Atezolizumab Heavy Chain

TCT AGA ACA ATG GGC TGG TCC TGC ATC ATC CTG TTC CTT GTT GCT ACT GCT ACC GGC GTT

S R T M G W S C I I L F L V A T A T G V

CAC TCT GAT GTT CAA CTT CTC GAG GAG GTC CAG CTC GTC GAG TCC GGC GGC GGC CTC GTC

H S D V Q L L E E V Q L V E S G G G L V

CAG CCC GGC GGC TCC CTC CGC CTC TCC TGC GCC GCC TCC GGC TTC ACC TTC TCC GAC TCC

Q P G G S L R L S C A A S G F T F S D S

TGG ATC CAC TGG GTC CGC CAG GCC CCC GGC AAG GGC CTT GAG TGG GTC GCC TGG ATC TCC

W I H W V R Q A P G K G L E W V A W I S

CCC TAC GGC GGC TCC ACC TAC TAC GCC GAC TCC GTC AAG GGC CGC TTC ACC ATC TCC GCC

P Y G G S T Y Y A D S V K G R F T I S A

GAC ACC TCC AAG AAC ACC GCC TAC CTC CAG ATG AAC TCC CTC CGC GCC GAG GAC ACC GCC

D T S K N T A Y L Q M N S L R A E D T A

GTC TAC TAC TGC GCC CGC CGC CAC TGG CCC GGC GGC TTC GAC TAC TGG GGC CAG GGC ACC

V Y Y C A R R H W P G G F D Y W G Q G T

CTC GTC ACC GTC TCC TCC GCT AGC ACC AAA GGT CCA TCG GTC TTT CCA CTG GCA CCT TCT

L V T V S S A S T K G P S V F P L A P S

TCC AAG AGT ACT TCT GGA GGC ACA GCT GCA CTG GGT TGT CTT GTC AAG GAC TAC TTT CCA

S K S T S G G T A A L G C L V K D Y F P

GAA CCT GTT ACG GTT TCG TGG AAC TCA GGT GCT CTG ACC AGT GGA GTG CAC ACC TTT CCA

E P V T V S W N S G A L T S G V H T F P

GCT GTT CTT CAG TCC TCA GGA TTG TAT TCT CTT AGC AGT GTT GTG ACT GTT CCA TCC TCA

A V L Q S S G L Y S L S S V V T V P S S

AGC TTG GGC ACT CAG ACC TAC ATC TGC AAT GTG AAT CAC AAA CCC AGC AAC ACC AAG GTT

S L G T Q T Y I C N V N H K P S N T K V

GAC AAG AAA GTT GAG CCC AAG TCT TGT GAC AAG ACT CAT ACG TGT CCA CCG TGC CCA GCA

D K K V E P K S C D K T H T C P P C P A

```
CCT GAA CTT CTT GGA GGA CCG TCA GTC TTC TTG TTT CCT CCA AAG CCT AAG GAT ACC TTG
 P   E   L   L   G   G   P   S   V   F   L   F   P   P   K   P   K   D   T   L
ATG ATC TCC AGG ACT CCT GAA GTC ACA TGT GTA GTT GTG GAT GTG AGC CAT GAA GAT CCT
 M   I   S   R   T   P   E   V   T   C   V   V   V   D   V   S   H   E   D   P
GAG GTG AAG TTC AAC TGG TAT GTG GAT GGT GTG GAA GTG CAC AAT GCC AAG ACA AAG CCG
 E   V   K   F   N   W   Y   V   D   G   V   E   V   H   N   A   K   T   K   P
AGA GAG GAA CAG TAC GCC AGC ACG TAC AGG GTT GTC TCA GTT CTC ACT GTT CTC CAT CAA
 R   E   E   Q   Y   A   S   T   Y   R   V   V   S   V   L   T   V   L   H   Q
GAT TGG TTG AAT GGC AAA GAG TAC AAG TGC AAG GTC TCC AAC AAA GCC CTC CCA GCC CCC
 D   W   L   N   G   K   E   Y   K   C   K   V   S   N   K   A   L   P   A   P
ATT GAG AAG ACC ATT TCC AAA GCG AAA GGG CAA CCC CGT GAA CCA CAA GTG TAC ACA CTT
 I   E   K   T   I   S   K   A   K   G   Q   P   R   E   P   Q   V   Y   T   L
CCT CCA TCT CGC GAG GAA ATG ACC AAG AAC CAG GTC AGC TTG ACT TGC CTG GTG AAA GGC
 P   P   S   R   E   E   M   T   K   N   Q   V   S   L   T   C   L   V   K   G
TTC TAT CCC TCT GAC ATA GCT GTA GAG TGG GAG AGC AAT GGG CAA CCG GAG AAC AAC TAC
 F   Y   P   S   D   I   A   V   E   W   E   S   N   G   Q   P   E   N   N   Y
AAG ACT ACA CCT CCC GTT CTC GAT TCT GAC GGC TCC TTC TTC CTC TAC AGC AAG CTC ACA
 K   T   T   P   P   V   L   D   S   D   G   S   F   F   L   Y   S   K   L   T
GTG GAC AAG AGC AGG TGG CAA CAA GGG AAT GTC TTC TCA TGC TCC GTG ATG CAT GAG GCT
 V   D   K   S   R   W   Q   Q   G   N   V   F   S   C   S   V   M   H   E   A
CTT CAC AAT CAC TAC ACA CAG AAG AGT CTC TCC TTG TCT CCG GGT AAA TCT GAG AAG GAT
 L   H   N   H   Y   T   Q   K   S   L   S   L   S   P   G   K   S   E   K   D
GAG CTT TGA GAG CTC
 E   L   -   E   L
```

APPENDIX B

Sequence of Atezolizumab Light Chain

TCT AGA ACA ATG GGC TGG TCC TGC ATC ATC CTG TTC CTT GTT GCT ACT GCT ACC GGC GTT

S R T M G W S C I I L F L V A T A T G V

CAC TCT GAT GTT CAA CTT CTC GAG GAC ATC CAG ATG ACC CAG TCC CCC TCC TCC CTC TCC

H S D V Q L L E D I Q M T Q S P S S L S

GCC TCC GTC GGC GAC CGC GTC ACC ATC ACC TGC CGC GCC TCC CAG GAC GTC TCC ACC GCC

A S V G D R V T I T C R A S Q D V S T A

GTC GCC TGG TAC CAG CAG AAG CCC GGC AAG GCC CCC AAG CTC CTC ATC TAC TCC GCC TCC

V A W Y Q Q K P G K A P K L L I Y S A S

TTC CTC TAC TCC GGC GTC CCC TCC CGC TTC TCC GGC TCC GGC TCC GGC ACC GAC TTC ACC

F L Y S G V P S R F S G S G S G T D F T

CTC ACC ATC TCC TCC CTC CAG CCC GAG GAC TTC GCC ACC TAC TAC TGC CAG CAG TAC CTC

L T I S S L Q P E D F A T Y Y C Q Q Y L

TAC CAC CCC GCC ACC TTC GGC CAG GGC ACC AAG GTC GAG ATC AAG CGC ACC GTC GCC GCC

Y H P A T F G Q G T K V E I K R T V A A

CCC TCC GTC TTC ATC TTC CCC CCC TCC GAC GAG CAG CTT AAG TCT GGA ACT GCT TCT GTT

P S V F I F P P S D E Q L K S G T A S V

GTG TGC CTT CTG AAC AAC TTC TAT CCT AGA GAA GCC AAA GTA CAG TGG AAG GTT GAC AAT

V C L L N N F Y P R E A K V Q W K V D N

GCT CTT CAA TCA GGT AAC TCC CAG GAG AGT GTC ACA GAG CAA GAT TCC AAG GAT TCC ACC

A L Q S G N S Q E S V T E Q D S K D S T

TAC AGC CTC TCA AGT ACC TTG ACG TTG AGC AAG GCA GAC TAT GAG AAA CAC AAA GTG TAC

Y S L S S T L T L S K A D Y E K H K V Y

GCA TGC GAA GTC ACT CAT CAG GGC CTG TCA TCA CCC GTG ACA AAG AGC TTC AAC AGG GGA

A C E V T H Q G L S S P V T K S F N R G

GAG TGT TGA GAG CTC

E C - E L

APPENDIX C

Sequence of 2C8 Heavy Chain

TCT AGA ACA ATG GGC TGG TCC TGC ATC ATC CTG TTC CTT GTT GCT ACT GCT ACC GGC GTT

S R T M G W S C I I L F L V A T A T G V

CAC TCT GAT GTT CAA CTT CTC GAG CAG GTT CAG CTT CAA CAA TCT GGT CCT GGT CTG GTG

H S D V Q L L E Q V Q L Q Q S G P G L V

AAG CCT TCT CAG ACT CTT TCT CTT ACC TGC GCT ATC AGC GGT GAC ACC GTT TCT TCT AAT

K P S Q T L S L T C A I S G D T V S S N

ACC GCT GCT TGG AAC TGG ATC AGG CAG TCT CCT TCA AGA GGT CTT GAG TGG CTT GGT AGG

T A A W N W I R Q S P S R G L E W L G R

ACC TAC TAC AGG TCC AAG TGG TAC TCT GAT TAC GGC CTG TCT GTG AAG TCC CGG ATG ACC

T Y Y R S K W Y S D Y G L S V K S R M T

ATT AAC GCT GAC ACC AGC AAG AAC CAG GTG AGC CTT CAT CTT AAC TCT GTG ACC CCT GAG

I N A D T S K N Q V S L H L N S V T P E

GAT ACC GCT GTT TAC TAC TGT GCT AGA GAA GGT TCT GGT GGC ACC CTT ATC TAT TGG GGT

D T A V Y Y C A R E G S G G T L I Y W G

CAG GGT ACC CTC GTC ACC GTC TCC TCC GCT AGC ACC AAA GGT CCA TCG GTC TTT CCA CTG

Q G T L V T V S S A S T K G P S V F P L

GCA CCT TCT TCC AAG AGT ACT TCT GGA GGC ACA GCT GCA CTG GGT TGT CTT GTC AAG GAC

A P S S K S T S G G T A A L G C L V K D

TAC TTT CCA GAA CCT GTT ACG GTT TCG TGG AAC TCA GGT GCT CTG ACC AGT GGA GTG CAC

Y F P E P V T V S W N S G A L T S G V H

ACC TTT CCA GCT GTT CTT CAG TCC TCA GGA TTG TAT TCT CTT AGC AGT GTT GTG ACT GTT

T F P A V L Q S S G L Y S L S S V V T V

CCA TCC TCA AGC TTG GGC ACT CAG ACC TAC ATC TGC AAT GTG AAT CAC AAA CCC AGC AAC

P S S S L G T Q T Y I C N V N H K P S N

ACC AAG GTT GAC AAG AAA GTT GAG CCC AAG TCT TGT GAC AAG ACT CAT ACG TGT CCA CCG

T K V D K K V E P K S C D K T H T C P P

TGC CCA GCA CCT GAA CTT CTT GGA GGA CCG TCA GTC TTC TTG TTT CCT CCA AAG CCT AAG

C P A P E L L G G P S V F L F P P K P K

GAT ACC TTG ATG ATC TCC AGG ACT CCT GAA GTC ACA TGT GTA GTT GTG GAT GTG AGC CAT

```
 D   T   L   M   I   S   R   T   P   E   V   T   C   V   V   V   D   V   S   H
GAA GAT CCT GAG GTG AAG TTC AAC TGG TAT GTG GAT GGT GTG GAA GTG CAC AAT GCC AAG
 E   D   P   E   V   K   F   N   W   Y   V   D   G   V   E   V   H   N   A   K
ACA AAG CCG AGA GAG GAA CAG TAC AAC AGC ACG TAC AGG GTT GTC TCA GTT CTC ACT GTT
 T   K   P   R   E   E   Q   Y   N   S   T   Y   R   V   V   S   V   L   T   V
CTC CAT CAA GAT TGG TTG AAT GGC AAA GAG TAC AAG TGC AAG GTC TCC AAC AAA GCC CTC
 L   H   Q   D   W   L   N   G   K   E   Y   K   C   K   V   S   N   K   A   L
CCA GCC CCC ATT GAG AAG ACC ATT TCC AAA GCG AAA GGG CAA CCC CGT GAA CCA CAA GTG
 P   A   P   I   E   K   T   I   S   K   A   K   G   Q   P   R   E   P   Q   V
TAC ACA CTT CCT CCA TCT CGC GAT GAA CTG ACC AAG AAC CAG GTC AGC TTG ACT TGC CTG
 Y   T   L   P   P   S   R   D   E   L   T   K   N   Q   V   S   L   T   C   L
GTG AAA GGC TTC TAT CCC TCT GAC ATA GCT GTA GAG TGG GAG AGC AAT GGG CAA CCG GAG
 V   K   G   F   Y   P   S   D   I   A   V   E   W   E   S   N   G   Q   P   E
AAC AAC TAC AAG ACT ACA CCT CCC GTT CTC GAT TCT GAC GGC TCC TTC TTC CTC TAC AGC
 N   N   Y   K   T   T   P   P   V   L   D   S   D   G   S   F   F   L   Y   S
AAG CTC ACA GTG GAC AAG AGC AGG TGG CAA CAA GGG AAT GTC TTC TCA TGC TCC GTG ATG
 K   L   T   V   D   K   S   R   W   Q   Q   G   N   V   F   S   C   S   V   M
CAT GAG GCT CTT CAC AAT CAC TAC ACA CAG AAG AGT CTC TCC TTG TCT CCG GGT AAA TCT
 H   E   A   L   H   N   H   Y   T   Q   K   S   L   S   L   S   P   G   K   S
GAG AAG GAT GAG CTT TGA GAG CTC
 E   K   D   E   L   -   E   L
```

APPENDIX D

Sequence of 2C8 Light Chain

```
TCT AGA ACA ATG GGC TGG TCC TGC ATC ATC CTG TTC CTT GTT GCT ACT GCT ACC GGC GTT
 S   R   T   M   G   W   S   C   I   I   L   F   L   V   A   T   A   T   G   V
CAC TCT GAT GTT CAA CTT CTC GAG GAT ATT CAG CTG ACC CAG TCT CCG TCC TCT GTT TCT
 H   S   D   V   Q   L   L   E   D   I   Q   L   T   Q   S   P   S   S   V   S
GCT TCT GTT GGT GAT AGG GTG ACC ATT ACT TGC AGG GCT ACC CAG GGA ATT TCT TCT TGG
 A   S   V   G   D   R   V   T   I   T   C   R   A   T   Q   G   I   S   S   W
CTT GCT TGG TAT CAG CAG AAG CCT GGC AAG GCT CCT AAG CTG CTT ATC TAC GCT GCT TCC
 L   A   W   Y   Q   Q   K   P   G   K   A   P   K   L   L   I   Y   A   A   S
TCA CTT CAG TCT GGT GTG CCT TCT AGG TTC AGC GGT TCT GGT TCT GGT ACT GAG TTC ACC
 S   L   Q   S   G   V   P   S   R   F   S   G   S   G   S   G   T   E   F   T
CTG ACC ATC TCT TCA CTT CAG CCT GAG GAT TTC GCC ACC TAT TAT TGC CAG CAG GCT AAC
 L   T   I   S   S   L   Q   P   E   D   F   A   T   Y   Y   C   Q   Q   A   N
ACC CTT CCG CTG TTT ACT TTT GGT CCT GGC ACC AAG GTG GAC ATT AAG AGG ACC GTC GCC
 T   L   P   L   F   T   F   G   P   G   T   K   V   D   I   K   R   T   V   A
GCC CCC TCC GTC TTC ATC TTC CCC CCC TCC GAC GAG CAG CTT AAG TCT GGA ACT GCT TCT
 A   P   S   V   F   I   F   P   P   S   D   E   Q   L   K   S   G   T   A   S
GTT GTG TGC CTT CTG AAC AAC TTC TAT CCT AGA GAA GCC AAA GTA CAG TGG AAG GTT GAC
 V   V   C   L   L   N   N   F   Y   P   R   E   A   K   V   Q   W   K   V   D
AAT GCT CTT CAA TCA GGT AAC TCC CAG GAG AGT GTC ACA GAG CAA GAT TCC AAG GAT TCC
 N   A   L   Q   S   G   N   S   Q   E   S   V   T   E   Q   D   S   K   D   S
ACC TAC AGC CTC TCA AGT ACC TTG ACG TTG AGC AAG GCA GAC TAT GAG AAA CAC AAA GTG
 T   Y   S   L   S   S   T   L   T   L   S   K   A   D   Y   E   K   H   K   V
TAC GCA TGC GAA GTC ACT CAT CAG GGC CTG TCA TCA CCC GTG ACA AAG AGC TTC AAC AGG
 Y   A   C   E   V   T   H   Q   G   L   S   S   P   V   T   K   S   F   N   R
GGA GAG TGT TGA GAG CTC
 G   E   C   -   E   L
```

APPENDIX E

Restriction enzymes

*Xba*I restriction enzyme

*Bmt*I restriction enzyme

*Afl*II restriction enzyme

*Sac*I restriction enzyme

APPENDIX F

pBYR2e-K2Md expression vector

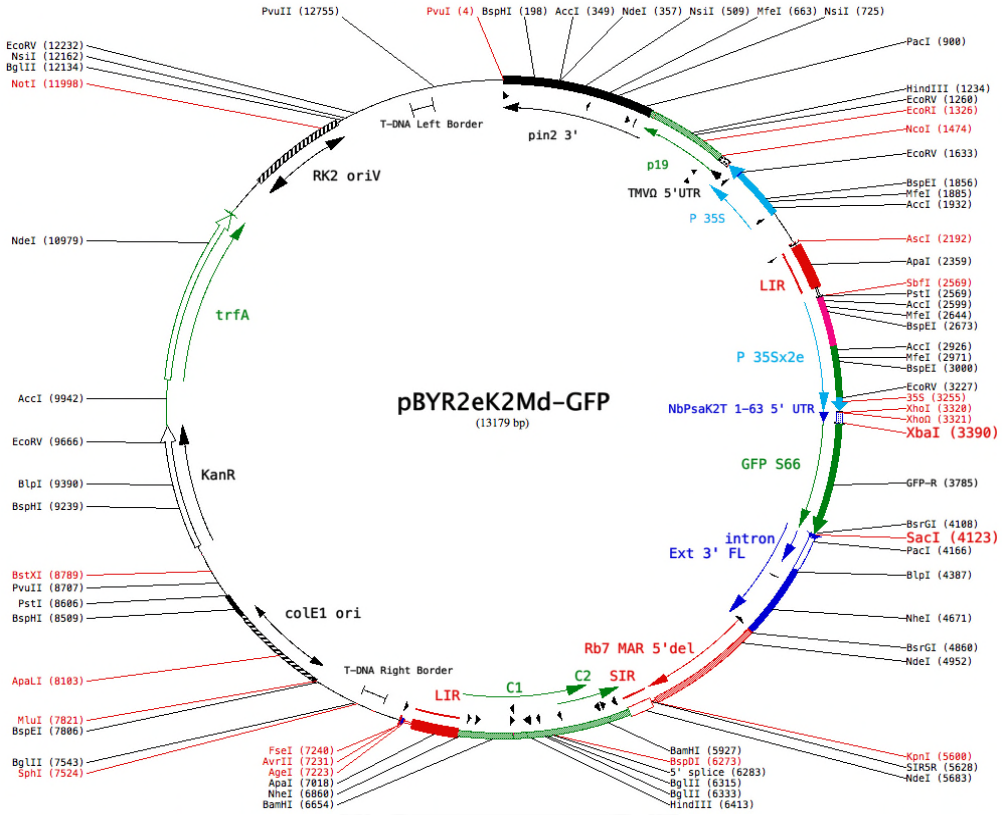

APPENDIX G

Sequence of DVD AT2C Heavy Chain

TCT AGA ACA ATG GGC TGG TCC TGC ATC ATC CTG TTC CTT GTT GCT ACT GCT ACC GGC GTT

S R T M G W S C I I L F L V A T A T G V

CAC TCT GAT GTT CAA CTT CTC GAG GAG GTC CAG CTC GTC GAG TCC GGC GGC GGC CTC GTC

H S D V Q L L E E V Q L V E S G G G L V

CAG CCC GGC GGC TCC CTC CGC CTC TCC TGC GCC GCC TCC GGC TTC ACC TTC TCC GAC TCC

Q P G G S L R L S C A A S G F T F S D S

TGG ATC CAC TGG GTC CGC CAG GCC CCC GGC AAG GGC CTT GAG TGG GTC GCC TGG ATC TCC

W I H W V R Q A P G K G L E W V A W I S

CCC TAC GGC GGC TCC ACC TAC TAC GCC GAC TCC GTC AAG GGC CGC TTC ACC ATC TCC GCC

P Y G G S T Y Y A D S V K G R F T I S A

GAC ACC TCC AAG AAC ACC GCC TAC CTC CAG ATG AAC TCC CTC CGC GCC GAG GAC ACC GCC

D T S K N T A Y L Q M N S L R A E D T A

GTC TAC TAC TGC GCC CGC CGC CAC TGG CCC GGC GGC TTC GAC TAC TGG GGC CAG GGC ACC

V Y Y C A R R H W P G G F D Y W G Q G T

CTC GTC ACC GTC TCC TCC GCT AGC ACC AAA GGT CCA CAG GTT CAG CTT CAA CAA TCT GGT

L V T V S S A S T K G P Q V Q L Q Q S G

CCT GGT CTG GTG AAG CCT TCT CAG ACT CTT TCT CTT ACC TGC GCT ATC AGC GGT GAC ACC

P G L V K P S Q T L S L T C A I S G D T

GTT TCT TCT AAT ACC GCT GCT TGG AAC TGG ATC AGG CAG TCT CCT TCA AGA GGT CTT GAG

V S S N T A A W N W I R Q S P S R G L E

TGG CTT GGT AGG ACC TAC TAC AGG TCC AAG TGG TAC TCT GAT TAC GGC CTG TCT GTG AAG

W L G R T Y Y R S K W Y S D Y G L S V K

TCC CGG ATG ACC ATT AAC GCT GAC ACC AGC AAG AAC CAG GTG AGC CTT CAT CTT AAC TCT

S R M T I N A D T S K N Q V S L H L N S

GTG ACC CCT GAG GAT ACC GCT GTT TAC TAC TGT GCT AGA GAA GGT TCT GGT GGC ACC CTT

V T P E D T A V Y Y C A R E G S G G T L

ATC TAT TGG GGT CAG GGT ACC CTC GTC ACC GTC TCC TCC GCT AGC ACC AAA GGT CCA TCG

I Y W G Q G T L V T V S S A S T K G P S

GTC TTT CCA CTG GCA CCT TCT TCC AAG AGT ACT TCT GGA GGC ACA GCT GCA CTG GGT TGT

V F P L A P S S K S T S G G T A A L G C

CTT GTC AAG GAC TAC TTT CCA GAA CCT GTT ACG GTT TCG TGG AAC TCA GGT GCT CTG ACC

L V K D Y F P E P V T V S W N S G A L T

AGT GGA GTG CAC ACC TTT CCA GCT GTT CTT CAG TCC TCA GGA TTG TAT TCT CTT AGC AGT

S G V H T F P A V L Q S S G L Y S L S S

GTT GTG ACT GTT CCA TCC TCA AGC TTG GGC ACT CAG ACC TAC ATC TGC AAT GTG AAT CAC

V V T V P S S S L G T Q T Y I C N V N H

AAA CCC AGC AAC ACC AAG GTT GAC AAG AAA GTT GAG CCC AAG TCT TGT GAC AAG ACT CAT

K P S N T K V D K K V E P K S C D K T H

ACG TGT CCA CCG TGC CCA GCA CCT GAA CTT CTT GGA GGA CCG TCA GTC TTC TTG TTT CCT

T C P P C P A P E L L G G P S V F L F P

CCA AAG CCT AAG GAT ACC TTG ATG ATC TCC AGG ACT CCT GAA GTC ACA TGT GTA GTT GTG

P K P K D T L M I S R T P E V T C V V V

GAT GTG AGC CAT GAA GAT CCT GAG GTG AAG TTC AAC TGG TAT GTG GAT GGT GTG GAA GTG

D V S H E D P E V K F N W Y V D G V E V

CAC AAT GCC AAG ACA AAG CCG AGA GAG GAA CAG TAC AAC AGC ACG TAC AGG GTT GTC TCA

H N A K T K P R E E Q Y N S T Y R V V S

GTT CTC ACT GTT CTC CAT CAA GAT TGG TTG AAT GGC AAA GAG TAC AAG TGC AAG GTC TCC

V L T V L H Q D W L N G K E Y K C K V S

AAC AAA GCC CTC CCA GCC CCC ATT GAG AAG ACC ATT TCC AAA GCG AAA GGG CAA CCC CGT

N K A L P A P I E K T I S K A K G Q P R

GAA CCA CAA GTG TAC ACA CTT CCT CCA TCT CGC GAT GAA CTG ACC AAG AAC CAG GTC AGC

E P Q V Y T L P P S R D E L T K N Q V S

TTG ACT TGC CTG GTG AAA GGC TTC TAT CCC TCT GAC ATA GCT GTA GAG TGG GAG AGC AAT

L T C L V K G F Y P S D I A V E W E S N

GGG CAA CCG GAG AAC AAC TAC AAG ACT ACA CCT CCC GTT CTC GAT TCT GAC GGC TCC TTC

G Q P E N N Y K T T P P V L D S D G S F

TTC CTC TAC AGC AAG CTC ACA GTG GAC AAG AGC AGG TGG CAA CAA GGG AAT GTC TTC TCA

F L Y S K L T V D K S R W Q Q G N V F S

TGC TCC GTG ATG CAT GAG GCT CTT CAC AAT CAC TAC ACA CAG AAG AGT CTC TCC TTG TCC

C S V M H E A L H N H Y T Q K S L S L S

CCT GGC AAG TCT GAG AAG GAT GAG CTT TAA GAG CTC GAA GTG ACA

P G K S E K D E L - E L E V T

APPENDIX H

Sequence of DVD AT2C Light Chain

```
TCT AGA ACA ATG GGC TGG TCC TGC ATC ATC CTG TTC CTT GTT GCT ACT GCT ACC GGC GTT
 S   R   T   M   G   W   S   C   I   I   L   F   L   V   A   T   A   T   G   V
CAC TCT GAT GTT CAA CTT CTC GAG GAC ATC CAG ATG ACC CAG TCC CCC TCC TCC CTC TCC
 H   S   D   V   Q   L   L   E   D   I   Q   M   T   Q   S   P   S   S   L   S
GCC TCC GTC GGC GAC CGC GTC ACC ATC ACC TGC CGC GCC TCC CAG GAC GTC TCC ACC GCC
 A   S   V   G   D   R   V   T   I   T   C   R   A   S   Q   D   V   S   T   A
GTC GCC TGG TAC CAG CAG AAG CCC GGC AAG GCC CCC AAG CTC CTC ATC TAC TCC GCC TCC
 V   A   W   Y   Q   Q   K   P   G   K   A   P   K   L   L   I   Y   S   A   S
TTC CTC TAC TCC GGC GTC CCC TCC CGC TTC TCC GGC TCC GGC TCC GGC ACC GAC TTC ACC
 F   L   Y   S   G   V   P   S   R   F   S   G   S   G   S   G   T   D   F   T
CTC ACC ATC TCC TCC CTC CAG CCC GAG GAC TTC GCC ACC TAC TAC TGC CAG CAG TAC CTC
 L   T   I   S   S   L   Q   P   E   D   F   A   T   Y   Y   C   Q   Q   Y   L
TAC CAC CCC GCC ACC TTC GGC CAG GGC ACC AAG GTC GAG ATC AAG CGC ACC GTC GCC GCC
 Y   H   P   A   T   F   G   Q   G   T   K   V   E   I   K   R   T   V   A   A
CCC GAT ATT CAG CTG ACC CAG TCT CCG TCC TCT GTT TCT GCT TCT GTT GGT GAT AGG GTG
 P   D   I   Q   L   T   Q   S   P   S   S   V   S   A   S   V   G   D   R   V
ACC ATT ACT TGC AGG GCT ACC CAG GGA ATT TCT TCT TGG CTT GCT TGG TAT CAG CAG AAG
 T   I   T   C   R   A   T   Q   G   I   S   S   W   L   A   W   Y   Q   Q   K
CCT GGC AAG GCT CCT AAG CTG CTT ATC TAC GCT GCT TCC TCA CTT CAG TCT GGT GTG CCT
 P   G   K   A   P   K   L   L   I   Y   A   A   S   S   L   Q   S   G   V   P
TCT AGG TTC AGC GGT TCT GGT TCT GGT ACT GAG TTC ACC CTG ACC ATC TCT TCA CTT CAG
 S   R   F   S   G   S   G   S   G   T   E   F   T   L   T   I   S   S   L   Q
CCT GAG GAT TTC GCC ACC TAT TAT TGC CAG CAG GCT AAC ACC CTT CCG CTG TTT ACT TTT
 P   E   D   F   A   T   Y   Y   C   Q   Q   A   N   T   L   P   L   F   T   F
GGT CCT GGC ACC AAG GTG GAC ATT AAG AGG ACC GTC GCC GCC CCC TCC GTC TTC ATC TTC
 G   P   G   T   K   V   D   I   K   R   T   V   A   A   P   S   V   F   I   F
CCC CCC TCC GAC GAG CAG CTT AAG TCT GGA ACT GCT TCT GTT GTG TGC CTT CTG AAC AAC
 P   P   S   D   E   Q   L   K   S   G   T   A   S   V   V   C   L   L   N   N
TTC TAT CCT AGA GAA GCC AAA GTA CAG TGG AAG GTT GAC AAT GCT CTT CAA TCA GGT AAC
 F   Y   P   R   E   A   K   V   Q   W   K   V   D   N   A   L   Q   S   G   N
TCC CAG GAG AGT GTC ACA GAG CAA GAT TCC AAG GAT TCC ACC TAC AGC CTC TCA AGT ACC
 S   Q   E   S   V   T   E   Q   D   S   K   D   S   T   Y   S   L   S   S   T
TTG ACG TTG AGC AAG GCA GAC TAT GAG AAA CAC AAA GTG TAC GCA TGC GAA GTC ACT CAT
 L   T   L   S   K   A   D   Y   E   K   H   K   V   Y   A   C   E   V   T   H
CAG GGC CTG TCA TCA CCC GTG ACA AAG AGC TTC AAC AGG GGA GAG TGT TGA GAG CTC
 Q   G   L   S   S   P   V   T   K   S   F   N   R   G   E   C   -   E   L
```

APPENDIX I

The typical phenotype of infiltrated *N. benthamiana* leaves on different dpi.

Agrobacterium containing Atezolizumab HC and LC

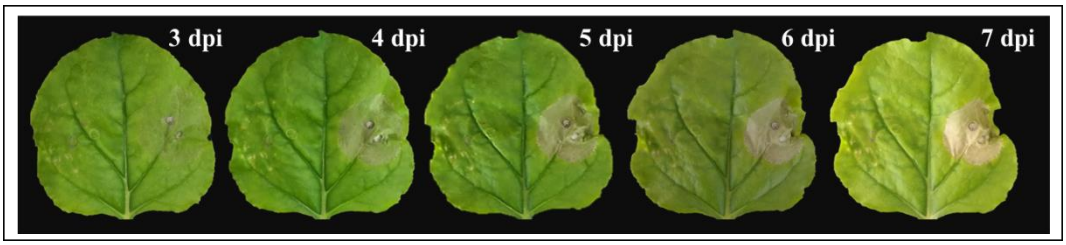

Agrobacterium containing 2C8 HC and LC

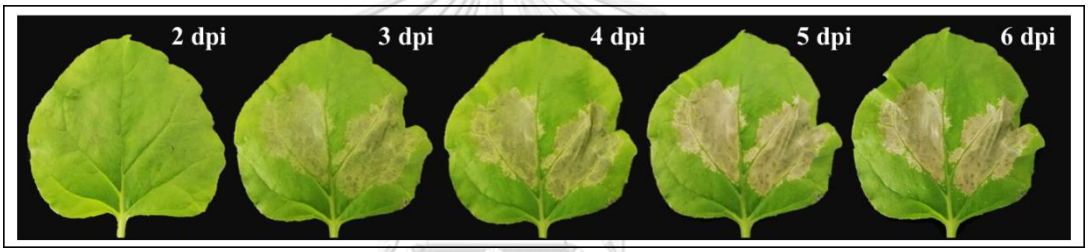

Agrobacterium containing DVD AT2C HC and LC

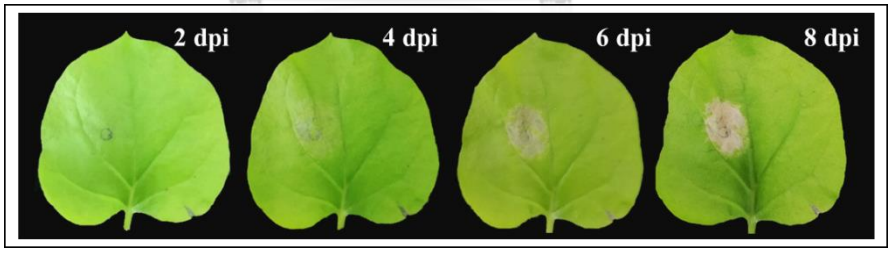

APPENDIX J

SEC chromatogram and data of integrated peaks for Atezolizumab

Plant-produced Atezolizumab

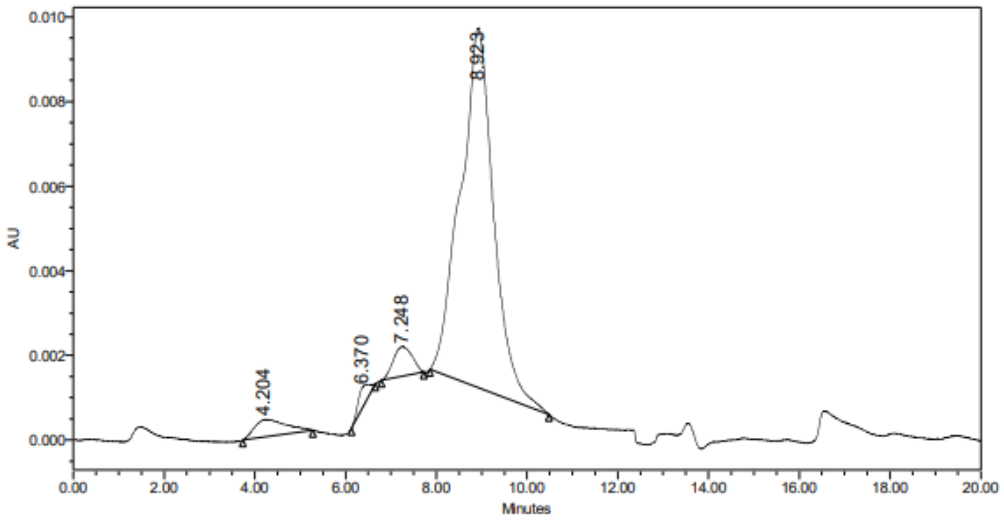

	RT	Area	% Area	Height
1	4.204	19821	4.12	415
2	6.370	7942	1.65	497
3	7.248	20307	4.22	708
4	8.923	433319	90.01	8493

Commercial Atezolizumab

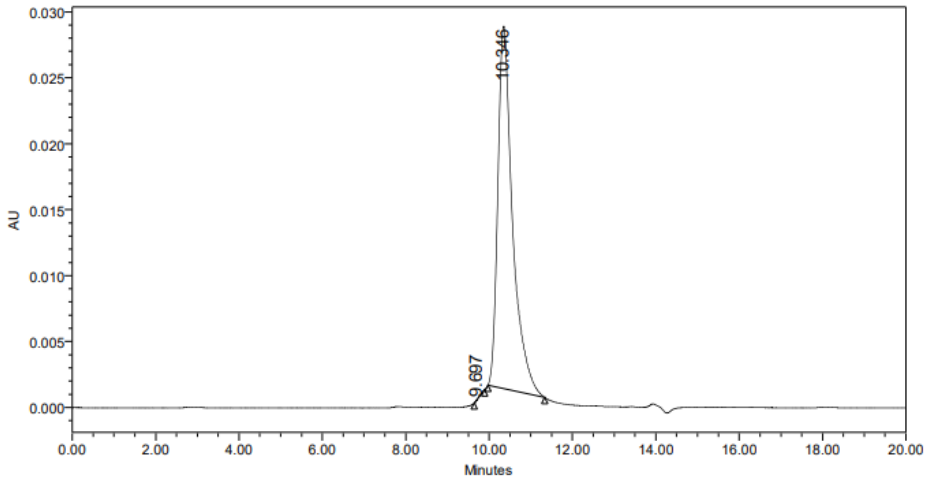

	RT	Area	% Area	Height
1	9.697	329	0.05	-37
2	10.346	670116	99.95	27456

APPENDIX K

SEC chromatogram and data of integrated peaks for 2C8

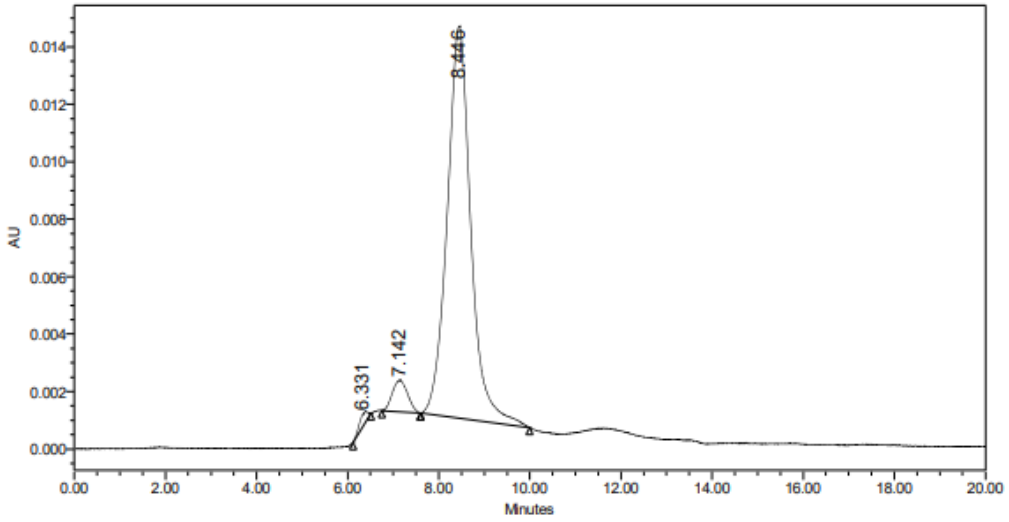

	RT	Area	% Area	Height
1	6.331	5279	1.01	441
2	7.142	25290	4.86	1093
3	8.446	489936	94.13	13635

SEC chromatogram and data of integrated peaks for DVD AT2C

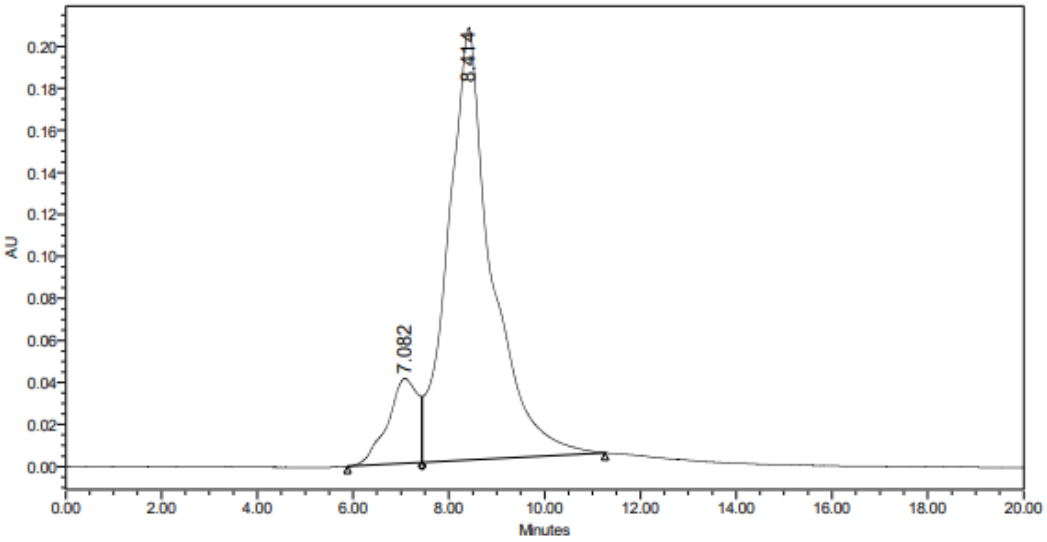

	RT	Area	% Area	Height
1	7.082	1785219	12.08	40329
2	8.414	12987780	87.92	205640

APPENDIX L

MS spectra of Atezolizumab (EEQYASTYR)

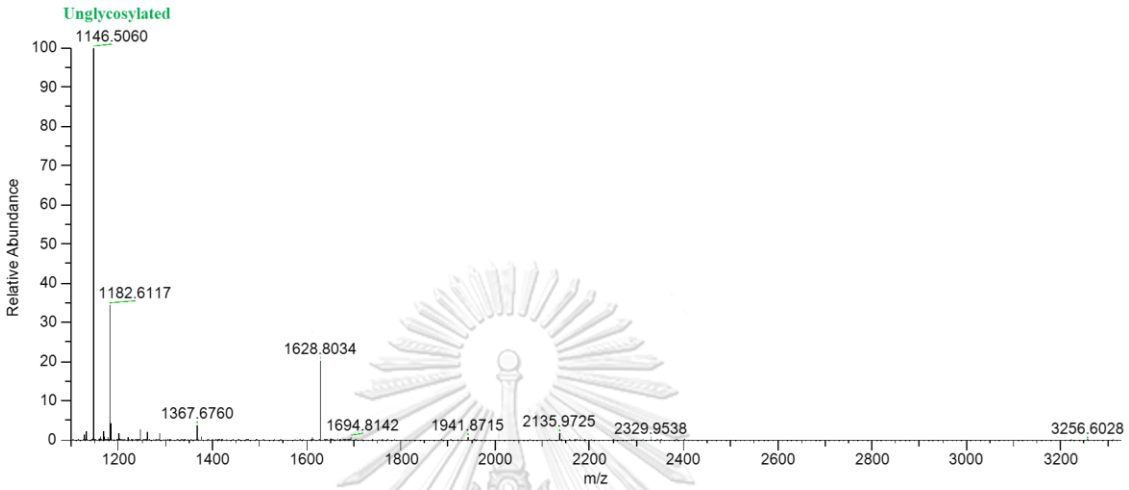

MS spectra of Tecentriq® (EEQYASTYR)

APPENDIX M

MS spectra of 2C8 (EEQYNSTYR)

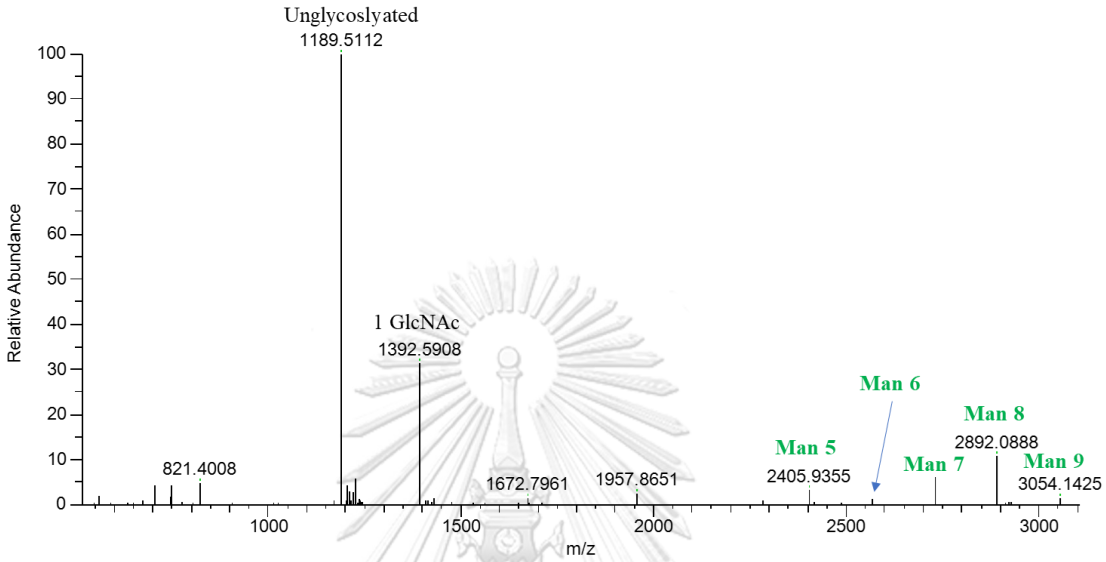

MS spectra of DVD AT2C (EEQYNSTYR)

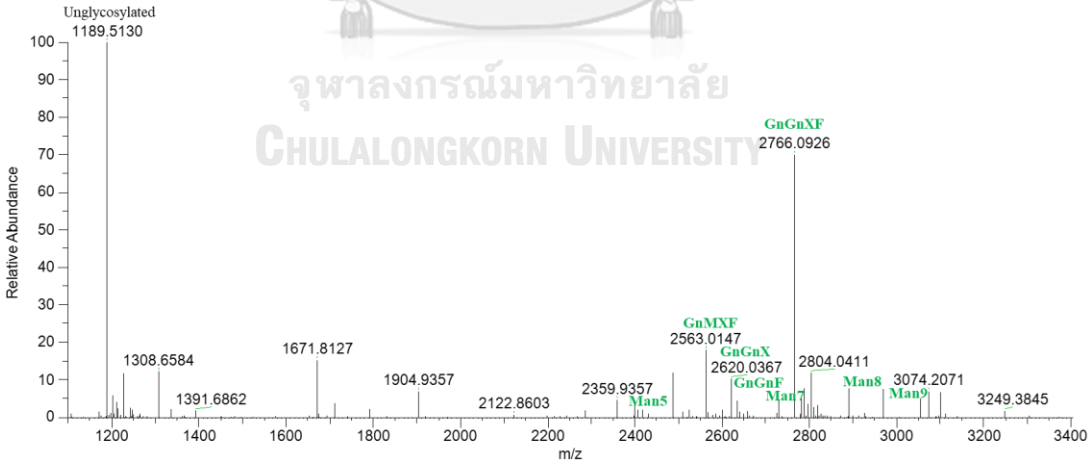

APPENDIX N

Mouse individual tumor changes of different groups

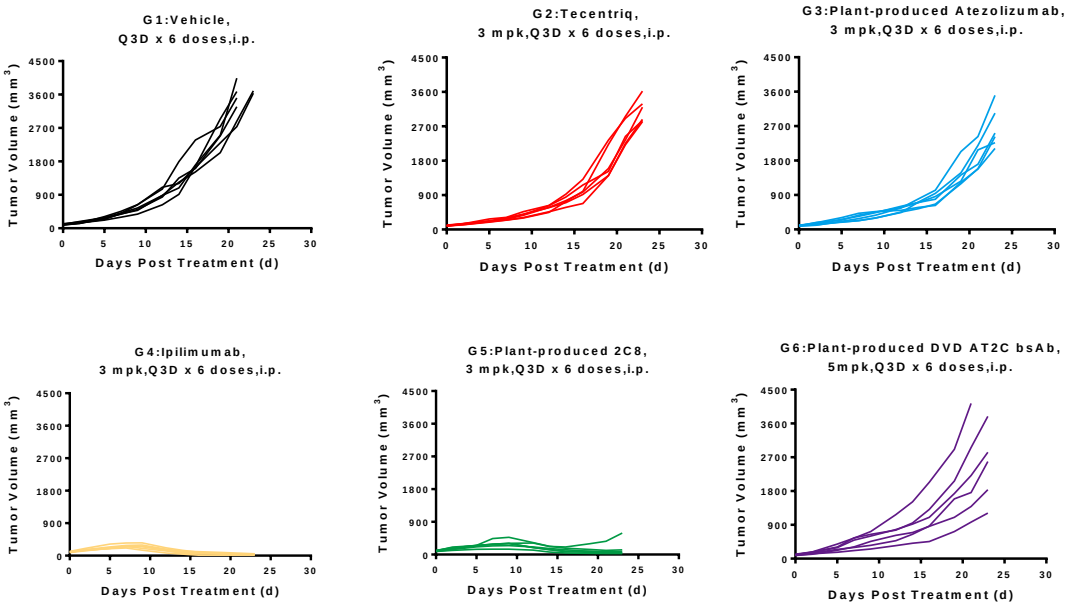

TGI_{TV} changes in different goups

G	D0	D2	D5	D7	D9	D12	D14	D16	D19	D21	D23
1	-	-	-	-	-	-	-	-	-	-	-
2	0.00 %	3.27 %	16.10 %	28.09 %	29.45 %	38.51 %	40.06 %	42.62 %	29.63 %	24.59 %	10.86 %
3	0.00 %	2.19 %	10.15 %	18.70 %	25.99 %	41.23 %	46.41 %	53.16 %	41.65 %	41.90 %	23.99 %
4	0.00 %	-9.88 %	14.08 %	31.21 %	52.72 %	83.22 %	92.70 %	96.04 %	97.97 %	98.83 %	99.17 %
5	0.00 %	-8.80 %	15.65 %	29.73 %	44.87 %	75.12 %	87.56 %	93.20 %	95.37 %	96.58 %	95.73 %
6	0.00 %	-2.26 %	-1.07%	-1.03%	6.33%	25.12 %	34.56 %	39.77 %	35.14 %	36.22 %	29.33 %

APPENDIX O

Tumor volume in different groups

G	Tumor Volume (mm^3)										
	D0	**D2**	**D5**	**D7**	**D9**	**D12**	**D14**	**D16**	**D19**	**D21**	**D23**
G1	100.91± 4.86	150.14± 8.34	264.24± 13.72	389.62± 20.81	530.60± 39.67	900.21± 68.63	1264.90± 122.43	1751.93± 127.13	2500.99± 130.60	3352.97± 201.59	3666.94± 30.93
G2	99.80 ± 3.97	143.26± 5.03	221.39± 12.13	280.02± 12.21	374.83± 24.72	552.62± 32.20	756.78± 48.91	1009.56± 88.29	1751.07± 171.11	2519.91± 135.12	3110.21± 129.51
G3	99.82 ± 4.36	144.96± 11.72	236.12± 19.03	314.01± 32.03	388.87± 31.17	522.90± 27.27	672.55± 39.04	818.24± 63.67	1438.31± 127.79	1929.33± 144.88	2644.84± 214.53
G4	100.06± 5.63	162.81± 9.80	227.34± 19.84	266.93± 19.47	251.42± 28.90	151.53± 19.75	92.43 ± 16.25	68.76 ± 13.67	48.98 ± 11.68	38.12 ± 8.96	28.47 ± 7.29
G5	99.85 ± 4.78	163.02± 13.49	224.80± 17.37	278.79± 39.01	298.44± 43.38	226.38± 32.88	159.53± 24.11	121.52± 25.18	117.86± 38.96	116.98± 51.8	152.85± 88.79
G6	99.97 ± 5.27	152.86± 10.46	271.91± 30.70	402.67± 59.38	507.03± 73.31	692.51± 116.93	857.02± 154.06	1104.71± 219.47	1688.09± 313.05	2239.13± 471.60	2451.29± 439.39

APPENDIX P

Tumor volume data

TV (mm^3)												
Group	Animal ID	D0	D2	D5	D7	D9	D12	D14	D16	D19	D21	D23
G1:Vehicle,Q3D x 6 doses,i.p.	653	86.19	133.18	313.9	453.92	635.81	1057.00	1794.99	2374.36	2741.07	3509.15	-
	681	93.84	129.44	256.5	387.42	483.50	881.94	1085.64	1705.41	2502.26	4041.79	-
	637	97.09	145.78	220.6	299.36	379.60	633.70	911.26	1666.30	2941.67	3680.71	-
	669	102.15	143.44	237.8	403.16	631.81	1104.00	1206.02	1635.59	2297.59	2733.76	3636.00
	641	105.11	182.23	286.0	411.37	546.94	884.18	1240.57	1517.81	2033.69	2880.86	3697.87
	643	121.11	166.77	270.6	382.49	505.95	840.44	1350.92	1612.09	2489.69	3271.54	-
G2:Tecentriq,3mpk,Q3D x 6 doses,i.p.	663	87.01	141.55	215.3	267.61	372.49	578.52	757.09	980.30	1596.76	2345.48	3201.86
	685	92.33	126.70	191.8	245.84	303.59	447.99	731.56	1000.35	2227.05	2961.40	3619.23
	699	97.01	151.07	227.2	305.72	386.59	625.23	848.23	1163.68	1522.29	2435.86	2850.04
	682	102.49	131.05	203.5	249.10	314.15	463.20	578.35	680.96	1410.57	2250.24	2881.35
	660	105.97	151.87	277.0	315.72	467.19	629.12	923.81	1314.15	2338.04	2908.79	3288.26
	654	113.99	157.34	213.7	296.14	404.94	571.67	701.63	917.91	1411.69	2217.68	2820.54
G3:Plant-produced Atezolizumab,3mpk,Q3D x 6 doses,i.p.	659	85.02	110.92	211.4	284.60	372.80	562.86	798.03	1023.97	2035.35	2427.33	3504.57
	672	92.54	181.71	244.9	374.29	455.03	573.31	697.59	862.17	1262.96	2080.85	2265.27
	642	98.55	119.32	196.7	230.96	296.96	454.39	543.41	660.12	1195.52	1587.54	2424.00
	691	101.71	134.68	264.5	343.62	440.44	604.12	707.27	788.93	1423.27	1703.29	2519.57
	651	104.90	173.77	310.7	420.79	465.70	499.38	574.17	629.71	1233.63	1582.29	2117.35
	666	116.19	149.38	188.6	229.79	302.30	443.32	714.84	944.54	1479.15	2194.68	3038.29
G4:Ipilimumab, 3mpk,Q3D x 6 doses,i.p.	650	83.00	138.34	199.9	262.37	201.06	128.17	86.18	71.77	55.93	40.29	26.85
	676	86.42	169.86	240.6	281.78	295.31	176.57	126.00	108.84	88.97	67.61	52.30
	656	99.98	154.00	203.7	246.20	250.91	149.26	59.25	48.38	44.67	34.90	20.13
	680	101.92	162.66	194.6	211.26	151.55	72.67	41.54	14.78	0.00	0.00	0.00

TV (mm³)												
Group	Animal ID	D0	D2	D5	D7	D9	D12	D14	D16	D19	D21	D23
	692	109.35	145.94	204.5	247.94	255.27	167.31	93.79	75.04	50.67	39.35	31.35
	667	119.70	206.05	320.7	352.00	354.39	215.21	147.80	93.76	53.65	46.56	40.18
G5:Plant-produced 2C8,3mpk,Q3D x 6 doses,i.p.	693	83.01	115.51	143.2	147.44	149.65	120.68	70.81	42.91	28.71	16.38	15.90
	679	89.97	137.67	212.7	237.37	246.35	208.77	168.09	131.25	89.55	72.98	55.70
	636	99.56	154.80	249.5	283.52	310.81	317.17	222.22	208.29	297.64	367.23	589.47
	635	103.89	203.04	248.3	276.96	301.13	195.31	134.06	76.83	60.66	51.29	41.66
	673	107.86	178.68	252.1	441.91	475.55	327.87	225.68	172.74	139.51	115.83	131.02
	670	114.85	188.40	243.1	285.52	307.13	188.46	136.34	97.11	91.07	78.16	83.34
G6:Plant-produced DVD AT2C bsAb,5mpk,Q3D x 6 doses,i.p.	652	83.79	116.71	222.8	312.38	458.30	621.72	694.93	860.69	1100.19	1389.89	1834.35
	683	88.12	130.25	171.9	215.24	258.57	348.42	410.69	454.50	720.74	971.87	1214.78
	687	100.25	147.52	245.2	296.85	356.11	478.24	651.88	867.12	1590.33	1760.82	2586.80
	678	102.21	167.70	295.4	491.69	601.17	775.17	920.18	1100.53	1734.45	2216.08	2831.94
	675	105.64	176.08	309.5	552.48	646.42	759.95	950.32	1311.53	2069.41	2961.02	3788.60
	694	119.84	178.91	386.7	547.39	721.63	1171.55	1514.10	2033.91	2913.42	4135.08	-

APPENDIX Q

P values based on tumor volume in different groups

Group	D0	D2	D5	D7	D9	D12	D14	D16	D19	D21	D23
G2 vs G1	0.872	0.636	0.135	0.031*	0.016*	<0.001 ***	<0.001 ***	<0.001 ***	0.003**	0.014*	0.176
G3 vs G1	0.874	0.721	0.322	0.129	0.028*	<0.001 ***	<0.001 ***	<0.001 ***	<0.001 ***	<0.001 ***	0.017*
G4 vs G1	0.902	0.385	0.196	0.017*	<0.001 ***	<0.001 ***	<0.001 ***	<0.001 ***	<0.001 ***	<0.001 ***	<0.001 ***
G5 vs G1	0.878	0.377	0.168	0.029*	<0.001 ***	<0.001 ***	<0.001 ***	<0.001 ***	<0.001 ***	<0.001 ***	<0.001 ***
G6 vs G1	0.892	0.851	0.785	0.789	0.703	0.021*	0.002**	<0.001 ***	0.001**	0.002**	0.006**
G3 vs G2	0.998	0.907	0.602	0.488	0.820	0.729	0.490	0.242	0.189	0.074	0.112
G5 vs G4	0.976	0.989	0.929	0.808	0.449	0.385	0.581	0.744	0.769	0.806	0.664
G6 vs G2	0.980	0.509	0.080	0.017*	0.039*	0.110	0.412	0.557	0.788	0.386	0.035*
G6 vs G3	0.982	0.587	0.209	0.077	0.063	0.055	0.136	0.084	0.291	0.339	0.520
G6 vs G4	0.990	0.494	0.120	0.009**	<0.001 ***	<0.001 ***	<0.001 ***	<0.001 ***	<0.001 ***	<0.001 ***	<0.001 ***
G6 vs G5	0.986	0.485	0.102	0.016*	0.002**	<0.001 ***	<0.001 ***	<0.001 ***	<0.001 ***	<0.001 ***	<0.001 ***

APPENDIX R

Tumor weight raw data

Group	Days after grouping	21	23	Group	Days after grouping	21	23
	Animal ID	Tumor weight ; g	Tumor weight; g		Animal ID	Tumor weight; g	Tumor weight;; g
G1:Vehicle, Q3D x 6 doses,i.p.	653	3.2867	-	G4:Ipilimumab,3mpk,Q3D x 6 doses,i.p.	650	-	0.0467
	681	4.7081	-		676	-	0.0543
	637	5.5413	-		656	-	0.0193
	669	-	4.4365		680	-	0.0000
	641	-	5.0731		692	-	0.0457
	643	4.8668	-		667	-	0.0621
G2:Tecentriq,3mpk,Q3D x 6 doses,i.p.	663	-	4.0889	G5:Plant-produced 2C8,3mpk,Q3D x 6 doses,i.p.	693	-	0.0106
	685	-	4.7053		679	-	0.0814
	699	-	3.7534		636	-	0.4570
	682	-	3.6086		635	-	0.0956
	660	-	4.9219		673	-	0.1594
	654	-	3.9443		670	-	0.0731
G3:Plant-produced Atezolizumab,3mpk,Q3D x 6 doses,i.p.	659	-	5.2074	G6:Plant-produced DVD AT2C bsAb,5mpk,Q3D x 6 doses,i.p.	652	-	1.6778
	672	-	2.9872		683	-	1.3474
	642	-	2.3652		687	-	3.7459
	691	-	3.5692		678	-	4.2603
	651	-	2.8256		675	-	4.5122
	666	-	3.2931		694	4.7511	-

APPENDIX S

Photos of terminal mice

D21: 5 mice (G1-653#, G1-681#, G1-637#, G1-643#, G6-694#) had been euthanized due to the tumor volume were more than 3000 mm^3.

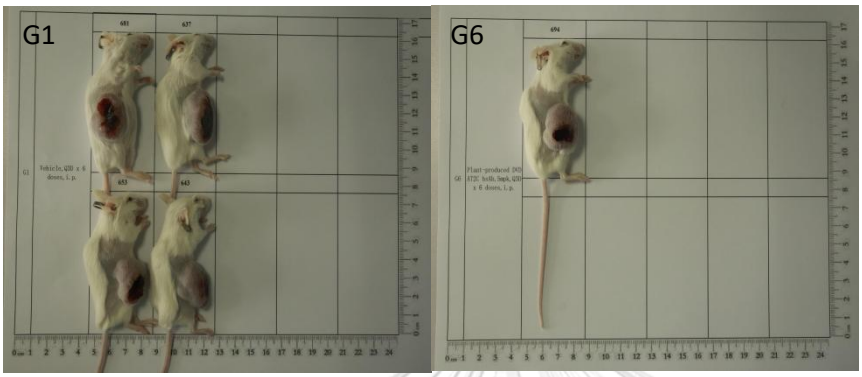

D23: The other mice had been euthanized at the endpoint.

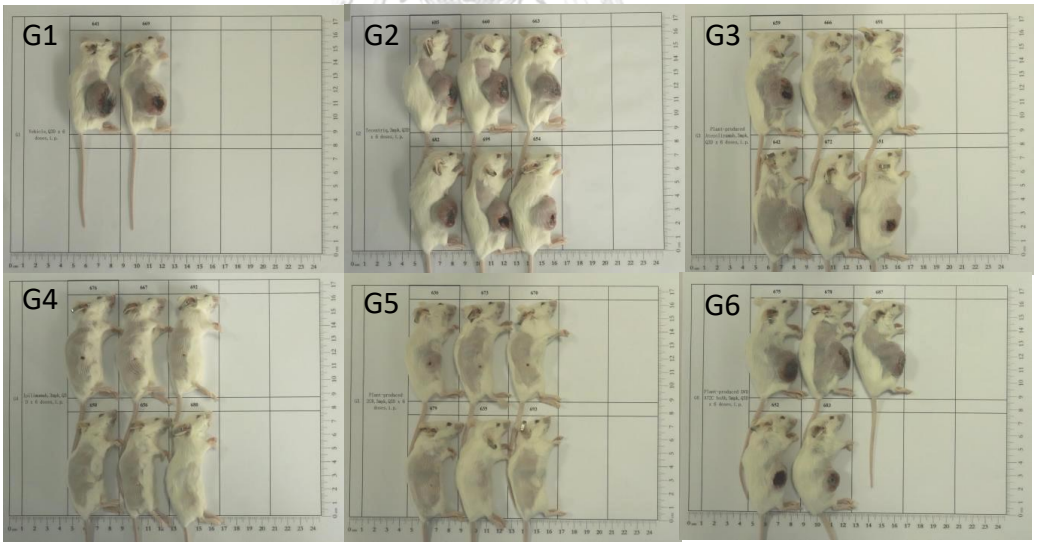

APPENDIX T

Photos of tumors

D21: 5 mice (G1-653#, G1-681#, G1-637#, G1-643#, G6-694#) had been euthanized due to the tumor volume were more than 3000 mm^3.

G1	Vehicle,Q3D x 6 doses,i.p.
G6	Plant-produced DVD AT2C bsAb,5mpk,Q3D x 6 doses,i.p.

D23: The other mice had been euthanized at the endpoint.

G1	Vehicle,Q3D x 6 doses,i.p.
G2	Tecentriq,3mpk,Q3D x 6 doses,i.p.
G3	Plant-produced Atezolizumab,3mpk,Q3D x 6 doses,i.p.
G4	Ipilimumab,3mpk,Q3D x 6 doses,i.p.
G5	Plant-produced 2C8,3mpk,Q3D x 6 doses,i.p.
G6	Plant-produced DVD AT2C bsAb,5mpk,Q3D x 6 doses,i.p.

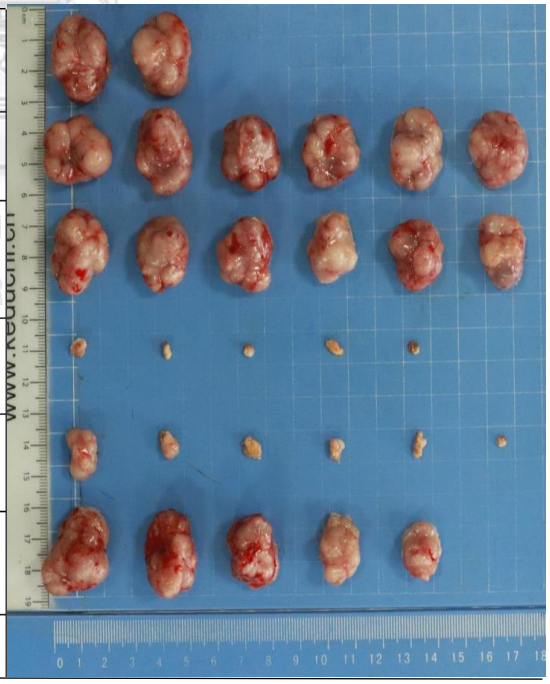

APPENDIX U

Body weight data

Body Weight (g)												
Group	Animal ID	D0	D2	D5	D7	D9	D12	D14	D16	D19	D21	D23
G1:Vehicle,Q 3D x 6 doses,i.p.	653	21.3	21.0	22.0	22.0	22.8	23.8	24.8	24.4	21.8	24.2	-
	681	23.5	22.0	22.6	22.5	23.3	24.2	24.6	25.0	26.1	27.5	-
	637	19.1	19.2	19.3	19.6	20.1	20.8	21.4	22.0	24.0	24.2	-
	669	17.8	17.3	17.7	18.3	18.7	19.5	20.2	19.7	20.1	20.7	21.6
	641	17.4	17.6	17.9	18.6	18.4	19.2	19.9	19.8	20.8	21.9	22.0
	643	18.6	18.5	18.4	19.3	19.0	19.8	21.0	20.8	22.0	22.9	-
G2:Tecentriq, 3mpk,Q3D x 6 doses,i.p.	663	20.0	20.4	19.7	20.7	20.6	21.2	21.1	21.4	22.1	22.5	22.6
	685	20.4	20.4	20.0	20.5	20.9	21.4	21.7	21.8	23.6	24.0	24.5
	699	22.9	22.2	21.8	22.8	22.7	23.1	23.4	24.1	23.1	24.6	25.5
	682	20.2	20.2	20.5	20.4	20.4	21.5	22.0	21.4	22.0	23.1	23.4
	660	22.0	21.3	21.7	21.9	22.0	23.2	23.6	23.0	24.6	25.1	25.5
	654	21.2	20.7	20.8	21.5	21.5	22.4	23.1	22.9	22.6	23.4	23.6
G3:Plant-produced Atezolizumab, 3mpk,Q3D x 6 doses,i.p.	659	19.8	19.1	19.5	20.3	20.7	21.1	21.7	21.6	23.5	22.7	24.5
	672	22.4	21.4	21.9	22.0	22.1	22.7	22.9	23.3	23.4	24.2	24.7
	642	21.4	21.3	21.4	22.0	21.6	22.6	22.3	22.6	23.6	24.4	24.3
	691	21.6	21.7	21.3	22.3	22.1	22.4	22.8	22.7	23.4	23.7	24.6
	651	21.3	21.3	20.9	21.6	21.3	21.7	21.9	22.6	23.2	23.8	24.5
	666	19.8	20.7	20.6	20.7	21.0	20.9	22.1	22.0	22.7	23.7	24.6
G4:Ipilimumab,3mpk,Q3D x 6 doses,i.p.	650	21.4	21.4	20.6	22.2	21.8	21.3	21.9	20.8	22.0	21.5	22.0
	676	22.1	21.5	21.9	23.3	23.1	22.8	22.8	22.4	22.2	23.5	23.8
	656	19.2	18.9	18.7	20.4	19.9	20.0	20.2	19.6	20.2	20.0	20.5
	680	20.3	20.7	20.3	20.9	20.5	21.0	20.9	21.1	21.2	21.7	22.5
	692	20.7	20.4	20.1	20.5	20.1	20.3	20.0	20.5	20.2	21.0	21.3
	667	20.9	21.5	21.4	21.3	21.3	21.7	21.5	21.4	21.7	22.4	22.1
G5:Plant-produced 2C8,3mpk,Q3D x 6 doses,i.p.	693	19.9	19.8	20.5	20.7	20.6	21.1	20.8	21.2	21.2	21.7	21.5
	679	22.0	21.6	22.2	21.5	22.1	22.3	22.7	22.8	22.1	22.7	22.4
	636	20.7	20.6	20.8	20.4	21.0	21.7	21.6	21.5	21.8	22.4	22.3
	635	21.0	21.5	21.2	21.3	22.0	21.5	21.3	21.5	21.9	22.1	22.3
	673	22.4	21.4	22.1	21.6	22.6	22.3	22.8	22.4	22.6	23.5	23.2
	670	20.3	20.4	20.5	20.5	20.8	21.1	21.0	20.8	20.9	21.9	21.5
G6:Plant-produced DVD AT2C bsAb,5mpk,Q3D x 6	652	20.4	19.8	20.0	20.1	20.7	21.6	22.0	21.6	22.8	22.4	23.4
	683	21.7	21.5	20.8	21.2	22.2	22.6	23.0	22.7	23.6	23.6	23.9
	687	18.4	18.8	18.4	17.9	18.4	19.1	19.0	19.3	20.3	21.2	22.1
	678	22.3	22.0	22.5	22.0	22.4	23.2	23.6	22.9	23.5	23.8	24.1

Body Weight (g)												
Group	Animal ID	D0	D2	D5	D7	D9	D12	D14	D16	D19	D21	D23
doses,i.p.	675	19.3	19.5	19.9	19.6	20.0	21.1	21.1	21.6	23.1	24.2	25.1
	694	21.8	21.6	21.4	21.7	22.2	23.0	22.7	23.2	24.6	25.1	-

VITA

NAME	Christine Joy I. Bulaon
DATE OF BIRTH	06 Nov 1996
PLACE OF BIRTH	Tarlac, Tarlac
INSTITUTIONS ATTENDED	Bachelor of Science (B.Sc.), University of Santo Tomas, Philippines Master of Science (M.Sc.), Chulalongkorn University, Thailand
HOME ADDRESS	Villa Lourdes Subdivision San Rafael Tarlac City
PUBLICATION	1. Shanmugaraj B, I Bulaon CJ, Phoolcharoen W. Plant Molecular Farming: A Viable Platform for Recombinant Biopharmaceutical Production. Plants (Basel). 2020 Jul 4;9(7):842. doi: 10.3390/plants9070842. PMID: 32635427; PMCID: PMC7411908. 2. Bulaon CJI, Shanmugaraj B, Oo Y, Rattanapisit K, Chuanasa T, Chaotham C, Phoolcharoen W. Rapid transient expression of functional human vascular endothelial growth factor in Nicotiana benthamiana and characterization of its biological activity. Biotechnol Rep (Amst). 2020 Aug 15;27:e00514. doi: 10.1016/j.btre.2020.e00514. PMID: 32884911; PMCID: PMC7453061. 3. Shanmugaraj B, Bulaon CJI, Malla A, Phoolcharoen W. Biotechnological Insights on the Expression and Production of Antimicrobial Peptides in Plants. Molecules. 2021 Jul 1;26(13):4032. doi: 10.3390/molecules26134032. PMID: 34279372; PMCID: PMC8272150. 4. Rattanapisit K, Bulaon CJI, Khorattanakulchai N,

Shanmugaraj B, Wangkanont K, Phoolcharoen W. Plant-produced SARS-CoV-2 receptor binding domain (RBD) variants showed differential binding efficiency with anti-spike specific monoclonal antibodies. PLoS One. 2021 Aug 11;16(8):e0253574. doi: 10.1371/journal.pone.0253574. PMID: 34379620; PMCID: PMC8357147.

5. Phakham T, Bulaon CJI, Khorattanakulchai N, Shanmugaraj B, Buranapraditkun S, Boonkrai C, Sooksai S, Hirankarn N, Abe Y, Strasser R, Rattanapisit K, Phoolcharoen W. Functional Characterization of Pembrolizumab Produced in Nicotiana benthamiana Using a Rapid Transient Expression System. Front Plant Sci. 2021 Sep 9;12:736299. doi: 10.3389/fpls.2021.736299. PMID: 34567049; PMCID: PMC8459022.

6. Shanmugaraj B, Malla A, Bulaon CJI, Phoolcharoen W, Phoolcharoen N. Harnessing the Potential of Plant Expression System towards the Production of Vaccines for the Prevention of Human Papillomavirus and Cervical Cancer. Vaccines (Basel). 2022 Dec 1;10(12):2064. doi: 10.3390/vaccines10122064. PMID: 36560473; PMCID: PMC9782824.

7. Christine Joy I. Bulaon, Hongyan Sun, Ashwini Malla, Waranyoo Phoolcharoen, Therapeutic efficacy of plant-produced Nivolumab in transgenic C57BL/6-hPD-1 mouse implanted with MC38 colon cancer, Biotechnology Reports, Volume 38, 2023, e00794, ISSN 2215-017X.